Spectroscopic Investigation of Chemiluminescence in Gasoline Homogeneous Charge Compression Ignition Engine

by

Rinaldo Augusta

A thesis submitted in partial fulfillment
of the requirements for the degree of

Master of Science

(Mechanical Engineering)

at the

University of Wisconsin – Madison

2004

Approved: _____

David E. Foster

Professor – Mechanical Engineering
University of Wisconsin – Madison

Date: _____

ABSTRACT

A spectroscopic diagnostic system has been designed to study the effects of different engine parameters on the chemiluminescence characteristic of HCCI combustion. Light emitted during the combustion process was collected by an optical fiber installed in the spark plug hole. An imaging spectrograph separated the light into the component wavelength and a high speed CCD camera captured the resulting light spectrum. The engine parameters studied in this work were intake temperature, fuel delivery method, fueling rate, air-fuel ratio, and intake charge preheating. Two different fuels were used in this experiment: pure isooctane and a primary reference fuel blend with an octane number of 87 (PRF 87). At each data point, a set of time-resolved chemiluminescence spectra were obtained, along with the cylinder pressure and exhaust emissions data.

Based on the results, it was determined that different engine parameters affect the start of ignition timing in HCCI combustion without altering the reaction pathways of the fuel. The thermal history of the air-fuel mixture greatly affects the ignition timing. However, once the ignition starts, the fuel follows the same reaction pathways and produces the same intermediate species regardless of the thermal history of the mixture.

The chemiluminescence spectra of HCCI combustion appear as several distinct peaks corresponding to emissions from CHO, CH_2O, CH, and OH superimposed on top of a CO-O continuum. A strong correlation was found between the chemiluminescence light intensity and the rate of heat release. At the lower fueling rate conditions, the light intensity was too weak for further analysis.

ACKNOWLEDGEMENTS

I would like to express my sincere gratitude to several people who have contributed to this work. First, I would like to thank Professor David E. Foster and Professor Jaal B. Ghandhi for their valuable advice, opinions, and encouragement. I would also like to thank my thesis committee members, Professor Scott T. Sanders and Professor Patrick V. Farrell for their valuable inputs and suggestions regarding my research work.

I would like to acknowledge the contributions of General Motors in providing the engine and most of the laboratory equipments. The contributions of James Eng from General Motors in terms of opinions and advice were invaluable throughout this project.

My co-workers in this project, Robert Iverson and Randy Herold, have provided me with valuable support in many aspect of this work. Their suggestions and advice helped me solved many issues related to this project. This project would not have been possible without their tremendous contributions in setting up the test cell. I would also like to thank Ralph Braun for his technical advice and assistance in the ERC and Lonny Peet for his contributions in this project.

Finally, my deepest appreciation goes to my parents and my family for their support, understanding, and encouragement throughout my study.

TABLE OF CONTENTS

LIST OF TABLES

LIST OF FIGURES

GLOSSARY OF NOMENCLATURES

A/F	air/fuel ratio
aTDC	after top dead center
bTDC	before top dead center
CA	crank angle
CA 10	10% burn location
CA 50	50% burn location
CA 90	90% burn location
cc	cubic centimeter
CH_2O	formaldehyde
CI	compression ignition (diesel) engines
CO	carbon monoxide
CO_2	carbon dioxide
COV	coefficient of variation
CR	compression ratio
deg	degree
EGR	exhaust gas recirculation
EI	emission index
EI_{CO}	emission index of carbon monoxide
EI_{HC}	emission index of hydrocarbons
EI_{NO}	emission index of nitrogen oxides
EPA	environmental protection agency

FWHM	full-width half-maximum
HC	hydrocarbons
HCCI	homogeneous charge compression ignition
IMEP	indicated mean effective pressure
N_2	nitrogen
NA	naturally aspirated
NO_x	nitrogen oxides
NTC	negative temperature coefficients
PP	peak pressure
PRF	primary reference fuel (mixture of isooctane and n-heptane)
PRF 87	primary reference fuel with an octane number of 87
RPM	engine revolutions per minute
s	seconds
SI	spark ignition
TDC	top dead center

Chapter 1 - Introduction

1.1 Background

The internal combustion engine is known as one of the major sources of air pollutants in the environment. The fuel oxidation process in the engine generates not only useful power, but also a considerable amount of pollutant emissions including Carbon Dioxide (CO_2), Carbon Monoxide (CO), Unburned Hydrocarbon (HC), Nitrogen Oxides (NO_x), and particulate matter.

CO_2 is mainly responsible for the global warming issue as it creates a reflective layer in the atmosphere that reflects heat from the earth back to the earth surface, increasing the earth's average temperature over time [1]. Carbon Monoxide (CO) is a very dangerous substance since it reduces the oxygen carrying capacity of blood stream. At low concentrations, CO inhalation can cause dizziness and nausea, while at higher concentrations it can be deadly [2]. Unburned hydrocarbon emission, a result of incomplete combustion process, is a common source of respiratory problems. Particulate emissions or soot also causes some respiratory problems. Both unburned hydrocarbon and soot emissions have been linked to some cancers in several studies [2]. High flame temperature generated during the combustion process is responsible for NO_x formation which causes various health problems as well as contributing to acid rain and global warming issues [2].

Scientific research has projected a significant increase in the amount of major air pollutants in the decades to come due to the increasing number of internal combustion engine production and usage. To avoid the potential problems related with air pollutants,

the U.S. government through the Environmental Protection Agency (EPA) is enforcing the limit on maximum amount of pollutants an engine is allowed to generate. The regulations are getting stricter in the years to come. Engine researchers throughout the world have been focused on improving engine performance and efficiency while reducing the amount of pollutants generated in order to meet more stringent regulations. The expected result of enforcing stricter NO_x emissions regulations is shown in Figure 1-1 [3] below.

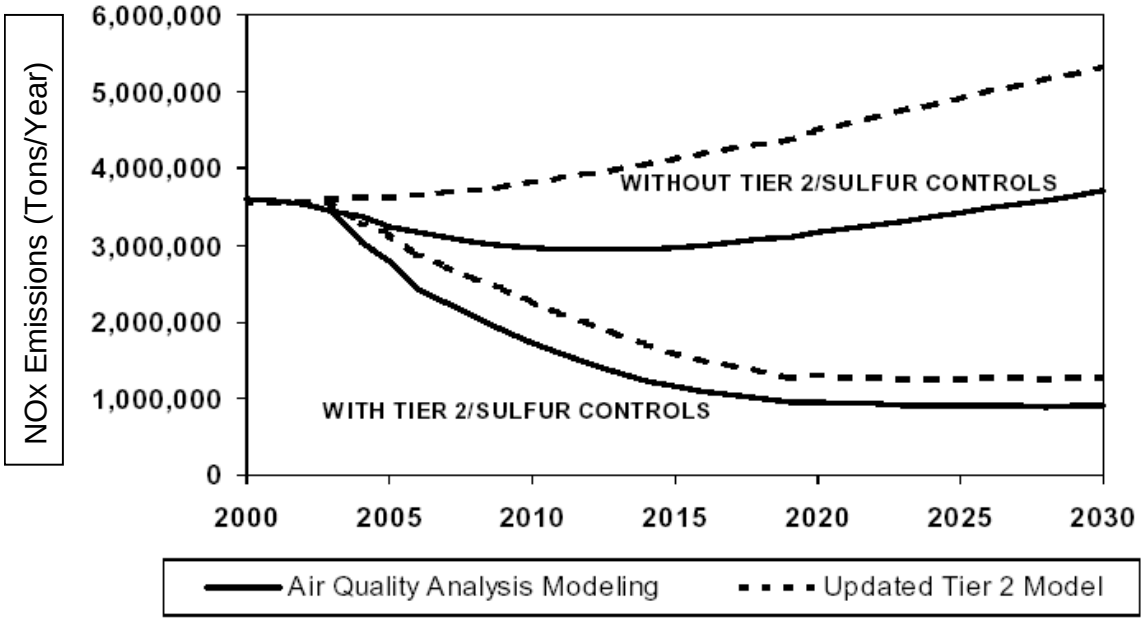

Figure 1-1 Projected NO_x emissions with and without stricter regulations [3]

It is clearly shown in figure 1-1 that NO_x emissions would increase substantially in three decades to come if the current emission regulation is maintained. However, with a stricter Tier-2 regulation, it is expected that the NO_x emissions will be significantly reduced from the current level. Meeting the stricter emissions regulation is not an easy

task for engine manufacturers. Considerable efforts have been placed in various areas to reduce the engine emissions or to remove certain pollutants from the exhaust gases.

One method to reduce engine emissions is a different combustion process known as Homogeneous Charge Compression Ignition (HCCI). This process is considered as an attractive alternative to other internal combustion engine types, namely Spark Ignition (SI) and Compression Ignition (CI) engine, due to its potential of high efficiency operation while producing significantly lower amount of NO_x and soot emissions. Both SI and CI engines have been widely used in commercial applications due to their capability of generating high power density under wide operating range while using readily available fuel. The goal of utilizing HCCI is to combine the advantages of SI and CI engines to create a more efficient and less polluting engines.

Each type of internal combustion engine has its own operating characteristic, advantages, and disadvantages which will be discussed in the following sections.

1.1.1 Spark Ignition (SI) Engine

In an SI engine, fuel is introduced into the intake system upstream of the cylinder to produce homogeneous air-fuel mixture. The mixture is inducted into the cylinder during the intake valve open period and compressed by the piston to high pressure and temperature. At a certain time close to top dead center, the mixture is ignited by an electrical discharge across the spark plug electrode. The flame will then propagate across the cylinder volume to completely oxidize the fuel inside the cylinder. The combustion process generates high pressure which then pushes the piston downward and rotates the crankshaft. The generated power can be used to move a vehicle or other applications.

Load control in SI engine is provided by means of a throttle which adjusts the opening of the intake port, thus controlling the mass flow rate of air-fuel mixture entering the cylinder. Throttling creates a pressure drop in the intake system which reduces the peak pressure attainable in the cylinder, thus limiting the amount of power produced by the engine.

The advantage of SI engines is that the ignition timing is easily controlled for optimum performance by varying the spark timing. SI engine also has high power density under naturally aspirated conditions due to the stoichiometric nature of the mixture. In addition, the homogeneous mixture produces negligible amount of particulate emission or soot.

In order to ensure flame propagation inside the cylinder and to facilitate catalytic clean-up of the exhaust, the air-fuel ratio of the mixture must be maintained at, or close to, stoichiometric. Flame propagation can not occur if the mixture is too lean or too rich. Stoichiometric air-fuel mixtures burn at very high temperature, producing significant NO_x emissions. Part of the homogeneous air-fuel mixture can also get trapped in the relatively cold crevice volume and does not burn. This unburned fraction leaves the engine as hydrocarbon emissions. The main challenge of SI engine development is controlling the amount of NO_x, CO, and unburned hydrocarbon emissions to meet the strict regulations.

The maximum compression ratio of an SI engine is limited by knocking constraints. If the air-fuel mixture is compressed to a certain pressure and temperature, it can auto-ignite prior to the spark timing, creating a high pressure fluctuation inside the cylinder. The auto-ignition process creates unpleasant pinging noise and can cause severe

mechanical damage to the engine. To prevent potential damage from this auto-ignition behavior, modern engines are equipped with knock sensor that retards the ignition timing appropriately when knock is detected. While this method may be useful in preventing engine damage, retarding the spark timing also reduces the engine efficiency.

1.1.2 Compression Ignition (CI) Engine

In a CI or Diesel engine, air is inducted into the cylinder and compressed by the piston during the compression stroke. Fuel is injected directly into the cylinder when the piston is close to top dead center, creating a locally rich or stoichiometric region that can auto-ignite and initiate the combustion process. Further oxygen and fuel mixing occurs in the cylinder as the fuel oxidation process continues until all the fuel is consumed or the cylinder temperature has cooled down to a point where the reactions can no longer take place.

In a Diesel engine, load control is provided by adjusting the amount of fuel injected into the cylinder on each cycle. The elimination of the throttle in the intake system increases the efficiency of Diesel engine compared to SI engine. In addition, Diesel engines typically have higher compression ratios to achieve the auto-ignition, and are not limited by knock

Compared to SI engine, a naturally aspirated Diesel engine has lower power density because of the leaner overall air-fuel ratio and lower maximum engine speed. The locally rich or stoichiometric region in the cylinder also burns at very high temperature and produces significant amount of NO_x emissions. The presence of locally rich regions is the source of soot formation. Simultaneous reduction of NO_x and soot emissions

becomes the main challenge for Diesel engine development to meet the strict emissions regulations.

1.1.3 Homogeneous Charge Compression Ignition (HCCI) Engine

HCCI is considered as an appealing alternative to SI and Diesel engines due to its capability of operating with higher efficiency while producing very low NO_x and soot emissions. HCCI can be seen as a hybrid between SI and Diesel engine, combining the advantages of both engines.

In an HCCI engine, a homogeneous air-fuel mixture is formed early in the cycle, either in the intake system prior to entering the cylinder, or directly in the cylinder early in the compression stroke. The mixture is compressed in the cylinder and allowed to auto-ignite. The auto ignition process occurs simultaneously in very short period of time leading to a small cycle-to-cycle variation. The short combustion duration is closer to the ideal constant volume combustion of the Otto cycle, thus maximizing the engine efficiency.

Since there is no flame propagation, the air-fuel mixture can be made very lean. In fact, it is often desirable to dilute the air-fuel mixture either with EGR or excess air to slow down the combustion process. The lean mixture burns at lower temperature compared to a stoichiometric mixture, resulting in significantly less NO_x emissions. Since the mixture is homogeneous, soot emissions are not a concern.

Despite these advantages, HCCI still poses some challenges that must be overcome before it can be widely used in practical application. The main limitation of HCCI is the narrow operating window which results from the lack of direct ignition

timing control. In an SI engine, the start of ignition is easily controlled by adjusting the spark timing, and in a Diesel engine ignition timing is controlled by varying the fuel injection timing. In HCCI, the start of ignition is mainly determined by the chemical kinetics reaction of the air-fuel mixture. Various methods have been proposed and investigated for HCCI ignition timing control, including intake charge preheating, internal or external EGR, and a stratified fuel injection system.

The lean nature of the air-fuel mixture limits the power density of HCCI engines and the amount of fuel that can be injected on each cycle is limited by knocking constraints. As the mixture becomes richer, the heat release rate becomes more rapid, producing an excessive pinging noise and possible mechanical damage. The lean mixture is also prone to reaction quenching which can result in incomplete combustion and considerable HC and CO emissions. In a low compression ratio engine, it is necessary to preheat the air-fuel mixture to a high temperature prior to entering the cylinder to ensure proper HCCI combustion. The preheating process reduces the mass flow rate of air-fuel mixture into the cylinder, further reducing the engine power density.

While HCCI operation has been demonstrated in both two-stroke and four-stroke engines under different operating conditions with different fuels, none of current technologies enable HCCI operation in the entire engine operating regime.

The reaction paths and nature of the combustion is not yet completely understood. Further research is necessary to gain better understanding of the combustion process and discover suitable methods for better ignition timing control before HCCI can be widely used in commercial applications.

1.2 Objectives and Approach

The objective of this work is to gain better understanding of HCCI combustion process and its reaction paths by performing time-resolved spectroscopic investigation of the light emitted naturally during combustion process. The combustion process emits light naturally through a process known as chemiluminescence. From analysis of the time-resolved light spectrum, different radical species can be identified at different stages of combustion process.

The experiments were performed on a single cylinder four-stroke engine built on Ricardo Hydra block and equipped with General Motors four-valve dual overhead camshafts cylinder head. Two separate fuel injection systems were installed in the engine. The first injector is a premixed fuel injection system which injects fuel approximately 1.5 meters upstream of the intake valves to ensure complete air-fuel mixture formation. The second fuel injector is installed at the intake port pointed directly to the intake valves to create some in-homogeneity in the mixture. Two types of fuel were used in this work: isooctane and a blend of primary reference fuels with an octane number of 87 (PRF 87). Isooctane was used to investigate the effects of varying intake temperature, fuel delivery method, fuel flow rate, and air-fuel ratio on the engine performance and light emission spectra. PRF 87 was used to study the effects of intake charge preheating throughout the intake system.

The operating window of the engine is governed by the lower and upper temperature limits. The lower temperature limit was defined as the point where the Indicated Mean Effective Pressure (IMEP) coefficient of variation (COV) is greater than 2%. The high temperature limit was defined as the point where the ringing index exceeds

8 V. Ringing index is a scaled measure of the cylinder pressure oscillation amplitude at a central frequency of 8.3 kHz as described by Eng [4]. From previous experience with this engine it is determined that the ringing index must be maintained below 8 V to prevent mechanical damage to the engine.

Various engine operating parameters, exhaust emissions, and cylinder pressure data were recorded simultaneously using computerized data acquisition systems. A set of time-resolved chemiluminescence spectra were obtained at each data point. The rate of heat release was calculated from the cylinder pressure data using a separate computer program.

1.3 Scope and Limitations

The experiments were performed on a single cylinder standard engine which was not specifically designed for optical diagnostic study. The spark plug hole was fitted with a custom threaded fiber optic adapter to gain optical access of the cylinder volume. Light was collected from a cone shaped volume at the center of the cylinder. When the piston is at TDC, the base diameter of the cone is 3.3 mm. It is assumed that the light collected by the fiber is an accurate representation of the chemiluminescence process throughout the cylinder volume.

The engine baseline operating conditions used in this work were established previously by Iverson [5]. The baseline data was used to ensure data consistency and operating conditions repeatability.

Chapter 2 - Literature Review

2.1 Overview

Over the last few decades, considerable efforts have been focused on HCCI combustion study by engine researchers throughout the world. The attraction to HCCI is mainly driven by its potential of producing power at higher efficiency while generating significantly less NO_x and soot emissions compared to SI and Diesel engine. In addition, HCCI combustion was found to have very low cycle-to-cycle variation due to the simultaneous auto-ignition of the air-fuel mixture throughout the cylinder [6, 7].

HCCI operates in the auto-ignition regime where the ignition process is mainly controlled by the kinetic history of the gas mixture in the cylinder. In order to gain a better understanding of HCCI combustion process, it is necessary to review the background of the fuel auto-ignition mechanisms. The first section of this chapter is focused on the chemical reactions related to auto-ignition of air-fuel mixture in HCCI combustion, followed by the mechanisms of pollutants formation. In the latter section, selected results of prior HCCI studies will be reviewed.

2.2 Chemical Kinetics

The auto-ignition process in HCCI combustion is a very complicated process with a large number of chemical reactions involving numerous intermediate chemical species. The reaction sequences and the corresponding chemical species formed are constantly changing with changes in temperature, pressure, and mixture composition [8]. Many of

the major species and chemical reactions involved in HCCI combustion have been identified through previous research results.

The auto-ignition behavior of the air-fuel mixture depends largely on the characteristics of the fuel itself [9]. The fuel's octane number determines its resistance to auto-ignition. N-heptane (n-C_7H_{16}), a reactive, straight-chain paraffinic fuel, has an octane number of zero. N-heptane tends to isomerize quite easily at relatively low temperature, thus makes it easier to auto-ignite. In HCCI operation, n-heptane exhibits distinguishable two-stage heat release; a cool-flame stage characterized by negative temperature coefficient (NTC) behavior, followed by the main heat release. The two-stage heat release behavior is less noticeable in fuels with highly complex branched structure such as isooctane (i-C_8H_{18}), which has an octane number of one hundred. Isooctane tends to hold its atoms more tightly which makes it more difficult to auto-ignite. In the case of fuel mixture of isooctane and n-heptane, the behavior is dependent upon the composition of the mixture [10].

The auto-ignition reactions can be divided into two regimes, namely the low temperature and high temperature reactions [8]. The low temperature reactions occur at temperature below 1000 K and consist mainly of the fuel molecule interactions with oxygen or other radicals to create fuel radical species. These low temperature reactions are mainly the pre-ignition kinetics. At higher temperature, above 1000 K, the high temperature reactions take over. During this period, the fuel and radicals oxidize to CO_2 and H_2O while releasing most of the fuel energy. Both of these regimes will be discussed in more detail in the following sections.

2.2.1 Low Temperature Reactions

Low temperature reactions are considered as the precursor of the main heat release and the main purpose of these reactions is to form radical pool which will react later during the main heat release period. The extent of low temperature reactions is highly dependent on the type of the fuel. A straight-chain fuel such as n-heptane is much more reactive at low temperature compared to isooctane which has a highly complex branched structure with less reactive methyl groups. Depending on the fuel, low temperature reactions can consume up to 10% of the fuel in the cylinder.

The initial reaction that occurs during low temperature reactions is the chain initiating reaction as shown in Reaction (2-1). In the reaction, R represents a free alkyl radical of unspecified composition (C_nH_{2n+1}) [11].

$$RH + O_2 \rightarrow R + HO_2 \qquad \text{(initiation)} \qquad (2\text{-}1)$$

Once the reaction system has created other radicals, the initiation reaction becomes less important route of radical R formation due to its endothermic nature. The major chain propagating reactions for creating free alkyl radical are listed below [8, 12].

$$RH + HO_2 \rightarrow R + H_2O_2 \qquad (2\text{-}2)$$

$$RH + OH \rightarrow R + H_2O \qquad (2\text{-}3)$$

Reaction (2-3) has the fastest rate of attack since the reaction is highly exothermic. Reaction (2-2) takes place throughout the low temperature reactions period to generate H_2O_2 which remains stable until the temperature reaches about 1000 K. At higher temperature, H_2O_2 breaks down into two OH molecules very rapidly as shown in Reaction (2-4), where M represents a non reactive species. OH is the main attacker of the

fuel, and as soon as OH is formed in large enough quantities, the reactions quickly accelerate toward the high temperature regime.

$$H_2O_2 + M \rightarrow OH + OH + M \qquad (2\text{-}4)$$

The predominant reactions and intermediate species that occur during low temperature reactions are detailed in Figure 2-1 below. In the figure, P represents any intermediate products including O-heterocycles, carbonyls, ketones, and alkenes, while R represents a free radical of unspecified composition [8].

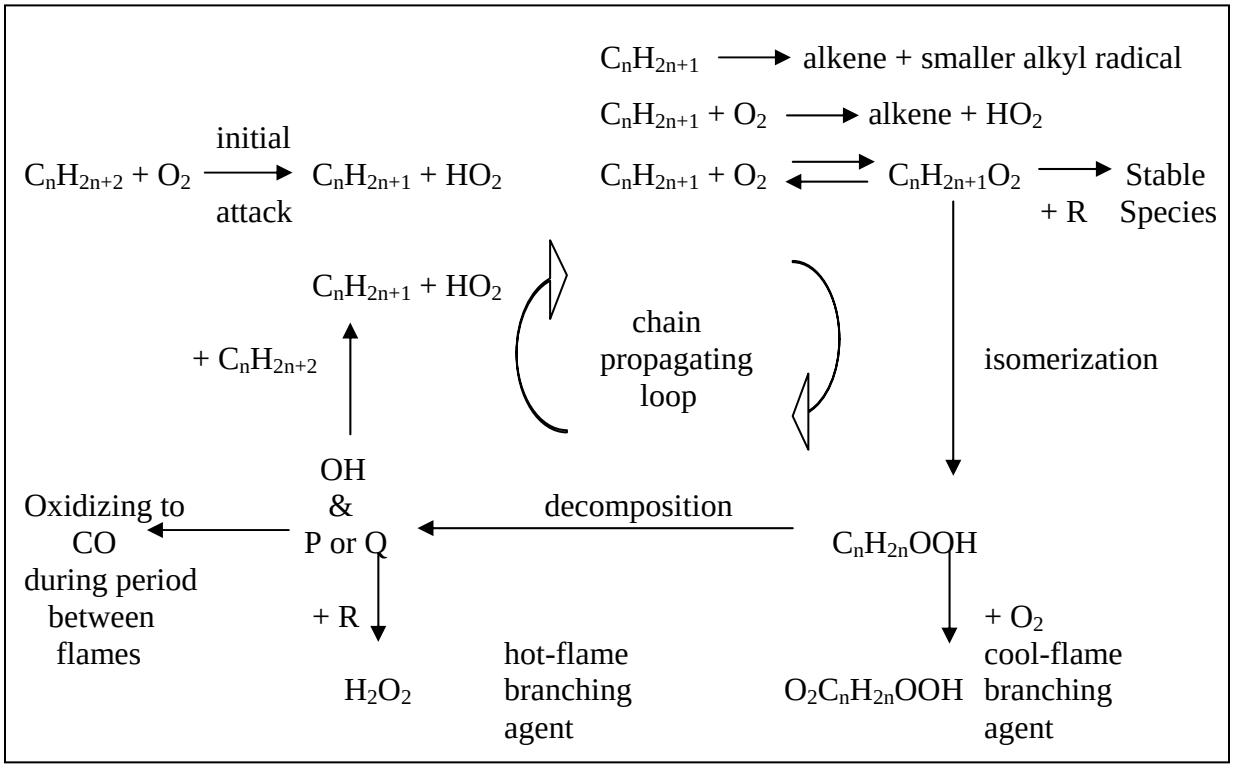

Figure 2-1 Low temperature reactions mechanisms [8]

As shown in Figure 2-1, the chain reaction is initiated by the interaction of fuel molecule with oxygen as in Reaction (2-1) to create a free alkyl radical R of unspecified composition (C_nH_{2n+1}) [8]. The hydrogen abstracted from the fuel typically comes from a

tertiary carbon atom since the C-H bonding is the weakest. If there is no tertiary carbon atom, the oxygen will attack the secondary carbon atom which has the next weakest C-H bond. Figure 2-2 shows an example of fuel molecular structure and the type of carbon atoms [13].

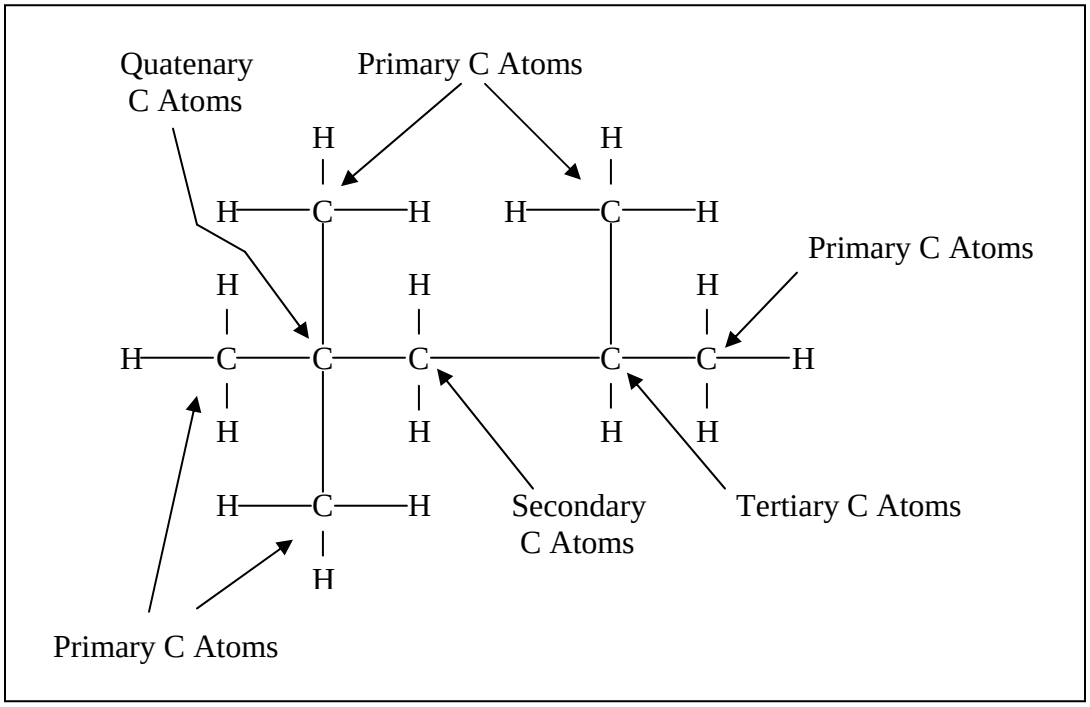

Figure 2-2 Isooctane molecular structure [13]

The alkyl radical will then follow one of the three possible reactions pathways. The first reaction path is for the alkyl radical to break down into an alkene and a smaller alkyl radical. Another possibility is for the alkyl radical to react with oxygen, forming a conjugate alkene along with an HO_2 radical. The third reaction path, which is a very important reaction in the chain propagating loop, is for the alkyl radical to bond with an oxygen atom, forming a peroxy radical (RO_2) as shown in Reaction (2-5). The equilibrium constant of RO_2 is highly temperature dependent; therefore the reaction can occur both ways depending on the temperature. At low temperature, the reaction tends to

form the RO_2 radical, while at higher temperature the RO_2 decomposition dominates. This temperature sensitivity leads to the NTC behavior of most fuels [8, 12].

$$R + O_2 \leftrightarrow RO_2 \quad (2\text{-}5)$$

The resulting RO_2 will then follow several reactions path depending on the environment as shown in Reaction (2-6 to 2-8).

$$RO_2 + R'H \rightarrow ROOH + R' \quad (2\text{-}6)$$

$$RO_2 \rightarrow QOOH \quad (2\text{-}7)$$

$$RO_2 \rightarrow R + O_2 \quad (2\text{-}8)$$

The pathway of RO_2 reaction is very important in determining the auto-ignition characteristic of the mixture. Following the first pathway, RO_2 reacts with a fuel molecule denoted R'H, abstracting an H atom from the fuel molecule, as shown in Reaction (2-6). The resulting ROOH will then produce an oxygenated radical and OH by breaking the O-O bond as in Reaction (2-9). The RO molecule will further react to form other radical species and generate an alkyl radical [8].

$$ROOH \rightarrow RO + OH \quad (2\text{-}9)$$

The second pathway (Reaction 2-7) is the major source of chain branching in low temperature reactions. Following this pathway, RO_2 internally abstract an H atom, forming a QOOH radical. The QOOH radical will then degenerate in several ways according to Reactions (2-10 to 2-12):

$$QOOH \rightarrow Q + HO_2 \quad (2\text{-}10)$$

$$QOOH \rightarrow QO + OH \quad (2\text{-}11)$$

$$QOOH + O_2 \rightarrow O_2QOOH \quad (2\text{-}12)$$

The QOOH molecule can release the entire OOH radical as in Reaction (2-10), and the Q molecule will turn into a fairly stable olefin. If the QOOH releases an OH radical as in Reaction (2-11), the resulting QO will turn into cyclic ether. Another possible way is for the QOOH to react with an oxygen molecule as in Reaction (2-12). If this occurs, the resulting molecule will isomerize into ketohydroperoxide and an OH radical. As the temperature reaches 800 K, the ketohydroperoxide will further decompose into at least two radicals.

At temperature higher than 800 K, the third pathway (Reaction 2-8) starts to become dominant. Following this pathway, the RO_2 molecule decomposes back into the original alkyl radical and oxygen molecule (R and O_2). This behavior is due to the temperature sensitivity of the equilibrium constant of that particular reaction. Once the temperature reaches 900 K, RO_2 decomposes as soon as it is formed; therefore the other two pathways can no longer take place. This behavior leads to Negative Temperature Coefficient (NTC) behavior in fuels that tend to form QOOH radicals [14].

2.2.2 High Temperature Reactions

High temperature reactions initiate at temperature above 1000 K when significant amount of OH has been formed. The high temperature reactions are highly dependent on the low temperature or cool flame reactions. The time delay between the low temperature and high temperature reactions depends on the cool flame intensity. Higher cool flame intensity results in shorter time delay between the two reactions regimes [8, 9].

The main fuel consumption reactions that occur during high temperature regime are listed below [8].

Initial Reactions

$$C_nH_{2n+2} + OH \rightarrow C_nH_{2n+1} + H_2O \quad (2\text{-}13)$$

$$C_nH_{2n+2} + O \rightarrow C_nH_{2n+1} + OH \quad (2\text{-}14)$$

$$C_nH_{2n+2} + H \rightarrow C_nH_{2n+1} + H_2 \quad (2\text{-}15)$$

Thermal Decomposition

$$C_nH_{2n+1} \rightarrow C_aH_{2a} + C_bH_{2b+1} \quad (2\text{-}16)$$

$$C_nH_{2n+1} \rightarrow C_nH_{2n} + H \quad (2\text{-}17)$$

Chain Branching

$$H + O_2 \rightarrow O + OH \quad (2\text{-}18)$$

The initial high temperature reactions are initiated by hydrogen abstraction of the fuel molecules by OH, oxygen, or hydrogen atom as shown in Reactions (2-13 – 2-15). The hydrogen abstraction is dominated by the OH route which produces alkyl radicals and water as in Reaction (2-13). The formation of water helps to increase the mixture temperature. Once the temperature reaches 1100 K, the C-C bonds in the fuel radicals begin to break, forming various combinations of smaller alkyl and alkene radicals according to Reactions (2-16) and (2-17). The decomposition reactions, however, is not a chain branching process. The most likely source of chain branching is Reaction (2-18) which produces OH and oxygen atom. Once this reaction starts, it will dominate the overall reactions and starts the main heat release. Milovanovic and Chen [9] noted that the main ignition temperature for almost all fuels are identical, which further suggests that high temperature chain branching is independent of the fuel type.

The various alkenes produced during the thermal decomposition sequences react with oxygen, forming water and carbon monoxide (CO), which will further oxidize into

carbon dioxide (CO_2) and water as in reaction (2-19) [8]. Glassman [11] also indicates that in the presence of HO_2, there is another route for CO oxidation as shown in reaction (2-20).

$$CO + OH \rightarrow CO_2 + H \quad (2\text{-}19)$$

$$CO + HO_2 \rightarrow CO_2 + OH \quad (2\text{-}20)$$

Reaction (2-20) only occurs during the initial stage of oxidation when high concentration of HO_2 exists; therefore Reaction (2-20) is rarely as important as Reaction (2-19) in most situations. Most of the energy release from the combustion process occurs during these CO oxidation reactions.

Throughout the combustion process, OH is involved in many different reactions, both in the low and high temperature regime. Early in the high temperature reactions, OH only exists in very low concentration due to a high degree of competition involving fuel molecules and hydrogen atoms. As such, CO oxidation reaction is delayed until most of the fuel and radicals have reacted. The delayed reaction also means that the majority of energy release does not occur until the end of the combustion process [8].

CO oxidation reaction can only occur above certain temperature. If the cylinder temperature drops before the reaction completes, significant amount of CO will be expelled along with the exhaust gases. This represents wasted energy and reduces the engine combustion efficiency.

2.3 Emissions Formation Mechanisms

The pollutant formation in the engine is highly dependent on the air-fuel mixture composition and the combustion temperature. Figure 2-3 shows the trends of exhaust

emissions of a spark ignition engine as a function of the fuel/air equivalence ratio [15]. The formation mechanism of major air pollutants from internal combustion engine will be discussed in this section.

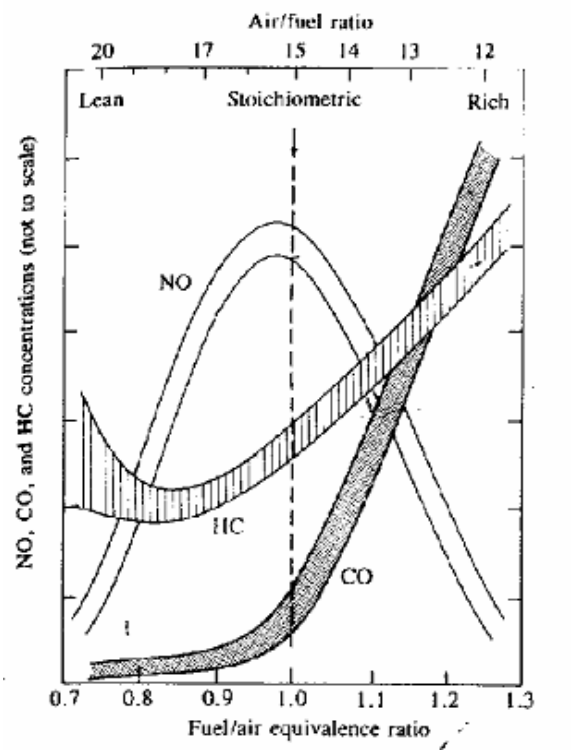

Figure 2-3 Trends of HC, CO, and NO from an SI engine as a function of equivalence ratio [15]

2.3.1 Nitrogen Oxides (NO_x)

One of the main challenges in pollutant emission control is reducing the amount of Nitrogen Oxide (NO_x), which is strictly regulated by the EPA. The main attraction to HCCI is the possibility of low NO_x emissions. The rate of NO formation is governed by Zeldovich mechanism, which with some approximations can be simplified as shown in Equation (2-1) [15]:

$$\frac{d[NO]}{dt} = \frac{6\times10^{16}}{T^{1/2}} e^{\frac{-69,090}{T}} [O_2]_e^{1/2} [N_2]_e \qquad (2\text{-}1)$$

Where $[]_e$ is the equilibrium concentration and T represents temperature. The equation is only valid at NO concentration close to zero, $[NO]/[NO]_e << 1$. The exponential term in the equation shows a strong dependence of the formation rate on temperature. The formation rate starts to increase very rapidly as the temperature reaches 1800 K, as shown in Figure 2-4. At temperature of 2000 K, the formation rate becomes extremely high.

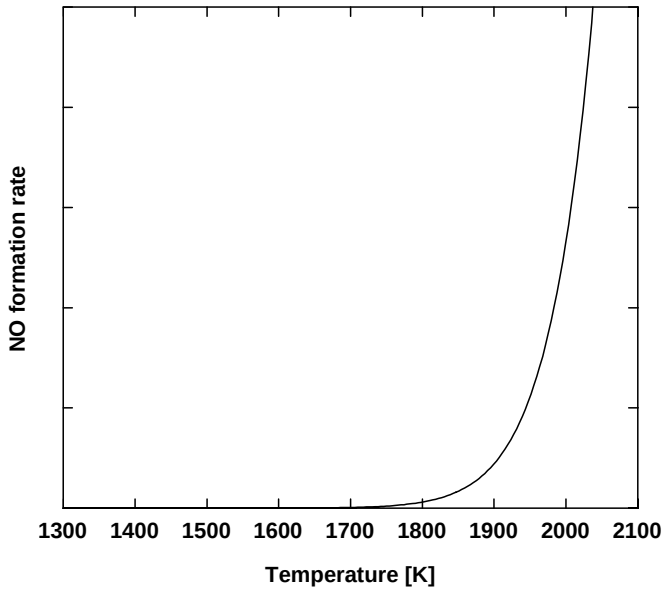

Figure 2-4 NO formation rate [16]

During HCCI combustion, the cylinder peak temperature is relatively low compared to SI or diesel combustion, which leads to a significant reduction of NO_x emissions. Christensen *et al*. [16] found that NO_x emissions in HCCI operation depend on the fuel characteristic. Fuels with higher octane number require higher temperature for auto-ignition, thus resulting in higher NO_x emissions.

2.3.2 Particulate Matter

Particulate matter or soot emission reduction is a main challenge in diesel engine development. The source of soot formation in diesel engine is the diffusion-limited combustion process and the presence of locally fuel-rich regions within the cylinder [15]. HCCI combustion is found to produce very low soot emissions due to the homogeneous nature of the mixture. However, soot emissions can be a problem once mixture heterogeneity is introduced in the cylinder.

2.3.3 Unburned Hydrocarbons

HCCI combustion tends to produce more unburned hydrocarbon (HC) emissions compared to conventional diesel combustion. The relatively low cylinder temperature during HCCI combustion often results in incomplete fuel oxidation. In addition, the low temperature combustion is more prone to flame quenching.

Research performed by Christensen *et al.* [17] found that HC emissions depend on the compression ratio, with higher compression ratio resulting in higher HC emissions. The trend occurs because the main combustion usually takes place after TDC on the expansion stroke. As the combustion progresses, the cylinder volume increases and the temperature decreases. The rate of volume and temperature change is more rapid with higher compression ratio, thus resulting in less time for complete fuel oxidation.

The main location for HC storage is in the crevice volume. As the premixed mixture is compressed in the cylinder, some fraction of the mixture gets trapped in the crevice volume. This trapped fraction can not auto-ignite because the temperature is too cold, and it leaves the cylinder along with the exhaust as HC emissions. As the

compression ratio is increased, a larger fraction of the mixture gets trapped in the crevice volume, contributing to higher HC emissions.

2.3.4 Carbon Monoxide

Carbon Monoxide (CO) emissions from HCCI engines are typically higher than conventional SI or CI engines. Similar to HC, high CO emission is an indication of incomplete fuel oxidation [18]. Christensen *et al.* [16-18] suggested that CO emissions are highly dependent on combustion temperature with higher intake temperature yielding lower CO emissions. This condition usually occurs close to the rich limit. At low load operation with lower intake temperature, a high concentration of CO can be generated. The author also noted that CO emissions increase with increasing compression ratio. The main reason for this behavior is the lack of time for complete fuel oxidation. With a higher compression ratio, the cylinder temperature decreases faster during the exhaust stroke and there is less time for complete oxidation of CO to CO_2.

High HC and CO emissions represent incomplete fuel oxidation processes, which means that part of the fuel energy is wasted along with the exhaust, resulting in poor combustion efficiency.

2.4 HCCI Combustion Research

The term HCCI is used to describe an operating regime in which premixed air-fuel mixture is allowed to simultaneously auto-ignite in the cylinder without using an auxiliary spark source or flame propagation. This combustion process has also been referred to by many different terminologies. In two-stroke studies, HCCI is also referred

to as Active Thermo-Atmosphere Combustion (ATAC) [6], Activated Radicals (AR) combustion [9], Toyota-Soken combustion [19], etc. In four-stroke engines, HCCI is also known as Controlled Auto-Ignition (CAI) [9], Compression Ignited Homogeneous Charge (CIHC) [8, 20], Premixed Charge Compression Ignition (PCCI) [9], etc.

The first HCCI combustion in two-stroke engine was demonstrated by Onishi *et al.* [6] in 1979. The authors observed a new operating regime where premixed air-fuel mixture can auto-ignite without using a spark plug. Compared to normal spark ignition operation, the auto-ignition process yielded smoother combustion with more consistent peak pressure and less misfiring cycles. In addition, the hydrocarbon emissions were noticeably lower. Optical investigation using Schlieren photography showed that the combustion occurred simultaneously at many different points throughout the cylinder without flame propagation. The authors called this auto-ignition behavior Active-Thermo Atmosphere Combustion (ATAC).

Noguchi *et al.* [19] presented similar auto-ignition behavior in an opposed piston two-stroke engine. The authors found that auto-ignition occurred at lower temperature and pressure compared to diesel operation. In addition, the combustion duration was significantly shorter compared to normal spark-ignition operation. The author called this combustion phenomenon Toyota-Soken combustion. Radical concentration measurement showed that CHO, HO_2, and O were the first species to be detected. As the combustion progressed, CH, C_2, and H were observed, followed by OH which was the last detected species.

The same type of auto-ignition behavior in four-stroke engines was first demonstrated by Najt and Foster [20]. The authors noted that the heat release rate in

HCCI operation was much smoother than knocking in spark ignition. Due to the low compression ratio of the engine, the intake charge had to be heated prior to entering the cylinder to achieve proper HCCI combustion. The authors found that the engine operational characteristics were highly sensitive to intake temperature. Equation (2-1) was developed to calculate the average energy release rate of HCCI combustion based on simplified chemical kinetics model.

$$AERR = \frac{C}{(vol)^{1.75}}(\phi)^{1.5}(DR)^{1.75}\exp(\frac{-E_{av}}{RT_{av}})$$

$AERR$ = Average Energy Release Rate (g-fuel/sec)

C = Proportionality Constant

vol = Cylinder clearance volume (cm^3)

ϕ = Equivalence Ratio

DR = Delivery Ratio

E_{av} = Pseudo-activation Energy (J/gmol)

R = Universal Gas Constant (J/gmol-K)

T_{av} = Average Charge Temperature (K)

Equation (2-1) successfully predicted the energy release rate for an engine speed range from 600 to 2500 RPM. This result concluded that the engine speed does not significantly alter the rate of energy release (*AERR*). It does, however, change the physical time (in seconds) available for complete fuel oxidation process. The study also found that the extent and nature of low temperature reactions depend largely on the fuel type. Conversely, the high temperature reactions remained unaffected by the fuel type.

In 1989, Thring [21] was the first to define an operating range concept for HCCI operation, which included satisfactory operating region, misfire region, power-limited

region, and knock region. In the power-limited region, even though the indicated power is not enough to overcome friction losses, the combustion was still quite steady and smooth without excessive pressure rise rate. Therefore, the power-limited region might still be acceptable in low load operating conditions. The author noted that high intake temperature, high EGR rate, or a combination of both was required for satisfactory HCCI operation. The author also suggested using HCCI mode at light load conditions where it is most efficient, and switch to conventional SI mode at high load conditions.

Previous research work on HCCI combustion has shown the capability of higher efficiency and lower emissions compared to conventional SI and CI engines. The challenges faced by HCCI researchers are low power density, narrow operating window, and lack of ignition control. While prior HCCI research has been focused in many different approaches, Milanovic and Chen [9] concluded that the prior work can be categorized into two approaches: modifying air/fuel mixture properties, and modifying the engine parameters. The two possible approaches will be discussed in the following sections.

2.4.1 Modifying Air/Fuel Mixture Properties

Various strategies have been investigated in prior HCCI research to alter the properties of the air-fuel mixture entering the cylinder. The main intention of modifying the mixture properties is to alter the reactivity of the mixture, which will determine the ignition timing as well as the rate of heat release.

Intake Temperature

Intake temperature adjustment is one of the easiest methods for ignition timing control in HCCI operation. Higher intake temperature results in more advanced ignition timing and a faster energy release rate. The main reason for this behavior is that higher temperature improves the mixture reactivity. As the intake temperature is increased past a certain upper limit, the energy release rate can become very rapid, resulting in unpleasant pinging noise and possible engine damage. In addition, high intake temperature reduces the engine volumetric efficiency due to lower mixture density. Prior studies found that HCCI combustion is very sensitive to intake charge temperature [5, 9, 22]. This control strategy is suitable only when the engine operating condition does not change regularly, since the intake temperature control does not offer sufficiently fast response time during transient condition.

Air-Fuel Ratio / Equivalence Ratio

The equivalence ratio of the mixture has a significant effect on HCCI ignition timing and heat release rate. In general, the heat release rate becomes more rapid as the mixture becomes richer. HCCI combustion can occur at very lean conditions, which results in lower peak temperature and NO_x emissions compared to conventional SI and diesel engines. However, there is a limit to maximum air-fuel ratio that the engine can run. Beyond this limit, the combustion becomes unstable with higher cycle-to-cycle variations. The HC and CO emissions also increase rapidly which indicate incomplete fuel oxidation. At the rich limit, the engine operation is limited by a situation similar to knocking in SI engines. Previous work by Noda and Foster [22] concluded that intake air

temperature has more pronounced effect on HCCI combustion compared to equivalence ratio.

It is also interesting to note that Iverson [5] found that increasing air-fuel ratio at lower fueling rate actually improved the combustion by widening the operating range, increasing the peak pressure, and reducing combustion variability. It is thought that the improvement stemmed from an increase in the amount of oxygen available in the cylinder as the air-fuel ratio is increased.

Exhaust Gas Recirculation (EGR)

EGR has been widely used as an alternative control method in prior HCCI research [6, 19, 20]. The EGR strategy can be divided into two categories, trapping internal EGR and adding external EGR. Internal EGR can be trapped in the cylinder by adjusting the exhaust valve timing to close early. The trapped residual is allowed to mix with fresh intake charge from the next cycle. Internal EGR usually increases the air-fuel mixture temperature, therefore reducing the amount of required preheating. The resulting air-fuel mixture temperature, which determines the ignition timing and heat release rate, can be controlled by adjusting the amount of internal EGR.

In other cases, external EGR is introduced back into the intake system and allowed to mix with fresh intake charge prior to entering the cylinder. The external EGR temperature is typically much lower than internal EGR, therefore the main purpose of external EGR is to dilute the intake charge to delay the ignition timing and slow down the heat release rate by absorbing the energy released from the combustion process.

Fuel Reformation / Intake Charge Preheating

Prior investigation by Iverson [5] found that extreme preheating of certain air-fuel mixtures in the intake system can alter the composition and auto-ignition resistance of the mixture. The engine operating window was found to shift as the intake charge temperature history was altered. Proper HCCI combustion could be achieved at lower intake temperature provided the intake charge has been previously exposed to higher temperature earlier in the intake system. Samples of the intake charge prior to entering the cylinder were collected and analyzed using Gas Chromatograph Mass Spectroscopy (GC Mass Spec). The analysis revealed an increase in some oxygenated species concentration as the intake system temperature was increased. The presence of these oxygenated species was believed to reduce the fuel auto-ignition resistance. This particular behavior was only observed when running the engine using gasoline and a Primary Reference Fuel blend with an octane number of 87 (PRF 87). Such a trend was not observed when running with isooctane.

2.4.2 Modifying engine operation parameters

Besides modifying the air-fuel mixture, the engine parameters can also be modified to alter the time-temperature history of the intake charge. Several parameters that have been observed previously are compression ratio, engine speed, valve timing, forced induction, and fuel delivery method. Each of these parameters will be discussed further in this section.

Compression Ratio

Compression ratio determines the pressure and temperature of the mixture at the end of compression process. A higher compression ratio corresponds to higher pressure and temperature, which results in advanced ignition timing. Early HCCI studies employed a low compression ratio engine to achieve slower heat release rate. More recently, higher compression ratios have been used to reduce the need for intake charge preheating and to increase the thermal efficiency [17, 20, 21]. Christensen *et al.* [17] used a variable compression ratio engine to investigate the effects of compression ratio on HCCI operation. They found that higher compression ratio does not improve the indicated efficiency as much as expected, due to a decrease in combustion efficiency. The authors also found that higher compression ratio generates higher HC and CO emissions.

In dual-mode engines, high compression ratios can also become problematic when the engine is operating in SI mode. An alternative solution for this problem is to utilize a variable compression ratio; however with current technology, the solution is still not feasible for practical applications

Engine Speed

Engine speed affects the time available for chemical reactions and heat transfer to occur. Higher engine speed corresponds to shorter time available for heat transfer from hot intake charge to the cold cylinder walls, resulting in higher mixture temperature prior to ignition. However, higher engine speed also retards the ignition timing, which occurs because there is less time for the chemical reactions to occur at higher speed. In HCCI combustion, the chemical reactions require a certain amount of time to reach completion.

If there is not enough time available, the combustion process can not reach completion, which results in lower combustion efficiency and high CO and HC emissions.

Variable Valve Timing

Variable Valve Timing (VVT) is a feasible control strategy to vary the amount of internal EGR. The trapped exhaust residual helps increase the mixture temperature in the cylinder, reducing the amount of required intake charge preheating.

The amount of trapped exhaust gases can be varied by adjusting the valve timing. There are two different VVT strategies to implement internal EGR: the sequential and simultaneous method [23]. In the sequential method, the exhaust valve is closed early in the exhaust stroke to trap significant portion of the exhaust gases in the cylinder. This trapped portion will then mixed with fresh intake charge from the following cycle.

In the simultaneous method, the exhaust valves operate normally during the exhaust stroke, expelling most of the exhaust gases to the exhaust port. During the intake stroke, there is a time period where both intake and exhaust valves are opened simultaneously. During this period, a portion of exhaust gases flows back into the cylinder and mix with fresh intake charge.

Forced Induction

Previous HCCI research has shown that utilizing forced induction or supercharging combined with proper intake temperature tuning can increase the maximum attainable IMEP and enlarge the air-fuel ratio range [24]. The main issue with forced induction is that the peak cylinder pressure can become too high which can limit its application in practical situation. The peak pressure issue can be addressed by using combination of EGR and forced induction [24].

Fuel Delivery Method / Charge Stratification

In most HCCI operation, fuel is injected into the intake system some distance away from the cylinder to ensure a complete mixing process. The air-fuel mixture entering the cylinder is assumed to be homogeneous. This particular fuel delivery method is known as premixed fuel injection. In reality, some spatial variations exist in the air-fuel mixture, even after a thorough mixing process [25, 26]. The spatial variations in the air-fuel mixture yield regions with different mixture composition within the cylinder, with some areas richer or leaner than the other. The richer regions tend to burn faster and hotter while generating more NO_x than other regions. Some investigations have been performed to observe the effect of charge stratification on the HCCI engine control and performance.

The most common way to introduce charge stratification into the air-fuel mixture is to change the fuel delivery method by utilizing a fuel injector mounted in the cylinder head to inject fuel directly into the cylinder. This concept is known as direct injection. Based on the fuel injection timing, the direct injection strategy can be divided into two categories, early injection and late injection. In the early injection strategy, fuel is injected into the cylinder early in the compression stroke to allow plenty of mixing time with air. This strategy was introduced in two similar concepts called Premixed Lean Diesel Combustion (PREDIC) [27-29] and Premixed Compression-Ignited (PCI) combustion [30]. Previous investigations found that the engine performance remained the same whether using early direct injection or premixed injection [31, 32].

In the late direct injection strategy, fuel is injected directly into the cylinder later in the compression stroke, close to TDC. It has been shown that this particular strategy is

beneficial in low load operation close to the lean limit [31]. In this operating region, premixed air-fuel mixture combustion typically produces high CO and HC emissions due to incomplete combustion. With the direct fuel injection method, the air-fuel mixture in the cylinder is more spatially stratified with some regions richer than the other. These richer region burns at higher temperature and help increasing the overall cylinder temperature, allowing more complete reactions throughout the cylinder.

Close to the rich limit, a direct fuel injection strategy has negative effects on the engine performance compared to premixed fuel injection. Aroonsrisopon *et al.* [31] found that the engine combustion becomes less stable while producing higher CO and HC. The authors suggested that this detrimental effect results from fuel spray impingement on the relatively cold cylinder wall. Part of the fuel that impinges the cylinder wall becomes to cold to react completely. This fuel fraction leaves the cylinder as unburned HC emissions.

Using a direct injection strategy, Marriott *et al.* [32] were able to partially control the ignition timing, which demonstrated that charge and thermal stratification might be useful in HCCI control.

Another strategy to create spatial heterogeneities in the fuel distribution was demonstrated by Suzuki *et al.* [33] and Odaka *et al.* [34] in a concept called Homogeneous Charge Diesel Combustion (HCDC). In this concept, a premixed charge is created in the intake system and a relatively small amount of fuel is injected directly into the cylinder close to TDC. Using this strategy, the authors were able to control the ignition timing by adjusting the timing and the amount of directly injected fuel. NO_x and

soot emissions were found significantly lower compared to conventional Diesel combustion.

Girard *et al.* [25] performed an experiment to quantify the effects of port fuel injector location on the mixture homogeneity and engine performance. Two fuel injectors were installed in the intake port at different distances from the intake valves. The author used a special probe to measure spatial variation of the fuel in the intake pipe and compared the results of two different injector locations. As expected, the mixture homogeneity improved with longer mixing time and distance. The more homogeneous mixture was found to generate smaller amounts of NO_x, HC, and CO emissions. The effect on engine performance, however, was not as pronounced. Besides a slight change in IMEP, the author did not notice any change in the cylinder pressure phasing or magnitude. This result was confirmed by simulation results that showed mixture homogeneity did not significantly affect the combustion phasing and heat release rate.

Richter *et al.* [26] performed another experiment to investigate the effect of air-fuel mixture spatial variations in HCCI combustion. In this work, one fuel injector was located directly at the cylinder head while the other was installed upstream of a mixing tank in the intake system. The engine was equipped with optical access to allow for Planar Laser Induced Fluorescence (PLIF) imaging of the cylinder. PLIF imaging was used to determine the locations of fuel molecules and OH radicals in the cylinder. The fuel distribution imaging showed more spatial variations when the fuel was directly injected into the cylinder. In contrast, imaging of OH locations for both fuel injectors did not show any obvious trends. Since the presence of OH indicates the start of combustion

location, this result implies that the start of combustion location does not depend on the air-fuel mixture homogeneity.

Iverson [5] employed a similar setup to observe the effects of the fuel delivery method on HCCI performance and emissions characteristics. In this work, air-fuel mixture in-homogeneity was introduced by injecting the fuel directly into the intake manifold about 10 cm upstream of the intake valves. The author found that without any thermal stratification, the overall engine performance remained the same no matter which fuel injectors were used. The only observed effect was a slight increase in NO_x and CO emissions with direct fuel injection, which was attributed to the presence of slightly richer region within the cylinder.

2.5 Optical Diagnostics

Optical diagnostics are one alternative to gain a better understanding of the combustion process. There are several techniques that have been employed in prior HCCI research including Chemiluminescence Spectroscopy [35-38], Absorption Spectroscopy [39], Planar Laser Induced Fluorescence (PLIF) [39-41], and Raman Scattering [39]. Some of these techniques will be reviewed in this section with more emphasis on Chemiluminescence Spectroscopy, as this particular technique is utilized in this work.

2.5.1 Chemiluminescence Spectroscopy

Chemiluminescence is natural light emission from the energy release of chemical reactions. An example of chemiluminescence reaction is shown in Reaction (2-21), where dimethyl sulfide reacts with fluorine to form products while releasing photons [42].

$$CH_3 - S - CH_3 + F_2 \rightarrow \text{products} + h\nu \text{ (light)} \quad (2\text{-}21)$$

Different chemical reactions and species related to the combustion process are known to emit photons at different wavelength; therefore the presence of such species can be detected by analyzing the chemiluminescence spectra. The list of some species related to combustion process along with the corresponding chemiluminescence wavelength is tabulated below in table 2-1 below [43].

Species	Wavelength (nm)
OH	306.4
CH	431.4
C_2	516.5
CHO	311.5, 318.6, 329.8, 337.6
CH_2O	395.2, 422.0 – 424.0

Table 2-1 List of species and emissions wavelengths

Noguchi [19] performed spectroscopic investigation of the chemiluminescence from HCCI combustion process in a two-stroke opposed piston engine. The author found that the species CHO, HO_2, and O were the first to appear during the combustion. As the combustion progress, CH, C_2, and H were detected, followed later by OH.

The same techniques have also been employed in four-stroke HCCI combustion studies. Hultqvist *et al.* [35] were able to obtain time-resolved chemiluminescence spectra during the cool-flame and main heat release period. The work was performed on a modified diesel engine that was equipped with four quartz window to provide optical access to the cylinder. The engine was fueled with a mixture of isooctane and n-heptane which exhibited cool-flame behavior. During the cool-flame period, the spectra showed some structure with distinct peaks. However, during the main heat release period, the

spectra appeared to be continuous from 250 to 550 nm, peaking at around 410 nm. Figure 2-5 shows the spectra of cool-flame and main heat release period [35].

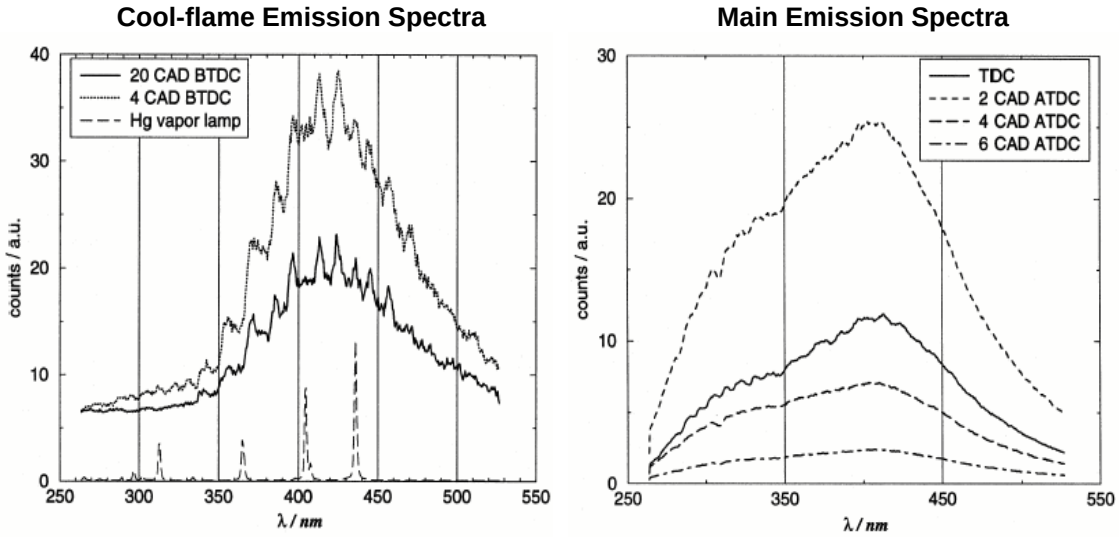

Figure 2-5 Time-resolved chemiluminescence spectra of HCCI combustion [35]

Kawahara *et al.* [36] obtained time-resolved chemiluminescence spectra from HCCI combustion fueled with Dimethyl-Ether (DME). An optical fiber probe was installed in the cylinder head to obtain the luminosity data from the cylinder. The spectra obtained during low temperature reactions showed peaks at 395 nm and 423 nm corresponding to HCHO emissions. During the main heat release period, strong broadband emission was observed between 350 to 550 nm, which was attributed to CO-O oxidation.

Kim *et al.* [38] performed analysis to compare the spectra of HCCI and SI combustion. The authors found noticeable difference between those two cases. During the main heat release period of HCCI, the time-resolved spectra are dominated by CO flame with formaldehyde bands. Peaks corresponding to OH, CH, and C_2 radicals were

not observed. The absence of C_2 in the spectra was attributed to the lack of soot formation in HCCI. In SI combustion spectra, the OH peak was visible throughout the combustion, while CH and C_2 peaks were only visible at the early stage of combustion. The authors also found a strong correlation between CO-O oxidation spectrum and the rate of heat release (ROHR) with the light intensity peak occurring slightly before the peak of ROHR. Figure 2-6 shows the phasing comparison of CO-O oxidation spectrum and ROHR [38].

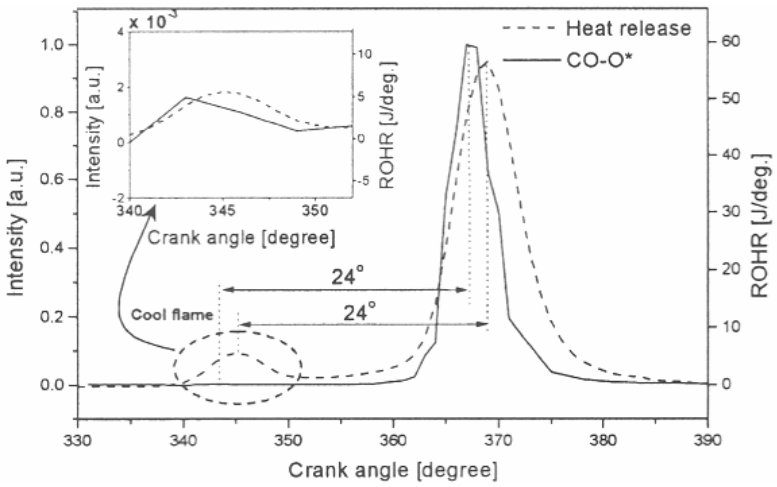

Figure 2-6 Comparison of CO-O spectrum and ROHR [38]

Many prior HCCI studies have employed chemiluminescence spectroscopy technique to gain a better understanding of the chemical reaction sequences during the combustion process. In addition, this technique has been utilized to observe the effects of charge in-homogeneity [37] and to measure local air-fuel ratio [44]. Chemiluminescence spectroscopy is one of the simplest optical diagnostic techniques as it does not require an external light source. The major limitation of this technique is the weak light intensity.

Often, the light intensity is close to the detection limit of the detection equipment, resulting in low signal-to-noise ratio.

2.5.2 Absorption Spectroscopy

Some species related to the combustion process are known to absorb lights at certain wavelengths. This phenomenon is the basis of the absorption spectroscopy technique. The setup of this technique is more involved than chemiluminescence spectroscopy, mainly because of the requirement for an external light source. Typically, a broad-band high intensity light source such as Xenon lamp is suitable for this application. Compared to chemiluminescence spectroscopy, this technique can yield better signal-to-noise ratio depending on the light source used.

Richter *et al*. [39] employed absorption spectroscopy technique to study the effect of different fuels on HCCI combustion. The results showed similar absorption spectra when using methanol, ethanol, or isooctane as the fuel. Distinct absorption features were observed at 310 nm and 284 nm, which correspond to OH radical absorption. When the engine was fueled with a mixture of isooctane and n-heptane, the spectra showed significant absorption in the UV region from about 20 degree bTDC until the start of main heat release, which was attributed to the presence of the cool flame.

2.5.3 Planar Laser Induced Fluorescence (PLIF) Imaging

In the PLIF technique, a laser beam is formed into a sheet by passing it through a certain optical arrangement. The laser sheet is then passed through an optically accessible combustion chamber. Certain species in the cylinder can be excited to a higher energy

state by absorbing the laser beam of appropriate wavelength. The excited species will emit photons at certain wavelength through a process called fluorescence. The resulting image can be captured with a CCD camera for further analysis to determine the spatial distribution of that species within the cylinder. An example of a PLIF experimental setup is shown in Figure 2-7 [39].

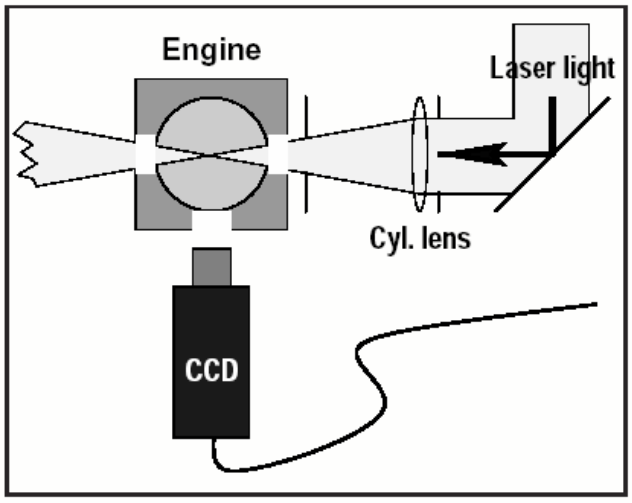

Figure 2-7 PLIF experimental setup example [39]

The PLIF technique is commonly used in HCCI research to study the spatial fuel distribution in the cylinder. Typically, the fuel used in HCCI research does not exhibit fluorescence behavior. Therefore, it is necessary to add a tracer with fluorescence characteristic into the fuel. It is important to make sure that the tracer has very similar properties with the fuel and follows the fuel completely. Richter *et al.* [39] used acetone as a tracer to study the effects of fuel injector location on the spatial fuel distribution within the cylinder. The authors also employed the same technique to determine the location of OH radical formation.

Collin *et al.* [41] employed a PLIF technique to simultaneously measure OH and formaldehyde concentration in an HCCI engine using two different laser sources. The

main challenges with the PLIF technique are the requirement of a high intensity laser source along with complicated optical arrangement to form the laser sheet.

Chapter 3 – Experimental Setup

The laboratory in room B131 ERB is equipped with two test engines, a standard single cylinder engine to study HCCI combustion, and an optically accessible engine for visualization experiments. All of the work presented in this thesis was performed in the standard engine; therefore this section will be focused on the setup of that particular engine and the data acquisition system. Figure 3-1 shows a picture of current standard engine setup.

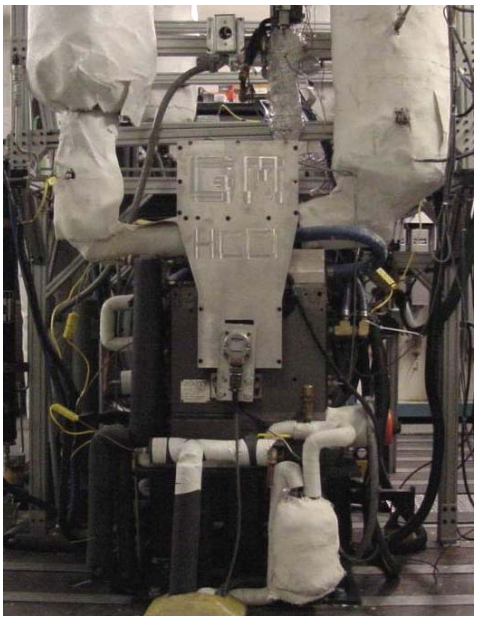

Figure 3-1 Standard engine setup

3.1 Engine System

3.1.1 Research Engine

The standard engine is a single cylinder four-stroke engine built on a Ricardo Hydra block. The cylinder head, which was provided by General Motors Research, was

originally designed for conventional spark ignition engine with port fuel injection. The cylinder head has a belt driven dual overhead camshafts that drive four valves. The engine parameters are listed in table 3-1.

Compression Ratio	10.95:1
Bore	86 mm (3.39 in)
Stroke	94.6 mm (3.72 in)
Displacement	550 cm^3 (33.58 in^3)
Clearance Volume	50.18 cm^3 (3.06 in^3)
Connecting Rod Length	152.5 mm (6.00 in)
Top Land Height	3.6 mm (0.142 in)
Intake Valve Diameter	30.0 mm (1.184 in)
Intake Valve Open	350 deg aTDC
Intake Valve Close	595 deg aTDC
Exhaust Valve Diameter	35.1 mm (1.382 in)
Exhaust Valve Open	131 deg aTDC
Exhaust Valve Close	375 deg aTDC

Table 3-1 Standard engine parameters

Due to possible interference between the piston and the valves, care must be taken in timing the engine to ensure that the piston does not hit the valves.

3.1.2 Coolant System

The engine is water cooled using a closed loop system. The loop consists of a coolant pump, immersion heater, coolant reservoir, cooling tower heat exchanger, and an overflow bottle. The coolant fluid is heated to a certain temperature with an immersion heater before it is circulated into the cylinder head and cylinder liner. From the engine, it

flows into the reservoir and heat exchanger before going back to the pump. Figure 3-2 shows a detailed schematic of the engine cooling system.

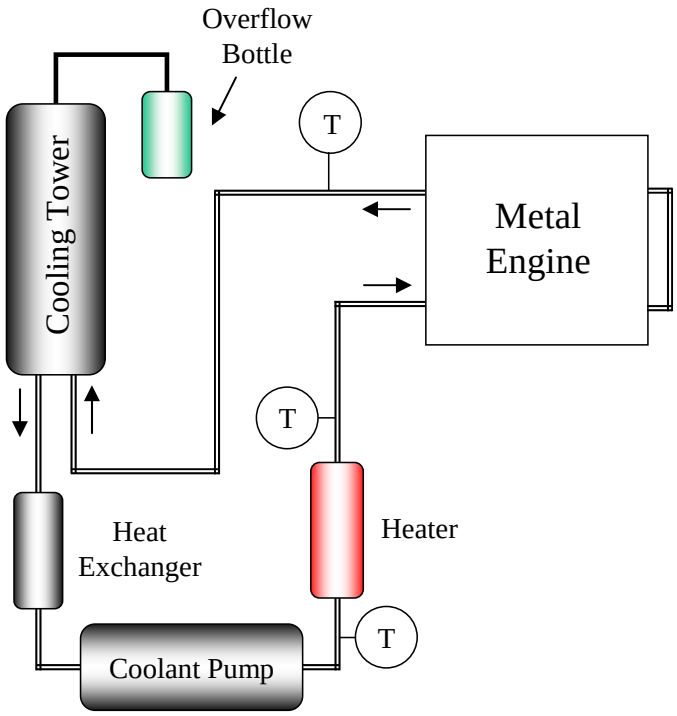

Figure 3-2 Coolant system schematic

A mixture of 50% distilled water and 50% ethylene glycol is used as the coolant fluid. Prior to running the engine, the coolant fluid is circulated through the engine while being heated to warm up the engine components. This helps the engine achieve steady state conditions faster. During engine operation, the coolant temperature is maintained constant at approximately 95°C by cooling it with city water in a cooling tower heat exchanger. The city water flow is regulated by a solenoid valve which is controlled by an Omega i-series dual output temperature controller. The same controller also regulates the power output of the immersion heater. To monitor the actual coolant temperature at the engine, another thermocouple is installed at the coolant line just after it leaves the engine.

During steady state operation, the coolant temperature leaving the engine is always within a range of 93 to 95°C.

The coolant line pressure is regulated using an automotive radiator cap on the reservoir. If the pressure rises above 70 kPa, a relief valve opens to allow coolant flow into the overfill bottle. Once the pressure drops below 70 kPa, the coolant from the overfill bottle is drawn back into the line. All coolant lines are ¾" OD copper tubing except the lines in and out the engine which are 5/8" ID silicone hoses. The heat exchanger is a cooling tower made of low carbon steel pipe with a diameter of 2".

3.1.3 Lubrication

The closed loop lubrication system consists of a gear pump, oil filter, relief valve, heat exchanger, and an immersion heater. The engine block is equipped with an internal oil gallery that supplies oil to the crankshaft and connecting rod bearings, as well as the camshafts in the cylinder head. The oil supply lines are 3/8" stainless steel tubing and the return lines are ¾" copper tubing. A detailed schematic of the engine lubrication system is shown in Figure 3-3.

To heat the oil to operating temperature, a 1000 W immersion heater is installed in the oil sump. Once the oil reaches the operating temperature of 90°C, the temperature is maintained constant using a heat exchanger in the supply line. Both the water flow to the heat exchanger and immersion heater power are controlled by an Omega i-series dual output temperature controller in the same manner as in the coolant system.

The pressure in the oil line is monitored using an Omega PX212 pressure transducer. If the pressure falls below 30 PSIG, the fuel pump and engine ECU power

supply will be cut off to prevent engine damage. An adjustable relief valve is installed in the supply line to allow oil flow into the sump when the oil line pressure rises above 40 PSIG.

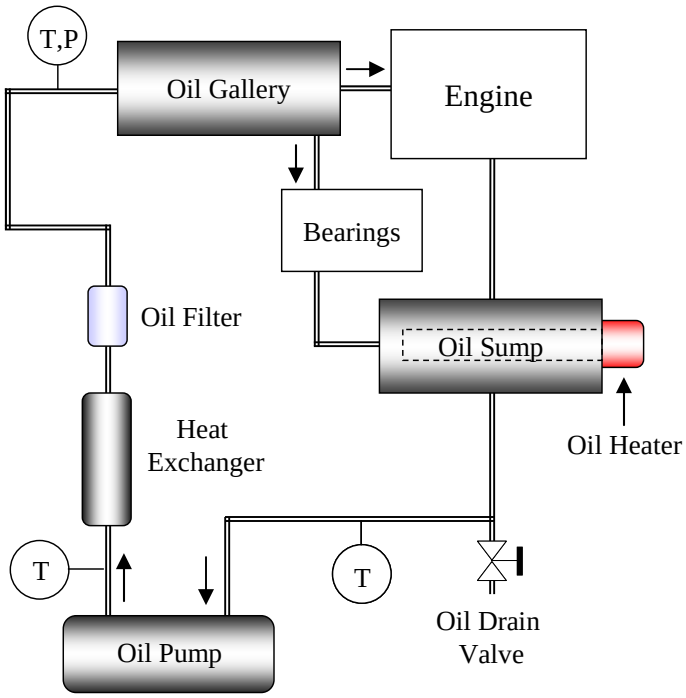

Figure 3-3 Oil system schematic

The oil used in the engine is standard 15W-40 engine oil and the oil filter is made by NAPA with part number 21515. The oil level can be checked through a sight glass mounted to the oil sump. To check the oil level, the oil filler cap needs to be removed to release the vacuum in the oil sump. The minimum and maximum oil level is marked in the sight glass. It is important to maintain the oil level within these limits to prevent damage to the immersion heater and the engine.

3.1.4 Dynamometer

The engine is coupled to a General Electric DC double ended dynamometer with a maximum speed rating of 4000 RPM and capable of providing 74.5 kW (100 HP) load to the engine. The dynamometer can spin in either clockwise or counter-clockwise direction. Due to the engine valve train design, the engine can only operate in clockwise direction; therefore only one engine can be coupled to the dynamometer at a time.

The dynamometer is controlled by Dyne Systems Co. DYN-LOC IV digital control system. The torque generated by the engine is measured using an Omega LC101-2K strain gage load cell which is capable of measuring force up to 8900 N (2000 lbs). Due to the large size of the dynamometer, all brake specific values are close to zero and therefore they will not be considered in this work.

Both the dynamometer shaft and the engine flywheel are equipped with custom metal hubs that allow them to be coupled together using a Falk Wrapflex^{TM} flexible hard rubber coupling. The hard rubber coupler can be removed easily from the metal hubs to allow switching between standard and optical engine. In addition, the compact design of the coupling minimizes the required distance between the engines and dynamometer, thus allowing both engines to be installed in the available laboratory space.

3.2 Air and Fuel Delivery

The air and fuel delivery systems were designed to accommodate flow to both engines with the capability of shutting off the flow to the non-operating engine. All intake and exhaust system components were designed to handle extremely high temperatures required for HCCI operation. It is also very important to make sure that the

air/fuel delivery system is completely sealed from the laboratory environment to prevent any leakage. Air leaks into or out of the system can seriously affect the measurement results and exhaust leaks can be hazardous to the operator. A schematic of air/fuel delivery system can be seen in figure 3-4.

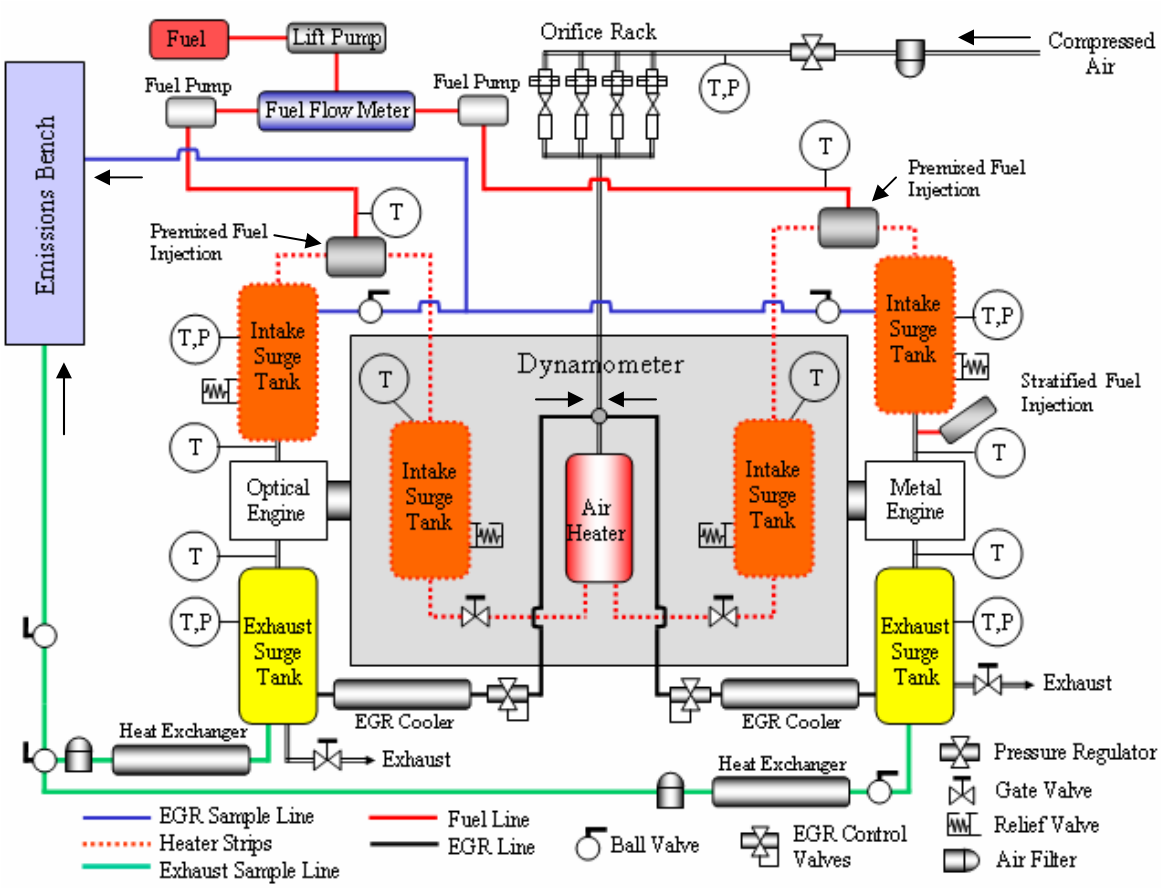

Figure 3-4 Air and Fuel Delivery Schematic

3.2.1 Intake Air

Compressed air at 85 PSIG and room temperature (70°F) is supplied to the laboratory continuously. The air is filtered prior to entering the intake systems and the flow to the engine is regulated by a pressure regulator and a set of calibrated orifices.

There are four orifices installed in the intake system which are selectable depending on the amount of required air flow. The orifice calibration curves are shown in figure 3-5.

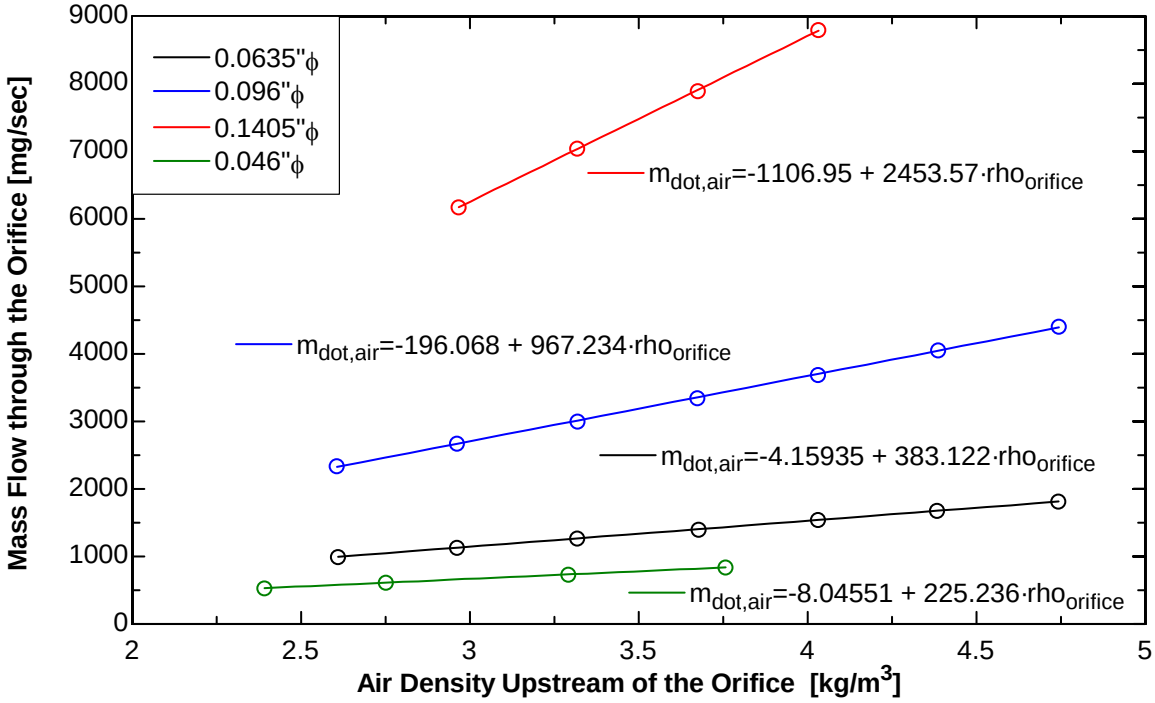

Figure 3-5 Orifice calibration curves

A Newport Micromega CN77000 controller is used to control the orifice upstream pressure by adjusting the signal to a Parker Pneumatics VIP-F pneumatic control board. This pneumatic control board controls a pneumatic pressure regulator. The Newport controller receives a pressure signal from an Omega PX212 pressure transducer. At steady state conditions, the orifice upstream pressure can be maintained within +/- 1 kPa of the set point.

The pressure and temperature measurement upstream of the orifice are essential for air flow rate calculation. The pressure and temperature were measured using a Dresser DXD combination pressure transducer and thermocouple which has higher accuracy compared to Omega PX212 transducer.

From the orifice, fresh air is allowed to mix with EGR from the engine and then flows through an inline heater before entering the first surge tank. When running with premixed fuel injection, fuel is injected into the intake system right after the first surge tank. The air-fuel mixture is allowed to mix completely in the second surge tank prior to entering the engine. Both surge tanks are 37.9 L (10 gal) steel tanks that were installed to damp out the pressure pulses generated during the intake stroke and to facilitate further mixing between fresh air, EGR, and fuel.

For safety reasons, a Kemp FA70-G flame arrestor is installed in the intake system to prevent flame propagation past the first surge tank. A 345 kPa (50 PSI) pop-off valve is installed in each surge tank to release high pressure in the intake system. Another 690 kPa (100 PSI) relief valve is installed in the second surge tank for back-up.

3.2.2 Intake Air Heating

To achieve HCCI combustion with proper phasing, the air-fuel mixture must be preheated to a high temperature prior to entering the cylinder. The fresh air and EGR mixture is initially heated by a Chromolox GCHI 3000 W inline gas heater, which is controlled in an on-off manner with an Omega i-series dual output controller. The main function of this inline heater is to maintain the air in the intake system at a uniform temperature. From the inline gas heater, the mixture flows through heated intake pipes and surge tanks combination. The pipes and tanks were wrapped with six heater strips to heat up the mixture to desired temperature. In addition, two heater strips were wrapped around the intake runner to facilitate fine adjustment of the intake charge temperature

entering the cylinder. The locations of the heater strips are shown in Figure 3-6, and the specifications are listed in Table 3-2.

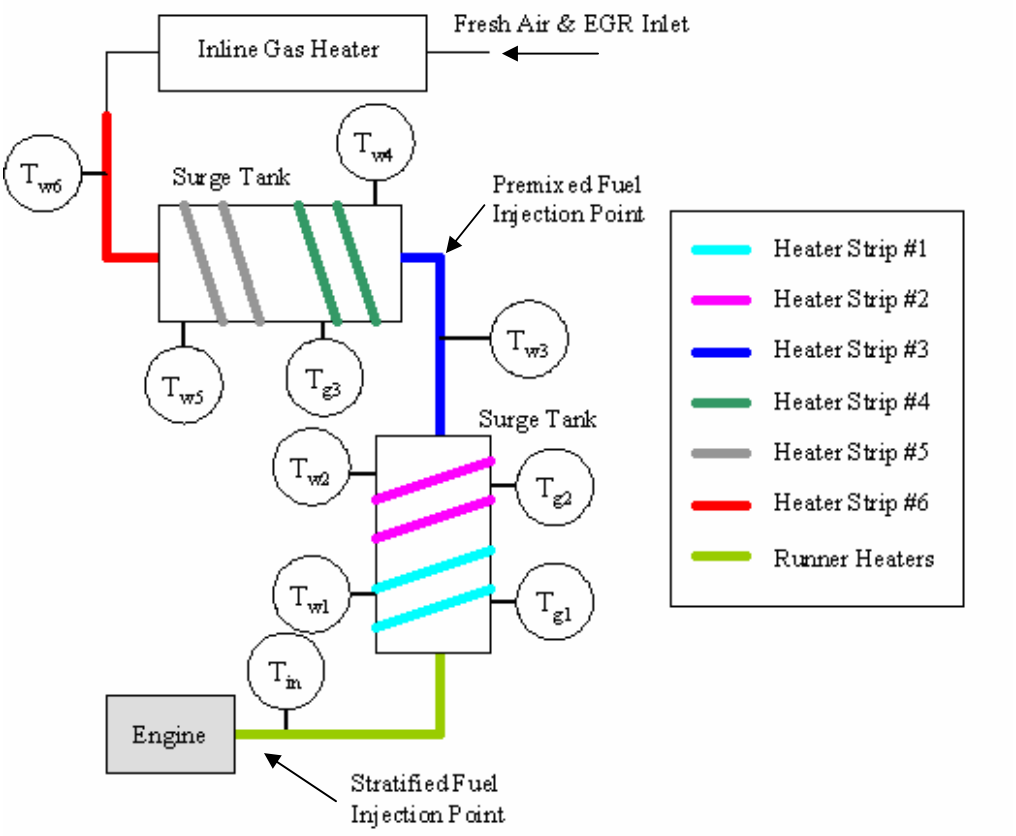

Figure 3-6 Intake Air Heating Diagram

Heater Number	Width (in)	Length (ft)	Power (W)
1	1	8	1256
2	2.5	10	2351
3	2.5	10	2351
4	2.5	10	2351
5	2.5	10	2351
6	1	8	1256
Runner 1	-	8	400
Runner 2	-	8	400

Table 3-2 Heater Strips specification

The intake pipes and surge tanks heater strips are controlled by an Omega CN616 controller. The controller adjusts the power to each heater strip independently based on the input signals received from six thermocouples measuring the intake pipes and surge tanks wall temperatures, denoted T_{w1} – T_{w6} in Figure 3-6. The gas temperatures are also measured at three different points along the flow with thermocouples denoted T_{g1} – T_{g3}. The control system is capable of maintaining a close agreement between the actual gas temperature and the average wall temperature, as shown in Figure 3-7.

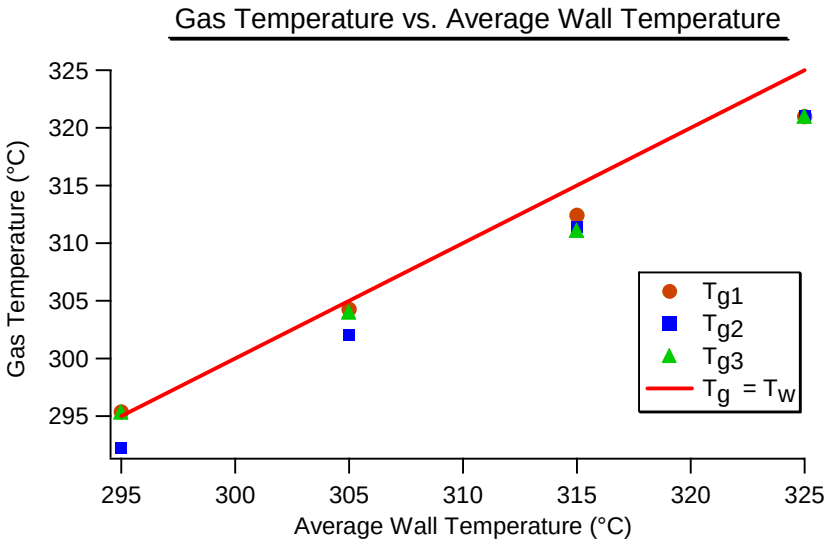

Figure 3-7 Gas temperatures versus average wall temperature

The intake runner heater strips are wired together in parallel and controlled by an Omega i-series temperature controller which receives an input signal from a thermocouple located in the intake runner approximately 10 cm upstream of the intake valves. By adjusting the power of these heater strips, the intake charge temperature leaving the second surge tank can be adjusted 40°C lower or 20°C higher prior to entering the cylinder. The intake heating system control strategy can maintain the intake temperature within 3°C below and 1°C above the set point temperature.

3.2.3 Exhaust Gas

Exhaust gas leaving the engine flows through an exhaust runner to an exhaust diffuser to ensure complete mixing of the exhaust gas components. Part of the exhaust is drawn into the emissions bench, another part flows back into the intake system as EGR, and the rest is drawn by the building exhaust system. A mixing diffuser is installed to ensure that the sample analyzed by the emissions bench is accurate representation of the exhaust gas.

The building exhaust system maintains a constant pressure of 97 kPa absolute (14 PSIA). The pressure can be changed by adjusting the gate valve located in the exhaust line right after the surge tank. For the results presented here, the exhaust pressure was maintained at 97 kPa.

3.2.4 Exhaust Gas Recirculation (EGR)

In HCCI operation, a significant amount of EGR is used to dilute the air-fuel mixture and to slow down the reaction. Part of the exhaust gas is circulated back into the intake system by means of a venturi with an area reduction of 95%. A diagram of the venturi is shown in figure 3-8. Fresh air is inducted into the intake system and accelerated as it flows through the reduced area section. This acceleration process creates lower pressure in that section which draws EGR to mix with the fresh air.

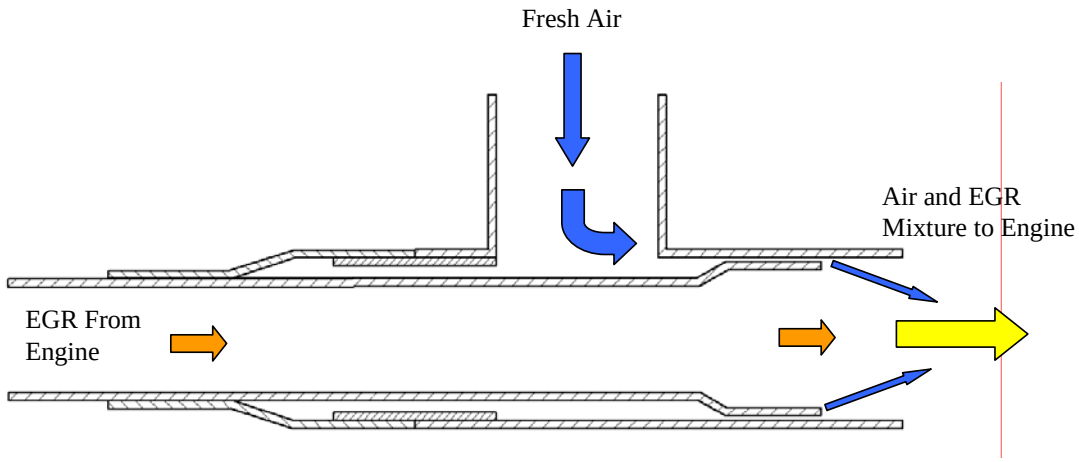

Figure 3-8 EGR Venturi diagram

The exhaust gas is cooled in an EGR cooler prior to entering the intake system to prevent the solder joints in the venturi area from melting. The coolant fluid in the EGR cooler is city water, whose flow is regulated with an Omega i-series controller in the similar manner as in the engine cooling system. The EGR temperature was maintained at 85°C. The mixture of EGR and fresh air then flows through the heated intake system leading to the engine.

The EGR percentage was calculated using equation 3.1. The ambient CO_2 volume fraction is measured in the inlet surge tank prior to running the engine. The volume fraction of CO_2 in the intake and exhaust surge tank is constantly measured by the emissions bench CO_2 analyzers.

$$EGR\% = \frac{CO_{2,In} - CO_{2,amb}}{CO_{2,Exh} - CO_{2,amb}} \times 100 \qquad (3.1)$$

3.2.5 Premixed Fuel Delivery

The fuel delivery system consists of a low pressure pump, high pressure pump, fuel injector, and air assisted injector. The air assisted injection system, which was designed by Mercury Marine, helps atomizing the fuel as it is injected into the intake system. The atomization process helps the fuel to mix with air more effectively. The low pressure fuel pump sends fuel from the fuel tank to a high pressure pump which supplies the fuel to the injector. Fuel is inducted into a cavity inside the injector before it is injected along with small amount of air into the intake air stream. A schematic of fuel delivery system can be seen in figure 3-9.

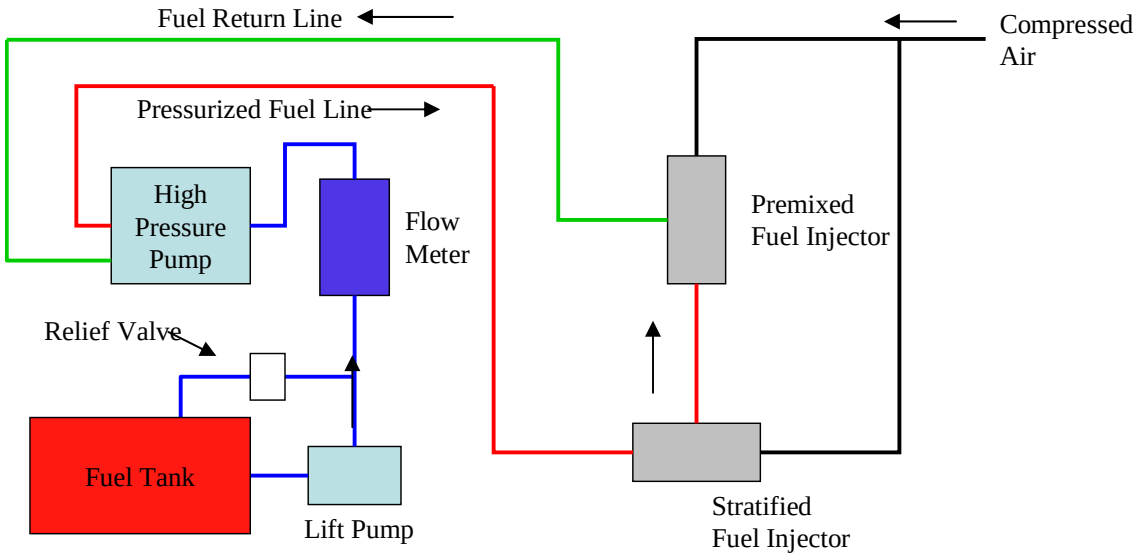

Figure 3-9 Fuel delivery schematic

The high pressure fuel pump actually consists of two separate pumps. A medium pressure pump which draws fuel from the float-controlled reservoir and the actual high pressure pump that sends fuel into the injector. The pressurized fuel line pressure is maintained at 90 PSIG (620.5 kPa) with a differential pressure regulator using the

injector air pressure as the reference. Figure 3-10 shows a schematic of the high pressure fuel pump.

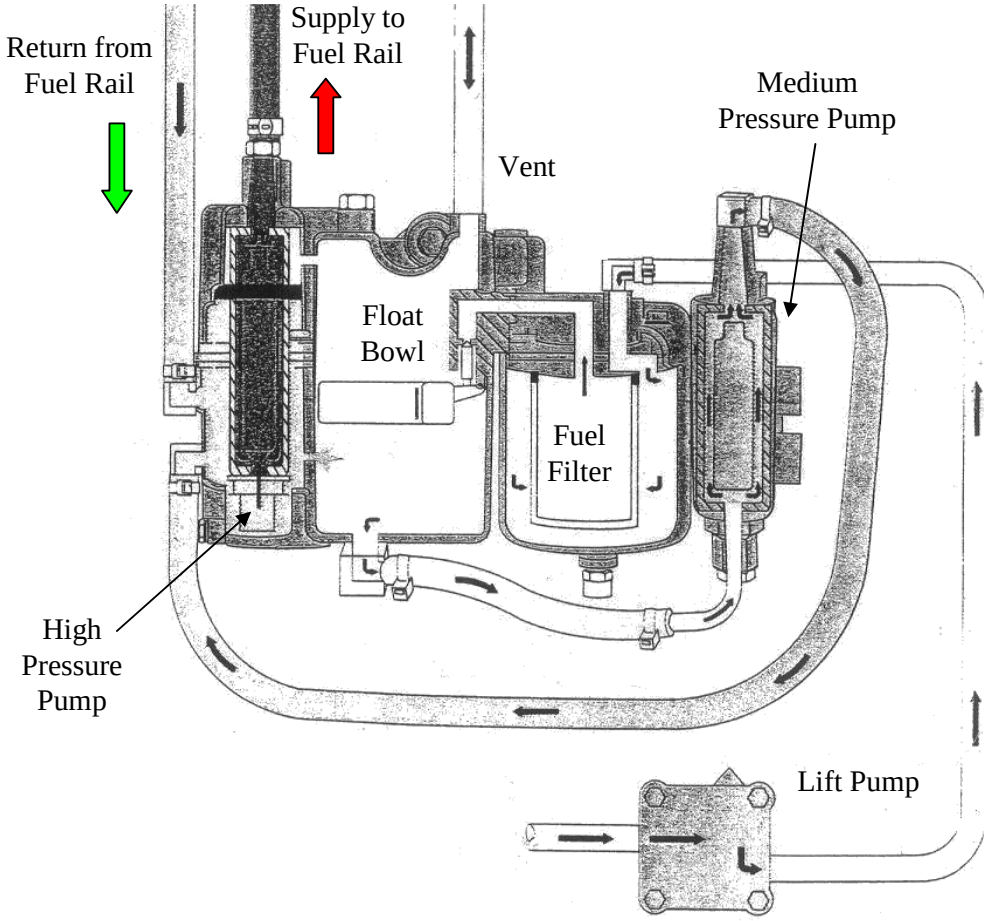

Figure 3-10 Fuel Pump Schematic

The mass flow of air through the air assisted injector was measured using an Omega PMA-A2309 mass flow meter and the value was added to the mass of air flow through the intake system to get the total air flow to the engine.

The low pressure fuel pump is equipped with a return line back to the fuel tank to prevent pressure build up in the fuel line. It is very important to route this return line back into the fuel tank so the fuel is not dumped into the laboratory.

When running the engine with premixed fuel injection, fuel was injected into the intake air stream right after the first surge tank, which is approximately 1.5 meters upstream of the intake valves to ensure formation of homogeneous air-fuel mixture prior to entering the cylinder. The OptiMax air assisted injection system is installed without any modification.

3.2.6 Stratified Fuel Delivery

A stratified fuel injection system was installed to observe the effect of fuel stratification on HCCI operation. The fuel injector was pointed near the intake valve by using a hypodermic tube to achieve a high level of stratification. The stratified injection system uses the same OptiMax air assisted injector as in the premixed fuel injection, but the fuel was injected into a heating chamber before going into the engine. The fuel was heated above the vaporization point, and the fuel flow into the engine was controlled by a Clean Air Partners (CAP) SP501D1 gas phase fuel injector. The injector was originally designed for use in a natural gas-fueled engine and is controlled by a 12-volt modulated signal.

The CAP injector is mounted to an adapter installed in the port injector hole in the cylinder head. The adapter is designed so that the hypodermic tubes are interchangeable. Different tubes can be installed to direct the fuel flow to a specific point in the intake port. A schematic of the stratified injector mounting adapter is shown in figure 3-11.

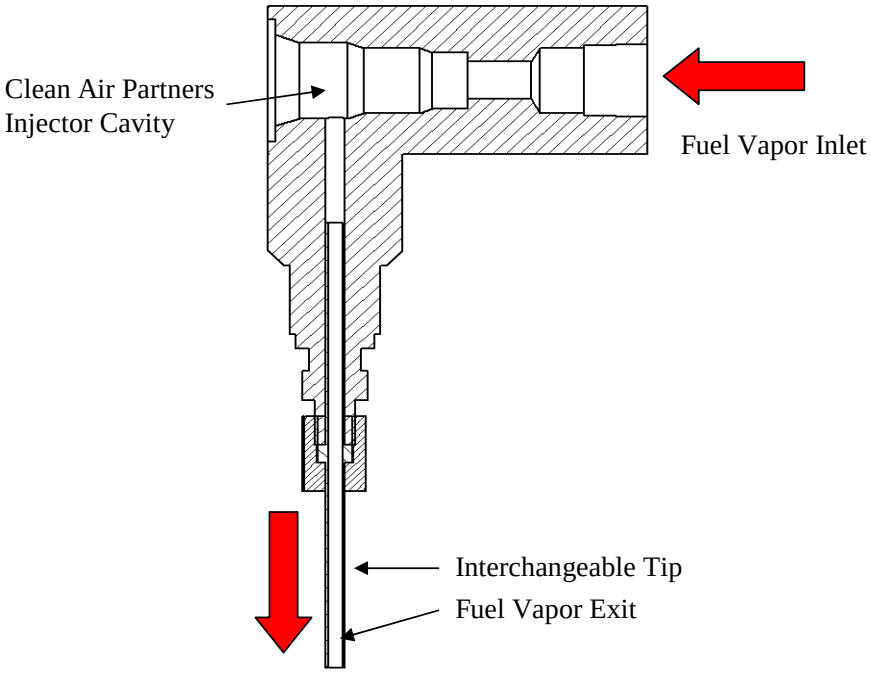

Figure 3-11 Stratified Fuel Injection Mounting Adapter

For safety reason, the amount of air and fuel inside the heating chamber is computer controlled and maintained very rich to prevent combustion inside the chamber.

The heating chamber was designed so that the fuel injected into the engine was at the same temperature as the intake stream, thus eliminating the temperature stratification effect. The heating chamber is wrapped with three 400 W rope heaters controlled by an Omega i-series temperature controller. The pressure inside the heating chamber was maintained constant at 250 kPa to ensure uniform fuel flow using a LabVIEW program that controls the power to the OptiMax air assisted injector upstream of the heating chamber. The pulse width and timing of both the OptiMax injector and CAP injector are controlled by MotoTune software. The CAP injector is actuated in every cycle with fixed timing and pulse width to maintain constant fueling rate. The pressure control strategy was capable of maintaining the heating chamber pressure within +/- 1% variation.

Since the goal of the fuel stratification experiments was to observe the effect of charge stratification without any thermal stratification, it was necessary to make sure that fuel entering the intake port was at the same temperature as the bulk air. It was previously found that with a short hypodermic tube, the fuel enters the intake port at a significantly lower temperature than the bulk air temperature, resulting in thermal stratification. To eliminate this effect, the hypodermic tube design was modified using a shell and tube heat exchanger principle. The idea was to use a longer tube to allow longer residence time of the fuel in the intake runner, allowing heat transfer to equalize the fuel and bulk air temperature. In the current design, the hypodermic tube length was approximately 76 cm (30 in.). It was made of stainless steel tubing with an outer diameter of 3.175 mm (0.125 in.) and an inner diameter of 2.286 mm (0.090 in.). The hypodermic tube was designed to point upstream of the intake runner and then looped back toward one of the intake valves. With this design, the ratio of the fuel injected per cycle volume to the tube volume was approximately 2.3. A schematic of the hypodermic tube design is shown in Figure 3-12. This current design successfully equalizes the fuel and bulk air temperature, thus eliminating thermal stratification.

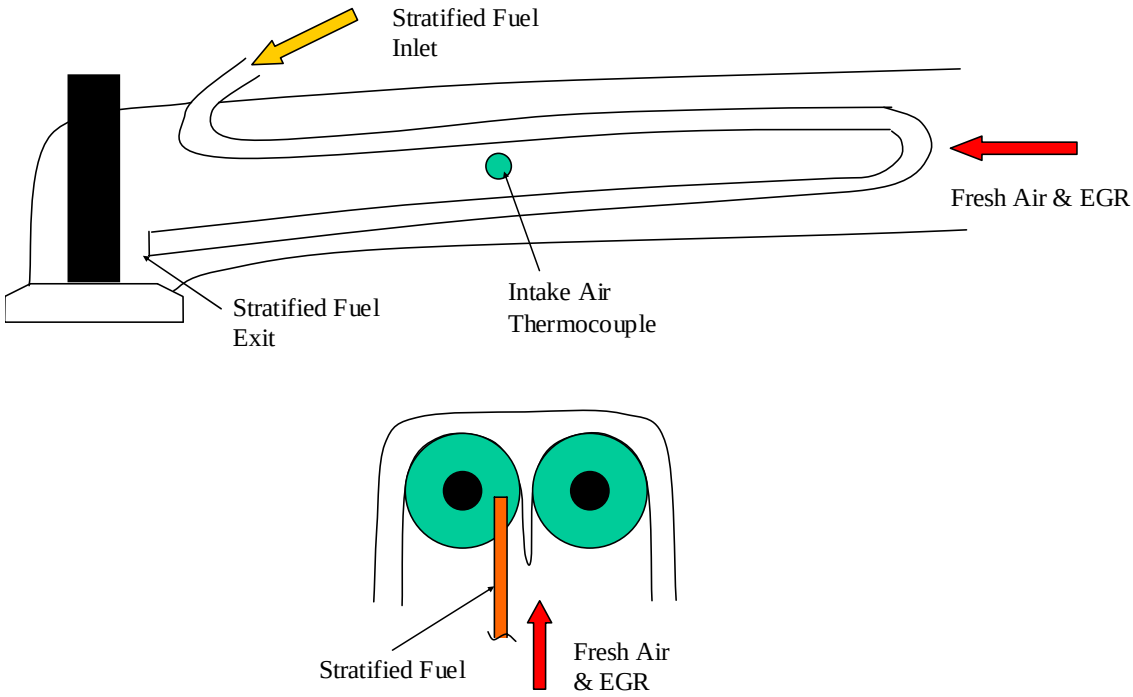

Figure 3-12 Hypodermic tube design

3.2.7 Fuels

The fuels used in this work were pure isooctane with an octane number of 100 and PRF 87, which is a volumetric mixture of 87% isooctane and 13% n-heptane with an octane number of 87. Both isooctane and n-heptane were supplied by Sigma-Aldrich, Inc. PRF 87 was used to examine the effects of intake charge heating in HCCI combustion. The properties of the fuels are listed on table 3-3.

	Isooctane	n-Heptane
Chemical Formula	C_8H_{18}	C_7H_{16}
Chemical Structure	$CH_3C(CH_3)_2CH(CH_3)_2$	$CH_3(CH_2)_5CH_3$
Purity	>99%	>99%
Molecular Weight	114.23 g/mol	100.20 g/mol
Boiling Point	99.2° C	98.5° C
Lower Heating Value	44.5 MJ/kg	44.93 MJ/kg
Specific Heat	2.09 kJ/kg-K[a] (1.59 kJ/kg-K)[b]	2.24 kJ/kh-K[a] (1.61 kJ/kg-K)[b]
Auto Ignition Temperature	418° C	204° C
Minimum Ignition Energy	27.0 mJ	14.5 mJ
Octane Number	100	0

[a] as a liquid at 25° C [b] as a vapor at 25° C

Table 3-3 Fuel Properties

3.3 Controls

3.3.1 Engine Operation Controls

The engine operation was controlled by an ECU developed by Mercury Marine for their OptiMax engine. The ECU is suitable for use in the engine because the fuel delivery system also utilizes the OptiMax system. The engine operating parameters such as injection timing and pulse width can be adjusted while the engine is running. All parameters are adjusted from a computer equipped with MotoTune software that interfaces with the ECU. The system is designed to handle eight different injectors and spark signals independently. The knock index analysis software, stratified injection heating chamber, and the CCD camera also receive triggers from the ECU.

3.3.2 Non Engine Controls

Various engine parameters are monitored and controlled continuously to ensure that the operating conditions are repeatable and consistent. Those parameters are

displayed at a control panel located in the test cell. The controllers used are Omega i-series dual output controllers and Omega CN7700 series controllers. The i-series controllers output are 0-12V proportional DC output and Solid State Relay (SSR) output. The CN7700 controllers have a 4-20 mA proportional output and SSR output. The controllers are wired together in parallel and connected to a computer with RS-485 communication protocol. The data were acquired using LabVIEW data acquisition program. The controlled parameter and its corresponding controller are listed on table 3-4. The parameters read and recorded by the data acquisition program is marked by a * after the communication ID number.

Parameter	**Units**	**Comm. ID#**	**Input Type**	**Output Signal**
Oil Pressure	PSI	0040	Pressure Transducer	SSR - Cutout Relay
Stratified Injector Pressure	kPa	0041*	Pressure Transducer	SSR - Injector Power
Orifice Upstream Temperature	C	0042	Thermocouple	NA
Stratified Injector Temp.	C	0001*	Thermocouple	0-12 V DC - Relay
Oil Temperature	C	0002*	Thermocouple	SSR - Heater
				SSR - Solenoid Valve
Coolant Temperature	C	0003*	Thermocouple	SSR - Heater
				SSR - Solenoid Valve
Intake Air Temperature	C	0004*	Thermocouple	SSR - Heater
Exhaust Surge Tank Pressure	kPa	0005	Pressure Transducer	NA
Orifice Upstream Pressure	kPa	0006	Pressure Transducer	4 - 20 mA - Pneumatic Controller
Fuel Temperature	C	0007	Thermocouple	NA
EGR Temperature	C	0008	Thermocouple	SSR - Solenoid Valve
Heated Line #2 Temperature	C	0009	Thermocouple	SSR
Heated Line #1 Temperature	C	0010	Thermocouple	SSR
General Temperature Reading	C	0011	Thermocouple	NA

Parameter	Units	Comm. ID#	Input Type	Output Signal
Engine Coolant Temperature	C	0012*	Thermocouple	NA
Air Assist Injector Flow Rate	SLPM	0013*	Mass Flow Meter	NA
Exhaust Port Temperature	C	0014*	Thermocouple	NA
Intake Surge Tank Pressure	kPa	0015	Pressure Transducer	NA

*Values read and recorded by LabVIEW data acquisition program

Table 3-4 List of controllers input and output signal

3.4 Data Acquisition and Analysis

3.4.1 Emissions Analyzer

Exhaust gases from the engine are sampled by a Horiba Instruments emissions analyzer which was donated by General Motors Research. Table 3-5 lists the type of emission analyzers and the measured species.

Analyzer Type	Measured Species
Non-Dispersive Infrared (NDIR)	CO & CO_2
Magneto-pneumatic Analyzer (MPA)	O_2
Flame Ionization Detector (FID)	Hydrocarbons
Chemiluminescent Analyzer (CLA)	NO

Table 3-5 List of emissions analyzer and measured species

The emissions analyzer was first calibrated using a Horiba SGR-710C gas divider to ensure accurate exhaust emissions calculation. New calibration curves are used instead of the factory one considering the age of the instrument. At the start of each experiment, the analyzers are zeroed and spanned to the calibration value of the reference gas concentration.

This particular emissions bench is a dry type; therefore water must be condensed out of the exhaust gases prior to entering the analyzers. Exhaust gas flows through a heat exchanger immediately after the exhaust surge tank and the water in the exhaust is separated from the flow using a Parker Corp. Balston Division 33G filter. Inside the emissions bench, the exhaust gas also flows through a chiller bath to ensure complete removal of water. It is important to drain the excess water from the emissions bench often to prevent damage to the instrument.

The output from the emission analyzers are sent to a data acquisition computer and displayed real time along with the calculated air/fuel ratio. For data analysis purposes, the emissions values are collected for 1 minute period and averaged.

3.4.2 Crank Angle Position

The crank angle position is determined by a BEI model H25 optical encoder mounted to the crankshaft. The encoder has a resolution of 720 pulses per revolution, corresponding to one pulse every half degree. The encoder “A” pulse is read by the DSP system to correlate the pressure signal with the engine volume. In addition, there is a “Z” pulse from the encoder to mark the top dead center location. The encoder top dead center signal is aligned with the crankshaft top dead center position using method described in the paper by Lancaster *et al.* [45].

3.4.3 Cylinder Pressure

The cylinder pressure was measured with a Kistler 6125B quartz pressure transducer. The pressure transducer has a ground insulated design which prevents

electrical interference. The measurement range of the transducer is from 0 to 25,000 kPa with an overload pressure of 30,000 kPa. With this particular transducer, thermal shock is not a concern due to the small variation (≤ +/- 2%) in pressure sensitivity over a temperature range of -50 to 350°C. The pressure transducer has a linear response characteristic and the slope of the calibration line is determined with a dead weight pressure tester.

A Kistler 5010B dual mode charge amplifier is used to convert the charge signal from pressure transducer to a voltage signal which can be read by the data acquisition system. During the experiments, the charge amplifier is operated in “Charge Mode” with a transducer sensitivity of 15.5 pC/MU and a scale of 10 MU/V.

From the charge amplifier, the signal is filtered with an 8 kHz low pass filter. This filtered signal is read by the DSP data acquisition system which consists of a model 4012 TRAQ controller module, an 8 channel 12 bit 100 kHz input module, and an 8 mega-samples memory module. The acquired data are analyzed with Redline ACAP v4.0 software which stores engine pressure data as well as calculates other engine parameters including IMEP, COV of IMEP, and peak pressure.

The pressure signal acquired by the cylinder pressure transducer does not give the actual cylinder pressure values. In order to get the actual cylinder pressure values, the DSP system needs a reference or pegging pressure. The reference pressure is determined by reading the intake surge tank pressure and assigning this value as the actual cylinder pressure when the piston is at BDC of the intake stroke. All other pressure values in the engine cycle can be determined from knowledge of the pegging pressure and calibration line slope.

The number of sequential engine cycle data that can be collected is limited by the DSP and computer storage capability. All cylinder pressure data collected in this work were averaged over 500 cycles to minimize cycle-to-cycle variation and obtain good representation of the engine operating conditions.

3.4.4 LabVIEW Data Acquisition Program

The engine control parameters and exhaust emissions are collected and analyzed by a LabVIEW data acquisition program. The signals were acquired using a National Instruments BNC 2090 16 channel input panel and a National Instruments PCI-6014 data acquisition card.

When the program was not recording data, it constantly monitors the engine operating parameters and displays real-time emission values as well as the air-fuel ratio. Every 30 seconds, the program displays averaged values of air flow rate, air-fuel ratio, and fuel flow rate. In addition, the program also displays averaged ringing index value every 50 consecutive cycles. In this mode, the program merely displays the values without recording any of them.

In data recording mode, the program reads and averages 30 consecutive readings from the specified Omega controllers as listed in Table 3-4. At the same time, it also averages the exhaust emission data over 1 minute period. After collecting control parameters and emission data, the program collects cylinder pressure data and analyzes the ringing index of 500 consecutive cycles. The average ringing index as well as the standard deviation is recorded and displayed. The procedure for ringing index calculation is detailed in the next section. Finally, the program averages the fuel flow rate data from

the Max meter over 5 minutes period. All the values are written into a text file which can be analyzed at a later time. It is important to note that the program does not update any real time displays when it is collecting cylinder pressure and fuel flow data, therefore the operator must pay attention particularly to the engine sounds to ensure that the operating condition does not change significantly during data recording period.

3.4.5 Ringing Index Analysis

Certain operating regimes in HCCI operation are characterized by severe cylinder pressure oscillations, very much like knocking behavior in spark ignition engines. In HCCI, this behavior is called ringing. This behavior generates not only irritating noise; at a certain intensity it can cause mechanical damage to the engine. Due to the possible risk of engine damage, it is very important to monitor the ringing intensity and avoid operating the engine at conditions that produces high intensity of ringing. The ringing intensity is characterized by the ringing index, calculated from the cylinder pressure data.

The ringing index calculation is performed by the LabVIEW data acquisition program. The program collects cylinder pressure data within the interval of 30 deg bTDC to 100 deg aTDC. The voltage signal from the charge amplifier is filtered with a band pass filter with high and low pass cutoff frequency setting of 6.3 kHz. The signal is multiplied by a factor of 500, and the program looks for a point with largest pressure oscillation. Ringing index is defined as the difference between the highest and lowest voltage values at that point. In data recording mode, the program calculates ringing index from 500 consecutive cycles and displays the average.

In determining the acceptable operating window, the upper limit of ringing index is set at 8 V, which corresponds to a peak-to-peak pressure variation of 16 kPa. If the ringing index rises above 12 V, the data acquisition program displays a warning message to alert the operator of potential problem.

3.4.6 Fuel Flow Measurement

The fuel flow to the engine can be calculated from the exhaust emission data. However, leakage in the air-fuel delivery system can seriously affect the emission values. To obtain physical measurement of the fuel volumetric flow rate, a Max Machinery Co. model 284 512 flow meter was installed in the fuel line. This flow meter is a positive displacement meter with very small displacement volume to ensure accuracy in small flow rate measurement.

The OptiMax fuel delivery system utilizes a fuel return line and float bowl in the high pressure pump which causes pulsations in the fuel flow. The flow meter always measure positive volume no matter which direction the fuel is flowing, therefore it is necessary to prevent reverse flow through the meter. Check valves were installed in the fuel lines for that purpose. To improve the measurement accuracy, the fuel flow rate data are collected over 5 minutes period and averaged to minimize the effects of pulsating flow.

It is also important to make sure that the fuel flow rate from the exhaust emissions calculation agrees with the flow meter measurement within acceptable error. Significant difference between those two values indicates potential leakage or other problems. The

procedure for calculating the air-fuel ratio from the exhaust emissions data is listed in Appendix B.1.

3.5 Optical Detection Equipment

The setup for the light emission detection experiments consists of an imaging spectrograph, CCD camera, optical fiber, and a desktop computer. The optical fiber transmits lights from the engine cylinder to the spectrograph and CCD camera. The desktop computer controls the operation of the spectrograph and the CCD camera, as well as stores the data for further analysis. Each of these instruments will be discussed in this section. A schematic of the current equipment setup is shown in Figure 3-13.

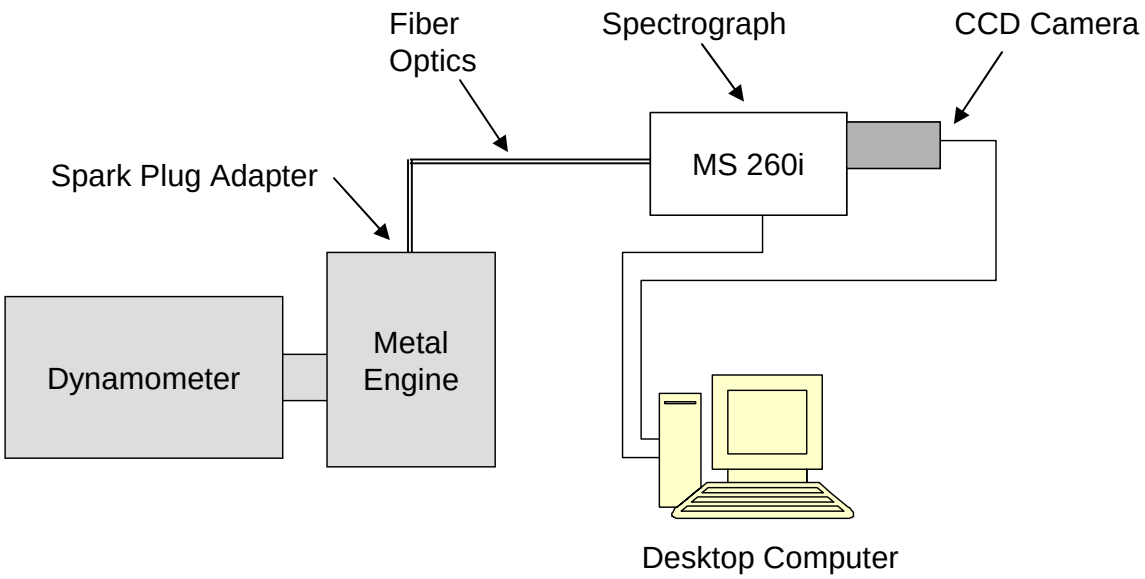

Figure 3-13 Chemiluminescence detection equipment setup

3.5.1 Imaging Spectrograph

An imaging spectrograph was used to separate the light collected from the engine into its component wavelengths. The resulting spectra were captured by a CCD camera and further analyzed to determine which chemical species exists at different stages of the combustion process. The spectrograph used in this work was an Oriel MS260i 1/4m imaging spectrograph with an input F/# of 3.9 and unequal input and exit focal lengths of 220 and 257 mm, respectively. An image of the input slit is projected at the output plane by a set of computer optimized toroidal mirrors with 1.1 horizontal and 1.6 vertical magnifications. The optical configuration of the imaging spectrograph is shown in Figure 3-14.

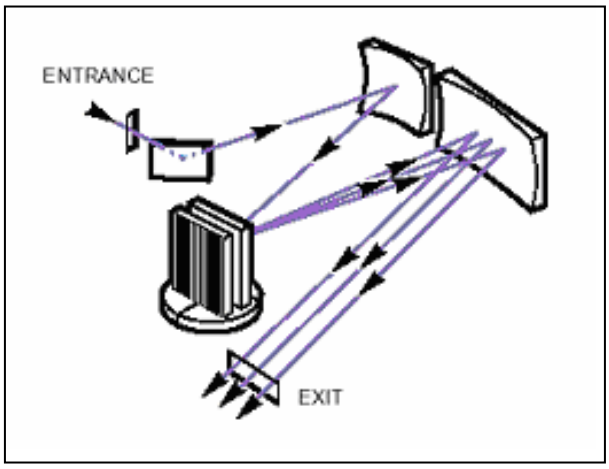

Figure 3-14 Spectrograph Optical Configuration

The spectrograph is equipped with two different, interchangeable gratings. Gratings selection and position are controlled through a computer. The gratings specifications are listed in Table 3-6.

Line Density (l/mm)	Blaze Wavelength (nm)	Peak Efficiency (%)	Spectral Resolution (nm)	Bandpass (nm)	Wavelength Region (nm)	Model
600	400	85	0.5	165	250-1300	74166
300	500	80	0.98	325	250-1150	74172

Table 3-6 Grating Specifications

A fast kinetics fiber optic adapter was installed in the spectrograph input to enable data acquisition in fast kinetics mode. In fast kinetics mode, light is incident only on a few rows at the upper part of the CCD while leaving most of the CCD area un-illuminated. The un-illuminated part of the CCD is used as temporary storage of spectra. Fast kinetics mode enables very fast exposure times, on the order of microseconds.

The grating and spectrograph were calibrated by the manufacturer and the calibration was checked using a Mercury Argon spectral calibration lamp to ensure the accuracy.

3.5.2 CCD and Controller Card

The CCD used in this work was a 512x512 pixel CCD made by Andor Technology. Each pixel has a dimension of 13 micron x 13 micron. The CCD was positioned at the output port of the spectrograph and attached directly with a built-in mounting flange. It was connected to a PCI controller card in a desktop computer which controls the camera and spectrograph operation. The controller card was also supplied by Andor Technology and the model number is CCI-010 PCI. The controller card has a digitization rate of 1 MHz with minimum readout time of 1 microsecond per pixel. The fast readout rate of the CCD and controller card allows measurement in fast kinetics

mode to capture images at a very high rate. All functions of the CCD and spectrograph are controlled through the supplied Andor MCD software.

In order to minimize dark noise, the CCD is equipped with a high performance cooling system capable of cooling the CCD to –45°C. Further reduction in temperature is possible using an external power supply unit or external water source. A plot of the CCD dark current value as a function of temperature can be seen in Figure 3-15.

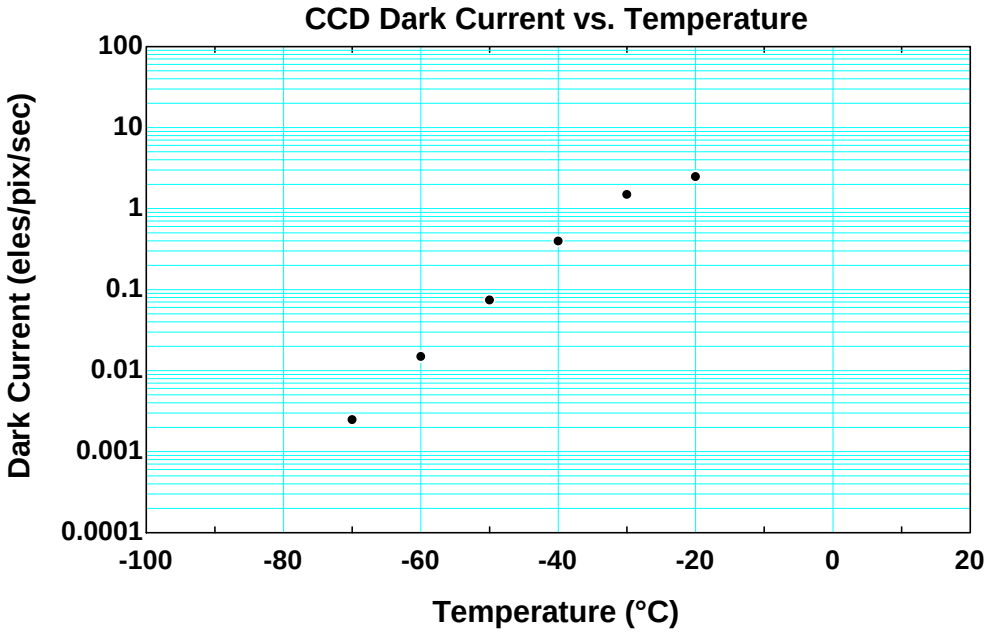

Figure 3-15 CCD dark current as a function of CCD temperature

3.5.3 Calibration Lamps

To ensure proper calibration of the spectrograph, an Oriel 6035 Hg(Ar) spectral calibration lamp was used. The lamp has distinct peaks at several wavelength values ranging from UV to visible. Table 3-7 lists the calibration wavelength and the irradiance at a distance of 25 cm.

Wavelength (nm)	Irradiance at 25 cm ($\mu W\ cm^{-2}$)
253.65	74.0
296.73	0.65
312.57	0.71
365.02	1.35
404.66	1.12
435.83	2.55
546.07	2.56
576.96	0.28
579.07	0.30

Table 3-7 Spectral calibration lamp wavelengths

The Hg(Ar) calibration lamp is powered by a DC power supply to ensure constant light intensity throughout the whole calibration process. The spectral calibration lamp is mounted in a fiber optic adapter with an SMA mount and the emitted light is transferred to the spectrograph using an UV-VIS optical fiber.

A Quartz Tungsten Halogen (QTH) lamp was used as a broadband light source to correct for the spectrograph and CCD camera sensitivity with wavelength. The QTH lamp was mounted inside a housing equipped with a collimating lens assembly. The collimated light was then focused into a fiber using a fiber optic focusing assembly.

The overall shape of the measured spectrum was compared to the published spectrum from the lamp manufacturer. A correction factor for each wavelength was then established to match the shape of the obtained spectrum to the actual spectrum. Figure 3-16 shows the light spectrum of the QTH lamp.

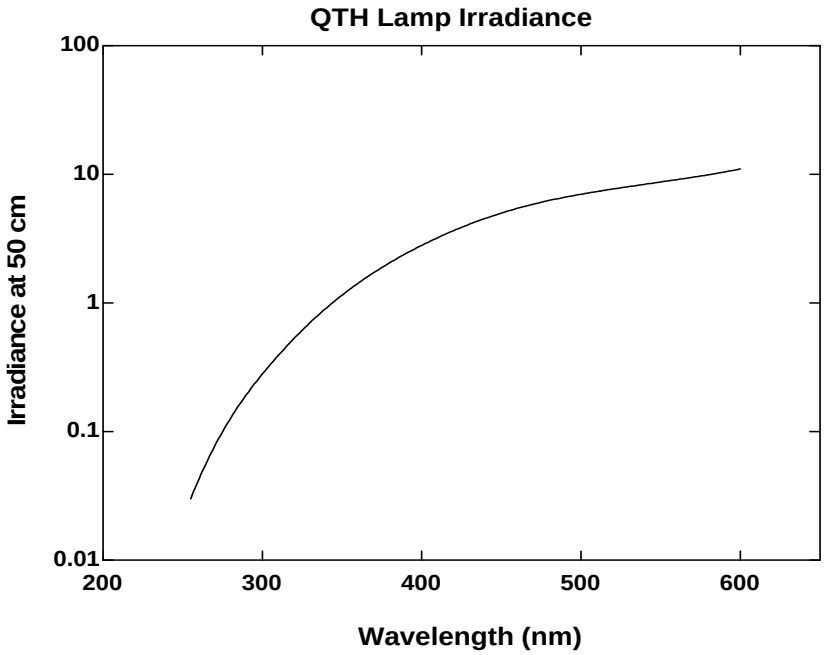

Figure 3-16 QTH lamp irradiance spectrum

3.5.4 Optical Fibers

For wavelength calibration purposes, a 2 meter section of fused silica optical fiber was used. The fiber has a numerical aperture (NA) of 0.22 and core diameter of 50 micron. Both ends are terminated with an SMA connector from the manufacturer. The high OH silica in the fiber is capable of transferring light from UV to visible (250 to 800 nm).

Optical access to the cylinder is required to collect the light emitted during combustion process. The spark plug hole was chosen as the best alternative to gain access to the cylinder for several reasons: the spark plug is not used in HCCI operation and the hole could be used as it is without further modification to the engine. In addition, the spark plug hole location is easily accessible, which facilitate easy fiber installation and removal.

A custom adapter was made to hold the optical fiber in place while maintaining the cylinder sealing. The adapter was made of stainless steel and threaded on the outside to fit into the spark plug hole. The fiber is attached permanently with epoxy in the center of the adapter. A drawing of the custom adapter is shown in Figure 3-17. The spark plug hole is located in the center of the cylinder and the fiber collects light from a cone-shaped volume in the center of the cylinder. When the piston is at TDC, the cone base diameter is approximately 3.3 mm. Figure 3-18 shows the location of the fiber optic adapter relative to the cylinder head and piston at top dead center.

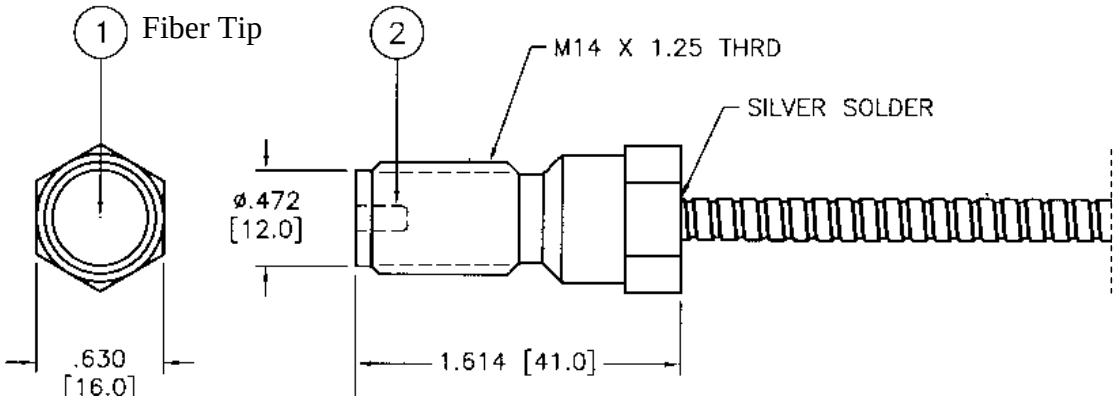

Figure 3-17 Custom fiber optics adapter

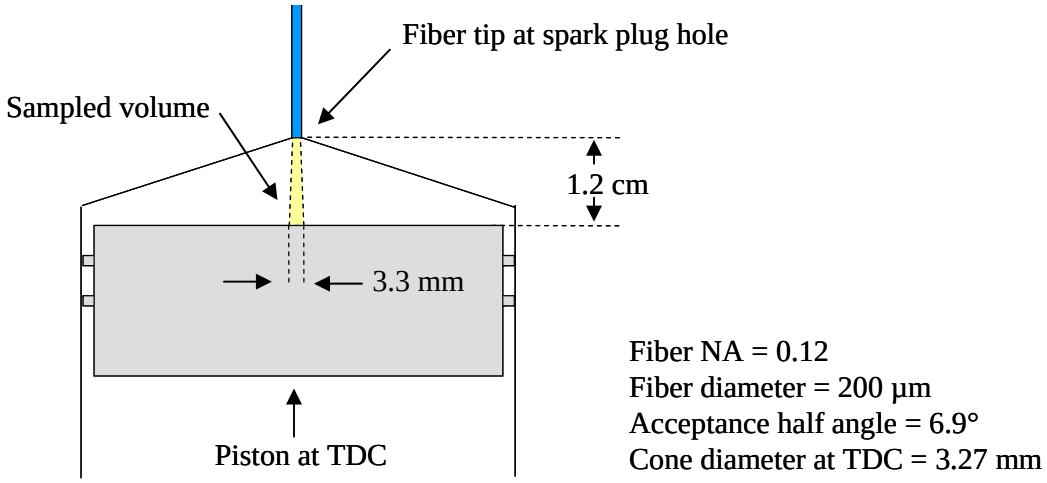

Figure 3-18 Fiber position schematic

Since the optical fiber is continuously exposed to the high temperature and pressure of the combustion chamber, it was important to choose a fiber that could withstand that environment. In addition, the size and numerical aperture of the fiber must be properly matched to the spectrograph and CCD. The fiber used in this work was Fiberguide Industries Superguide MG Fiber which transmits light from 180 to 1100 nm. The fiber has a core diameter of 200 µm and numerical aperture of 0.12 which matches the numerical aperture of the spectrograph. The fiber buffer material is aluminum with a temperature rating of 400°C continuous exposure. To further protect the fiber from the environment, it was wrapped in a flexible stainless steel material. The other end of the fiber was equipped with an SMA adapter that attaches directly to the spectrograph input. The fiber was removed from the engine for cleaning after a few days of running to ensure adequate light transmission and data consistency. The fiber manufacturer suggested cleaning the fiber tip with isopropyl alcohol and cotton swabs, but this method was not adequate to clean the deposits left in the fiber tip. A proper cleaning procedure involved

machine polishing the fiber tip with Colloidal Alumina polishing compound with particle size range from 50 to 70 nm and non-abrasive nylon polishing cloth.

Chapter 4 – Experimental Conditions

4.1 Experimental Parameters and Operating Conditions

The different engine parameters can be categorized into two general types, fixed parameters and variable parameters. Each of these parameters will be detailed in the following section.

4.1.1 Fixed Experimental Parameters

Several engine parameters were held constant throughout the experiments. These parameters are intake pressure, exhaust pressure, coolant temperature, oil temperature, and engine speed. These constant parameters are listed in Table 4-1.

Intake Pressure	97 kPa
Exhaust Pressure	100 kPa
Coolant Temperature	95°C
Oil Temperature	90°C
Engine Speed	1000 RPM

Table 4-1 Constant Engine Parameters

Intake Pressure

The intake pressure was maintained constant at a value close to atmospheric pressure in order to simulate a normally aspirated, wide open throttle condition. This condition was chosen to obtain the maximum efficiency benefit of running un-throttled. A constant intake pressure also eliminates the effects of pressure variation in the

chemical kinetics. The intake system components are properly sealed to prevent leakage in and out of the system.

Exhaust Pressure

The exhaust pressure was maintained constant at a slightly higher pressure than the intake system and building exhaust to allow for exhaust gases flow into the building exhaust and EGR system.

Coolant and Oil Temperature

The coolant and oil temperatures were maintained constant throughout the experiments to avoid variations in the cylinder head and wall temperatures. Variations in these temperatures can affect the thermal gradient and boundary layer thickness in the cylinder, which can alter the engine performance. The coolant and oil systems are equipped with electronically controlled heaters and heat exchangers which allow precise control of the fluid temperatures. More information about the coolant and oil temperature control strategy can be found on Section 3.1.2 and 3.1.3.

Engine Speed

The engine speed and load are controlled by a dynamometer. For all the results presented in this thesis, the engine speed was maintained constant at 1000 RPM.

4.1.2 Variable Experimental Parameters

Several engine parameters were varied to observe their effects on the engine performance and the light emission characteristics. Each variable parameter was varied while maintaining all other parameters constant to isolate the effects of that particular parameter.

The main variable parameter was the intake charge temperature, which was measured by a thermocouple located in the intake runner about 10 cm upstream of the intake valves. The temperature measurement is assumed to be the temperature of the intake charge as it enters the cylinder. This temperature can be adjusted by the operator through an electronic controller. Prior studies have showed that HCCI combustion timing and heat release rate is very dependent on the intake charge temperature.

Other variable parameters investigated in this work were fuel delivery method, fueling rate, air-fuel ratio, fuel type, and intake system upstream temperatures.

4.1.3 Dependent Parameter

The EGR percentage is a dependent parameter driven by the intake system temperature. The EGR system was designed to allow exhaust gas flow into the intake system to maintain a constant intake pressure of 97 kPa. The EGR was introduced into the intake system through a venturi, as described in Section 3.2.4. As the intake air temperature increased, the fresh air volume expands, and less EGR is inducted into the intake system. With a fuel flow rate of 10 mg/cycle and an air-fuel ratio of 20:1, the EGR rate was typically in the range of 35 to 40 percent.

4.1.4 Operating Window Definition

The engine operating window was defined as the range of intake temperatures that resulted in a ringing index less than 8.0 V and COV of IMEP less than 3%. The lower temperature limit was chosen to match the criterion used by General Motors in determining engine drivability. At COV greater than 3%, the combustion variation is

noticeable by the engine operator. If the intake temperature was decreased below the lower limit, the COV increased significantly.

The upper limit of ringing index was defined from previous experience by running the engine and monitoring the combustion noise. The cutoff value of 8.0 V is defined as the maximum ringing index at which the engine can be operated safely. Running the engine at high ringing index for a long period of time should be avoided to prevent engine damage. If the ringing index increases beyond 12.0 V, a warning message is displayed in the data acquisition program to alert the operator of potential problems.

4.2. Experimental Matrices

Four experimental matrices were established to observe the effects of different engine parameters on the engine performance and light emission characteristics. The operating conditions of each matrix are presented in this section

4.2.1 Matrix #1 Intake Charge Temperature

This experimental matrix was performed to observe the effects of different intake charge temperature on the emission spectra from the combustion process. For this data set, the fuel was injected upstream of the intake system. The data points were chosen at three different locations, two points close to each end of the operating window, and another point in the middle of the operating window. The details of this matrix are shown in Table 4-2.

Fuel Type	Isooctane
Fueling Rate	10 mg/cycle
Air-Fuel Ratio	20:1
Fuel Injection Type	Premixed
Engine Speed	1000 RPM
Intake Temperature	Variable

Table 4-2 Experimental Matrix #1

4.2.2 Matrix #2 Fuel Delivery Method

This data set was established to evaluate the effects of different fuel delivery methods on the emission spectra. In order to do this experiment, two fuel injectors were installed at different locations and the engine was run at operating conditions that result in similar operating conditions with both fuel injectors. The experimental matrix of this data set is shown in Table 4-3.

Fuel Type	Isooctane	
Fueling Rate	10 mg/cycle	
Air-Fuel Ratio	20:1	
Fuel Injection Type	Premixed	Stratified
Engine Speed	1000 RPM	
Intake Temperature	313°C and 320°C	

Table 4-3 Experimental Matrix #2

4.2.3 Matrix #3 Fueling Rate and Air-Fuel Ratio

Previous work on this engine found the combustion at lower fueling rate can be improved by increasing the air-fuel ratio. The purpose of this data set was to obtain and compare chemiluminescence spectra with lower fueling ratea at different air-fuel ratios. The intake temperature was fixed at 365°C for all three conditions to eliminate the effect of intake temperature. In addition, a comparison was also made with the higher fueling rate case. The experiment matrix for this data set is shown in Table 4-4.

Fuel Type	Isooctane			
Fueling Rate	5 mg/cycle			10 mg/cycle
Air-Fuel Ratio	20:1	25:1	30:1	20:1
Intake Temperature	365°C			320°C
Fuel Injection Type	Premixed			
Engine Speed	1000 RPM			

Table 4-4 Experimental Matrix #3

4.2.4 Matrix #4 Intake Charge Preheating (Fuel Reformation)

In the intake system, the air-fuel mixture is exposed to extremely high temperatures above 250°C. With a residence time of approximately 9 seconds, it is possible that the fuel undergoes some low temperature reaction in the intake system, which means that the fuel entering the cylinder could have been isomerized or partially reacted.

Previous work in this engine found that the engine operating window shifted depending on the upstream intake temperatures when running the engine with PRF 87 or gasoline. Such behavior was not observed when fueling with isooctane. Further analysis of the intake charge samples with GC Mass Spectroscopy showed an increasing concentration of certain oxygenated species with increasing upstream intake temperatures. These species were thought to be the result of low temperature reactions in the intake system, which very likely affects the fuel auto-ignition resistance.

The objective of this experiment was to observe the effects of intake charge preheating on the chemiluminescence spectra. The setup of the intake heating system, as shown in Figure 4-1, allows for independent control of each heater strip temperature. In this experiment, the heater strips (#1 - #6) were adjusted so that all the wall temperatures and gas temperatures ($T_{w1} - T_{w6,}$ $T_{g1} - T_{g3}$) are equal. This temperature is denoted T_{up}. The intake charge temperature entering the cylinder (T_{in}) can be adjusted to be lower or higher than T_{up} by manipulating the power to the intake runner heater strips.

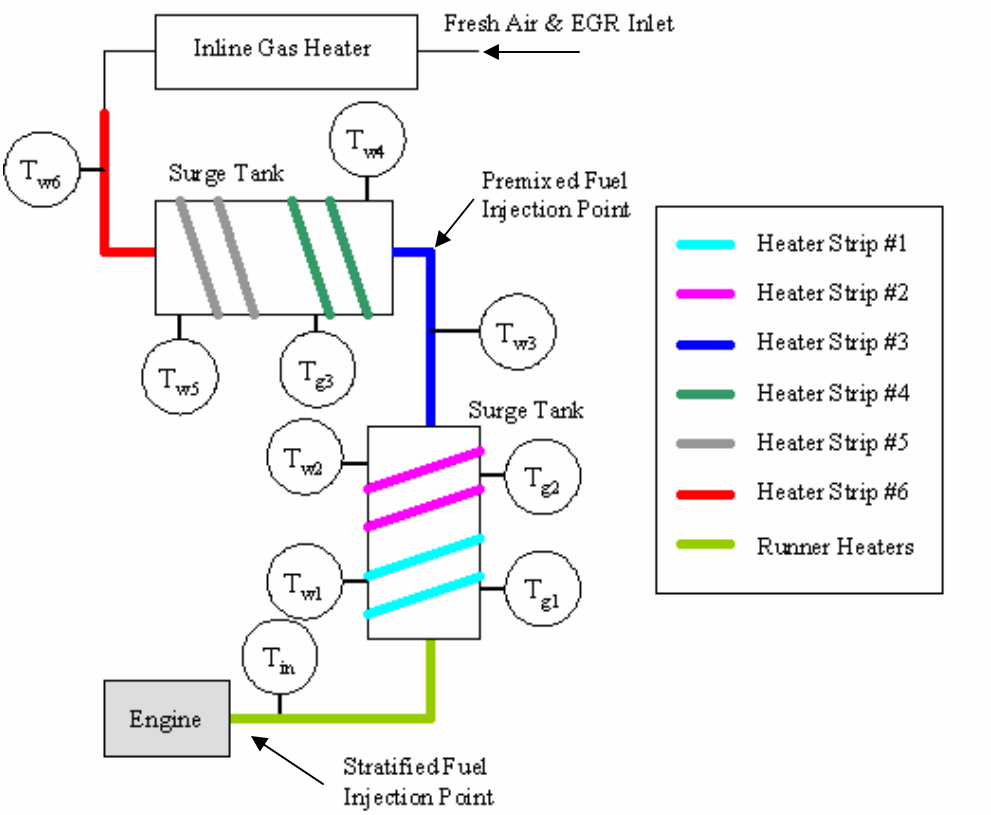

Figure 4-1 Intake Air Heating Diagram

Since similar behavior had been observed whether running the engine with PRF 87 or gasoline, the experiment was only performed with PRF 87. The data points were chosen to make two different comparisons. The first comparison is between the data point with highest upstream temperature and lowest possible intake temperature (Test #1) to the data point with lowest upstream temperature and highest possible intake temperature (Test #2). The second comparison is between Test #2 and Test #3 which had different upstream and intake temperature, but similar combustion phasing and heat release rate. The experiment matrix of this data set is shown in Table 4-5.

Fuel Type	PRF 87		
Fueling Rate	10 mg/cycle		
Air-Fuel Ratio	20:1		
Fuel Injection Type	Premixed		
Engine Speed	1000 RPM		
Test Number	1	2	3
Upstream Temperatures (T_{up})	295°C	270°C	285°C
Intake Temperature (T_{in})	260°C	297°C	285°C

Table 4-5 Experimental Matrix #4

Chapter 5 – Experimental Results and Discussion

Experimental results are presented in this chapter in the form of time-resolved chemiluminescence spectra obtained under various operating conditions. Each spectrum corresponds to a period of 400 μs or 2.4 CAD. The first section of this chapter is focused on the calibration of the spectrograph and CCD camera. The experimental results are presented in the later sections.

5.1 Spectrograph Wavelength Calibration

As already mentioned in Section 3.5.1, the purpose of the spectrograph is to split the incoming light into its component wavelength. The main component of the spectrograph is the grating, which can be moved to cover different ranges of wavelengths. The resulting light spectrum is captured by a CCD camera for further analysis.

In order to determine the actual wavelengths of the light spectrum, the spectrograph and CCD camera need to be calibrated. A Mercury Argon (Hg-Ar) spectral calibration lamp with several distinct peaks in the range of 250 – 550 nm was used for that purpose. The calibration lamp was attached to a fiber optic adapter and the light spectrum was captured by the CCD camera. The peaks in the spectrum were then assigned specific wavelength values corresponding to the calibration lamp specification. Based on this information, the CCD controller software automatically determined the wavelength values of the other pixels in the camera. The same procedure was repeated

for different grating positions to cover all the wavelength range of interest. Figure 5-1 shows the light spectrum of the calibration lamp for different grating positions.

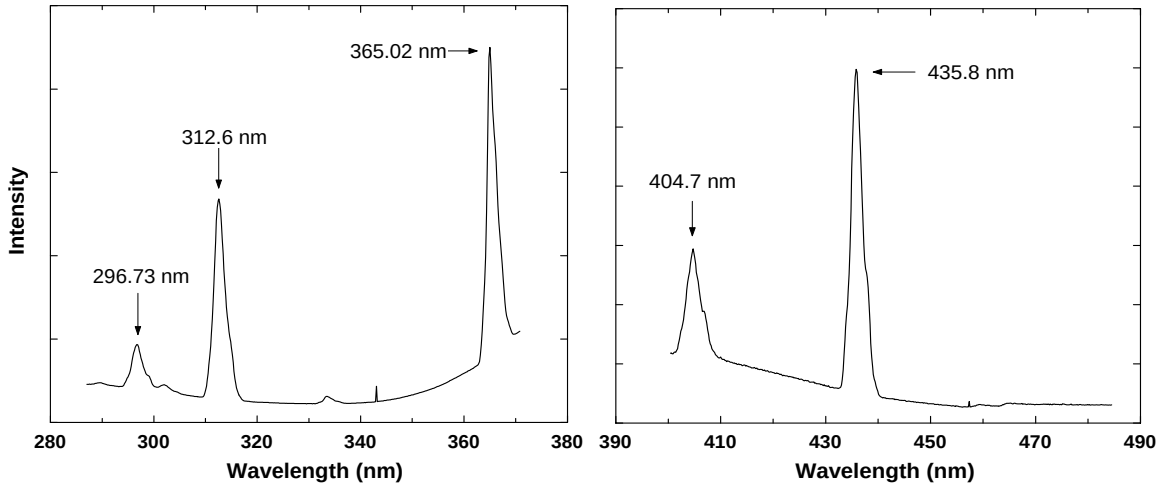

Figure 5-1 Spectral calibration lamp spectrum

The calibration lamp emission is characterized by several sharp peaks in the UV and visible wavelength region. However, in the spectrum above, the peaks appear to have a Full-Width Half-Maximum (FWHM) value of approximately 3 nm. In this case, the FWHM value was governed by the fiber optic diameter, which limited the spectral resolution of the detection instrument. The spectral resolution could be improved by using fiber optic with smaller diameter at the expense of light collection ability.

5.2 Correction Factor

The spectrograph components and the CCD camera have different response and efficiency at different wavelengths. To adjust for those differences, a correction factor was established. A Quartz Tungsten Halogen (QTH) broadband lamp was used as a light source for this purpose. The spectrum captured by the CCD camera was compared to the

lamp specification from the manufacturer and a multiplicative correction factor was established. The correction factor was calculated with a computer program to minimize the multiplication values to reduce the errors. The computer code used for the minimization is listed in Appendix B.4. The procedure was repeated for different grating positions to cover all the wavelength range of interest. Figure 5-2 shows an example of the difference between the light spectrum acquired by the CCD camera prior to correction and the actual lamp spectrum from the manufacturer. Figure 5-3 shows a plot of the established correction factor for a grating center position of 430 nm.

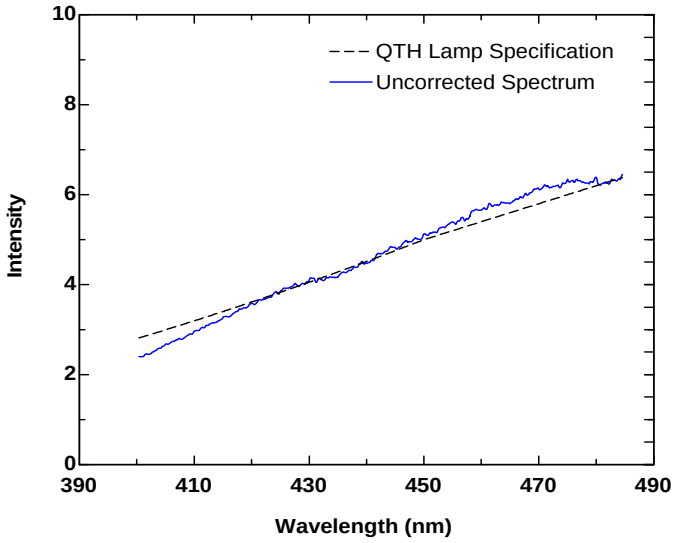

Figure 5-2 Spectrum comparison

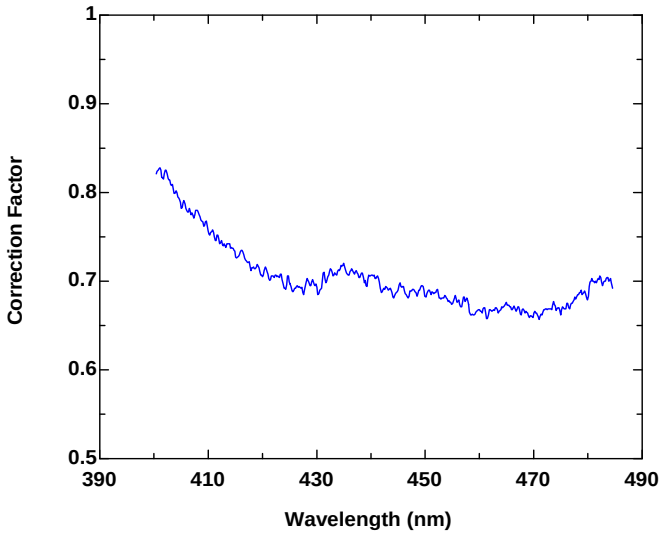

Figure 5-3 Correction factor for grating center position at 430 nm

The typical analysis procedures for light spectra acquired from the engine involved averaging over 500 cycles, background subtraction, and correction factor multiplication. The intensity value at each pixel was multiplied by the correction factor corresponding to that pixel to get the actual intensity value. It is important to note that the correction factor does not introduce or eliminate any feature of the spectrum. It only alters the overall slope of the spectrum. Peaks and species identification can still be performed without using the correction factor; however the correction factor was established to get a true representation of the light emitted during the combustion process.

5.3 Matrix #1 Effects of intake charge temperature

Prior HCCI studies have shown that HCCI combustion timing and heat release rate is highly dependant on intake charge temperature. This experimental data set was established to investigate the effects of intake charge temperature on the chemiluminescence spectra. Three data points were collected for this data set at three

different intake temperature settings with all other parameters being equal. Isooctane was used throughout this experiment with a fueling rate of 10 mg/cycle and an air-fuel ratio of 20:1. The fuel was injected by the premixed fuel injector approximately 1.5 meters upstream of the intake valves to obtain a homogeneous mixture. The engine performance and exhaust emissions values are listed in Table 5-1. Figure 5-4 shows the heat release rate of the three data points. It can be seen that increasing intake temperature resulted in more advanced combustion phasing with more rapid heat release rate.

Parameter	**Units**	**Test 1**	**Test 2**	**Test 3**
Intake Temperature	°C	320.3	312.7	316.7
IMEP	kPa	287.4	293.4	291.7
IMEP COV		1.5	1.2	1.2
Peak Pressure	kPa	3601	3239	3407
CA 10	deg aTDC	-1.00	2.75	1.25
CA 50	deg aTDC	1.75	6.25	4.50
CA 90	deg aTDC	4.50	10.25	8.00
EI NO	g/kg	1.27	0.35	0.61
EI CO	g/kg	13.0	15.9	14.7
EI HC	g/kg	16.2	22.8	19.6

Table 5-1 Engine performance and exhaust emissions values

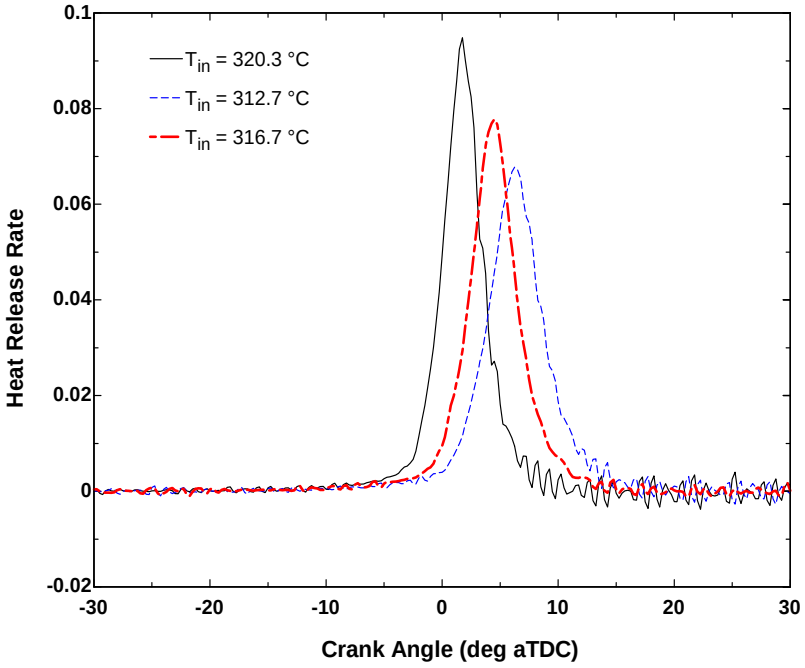

Figure 5-4 Heat release rate at different intake temperatures

The chemiluminescence spectra are shown in Figure 5-5 to 5-7. Comparing those three figures, it is obvious that the light intensity trend closely follows the rate of heat release. The highest intake temperature point has the most advanced light intensity phasing with highest light intensity. The results are similar at other wavelength ranges.

Despite the difference in phasing and intensity, the spectra features are similar between those three cases. All the peaks occur at the same wavelengths and they occur at the similar stage of heat release. Figure 5-8 shows the comparison of light spectra from three different cases taken at the timing closest to CA 50. In the figure, it can be seen that the three spectra have the same features with different intensity.

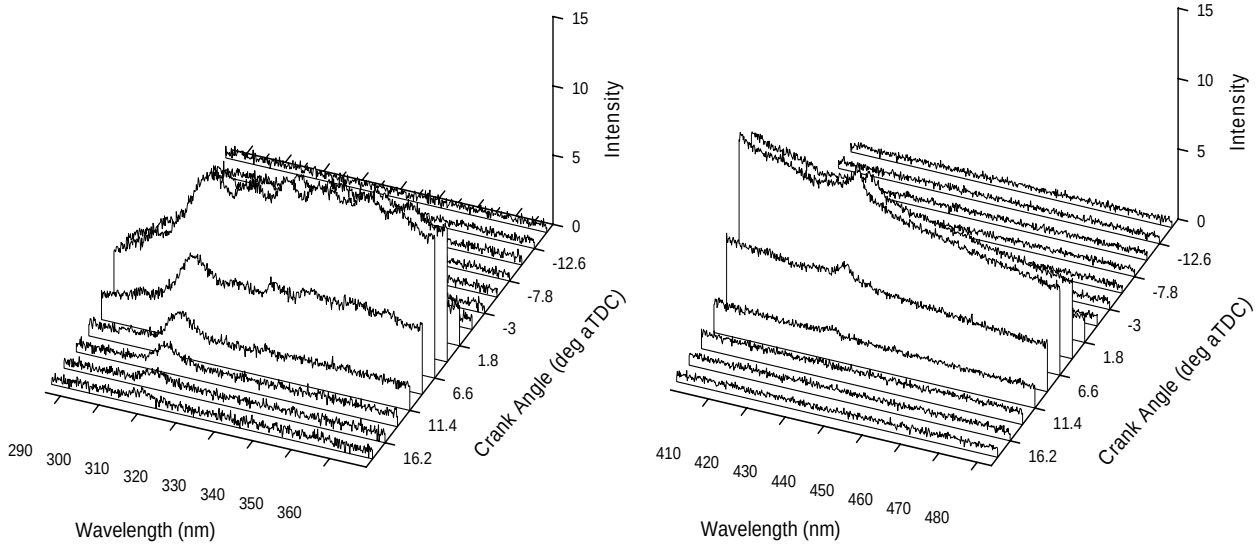

Figure 5-5 Spectra obtained at Tin = 312.7°C

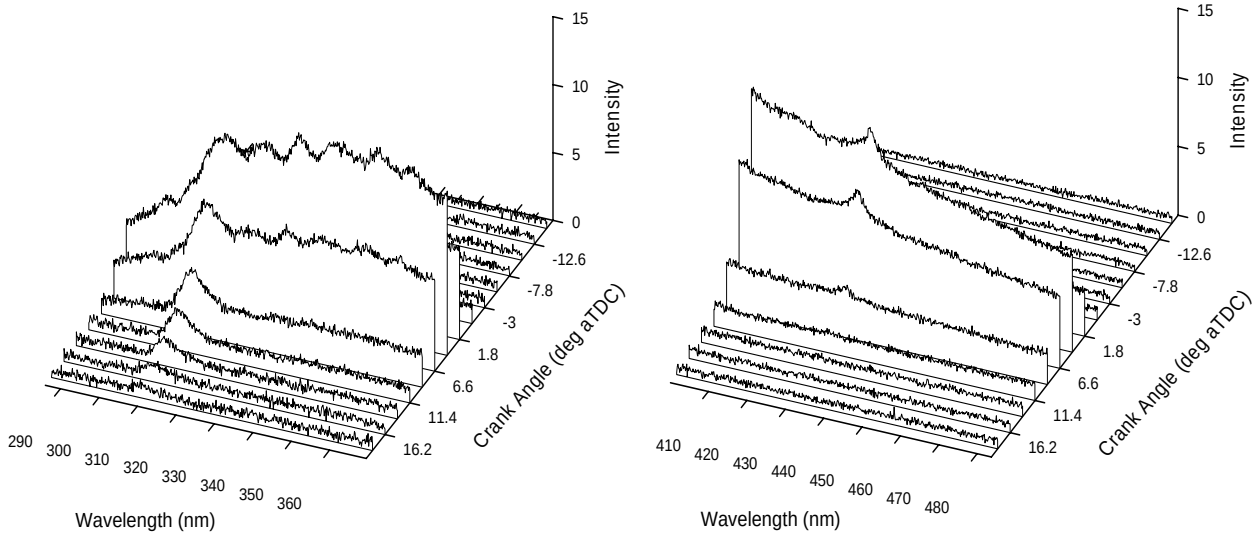

Figure 5-6 Spectra obtained at Tin = 316.7°C

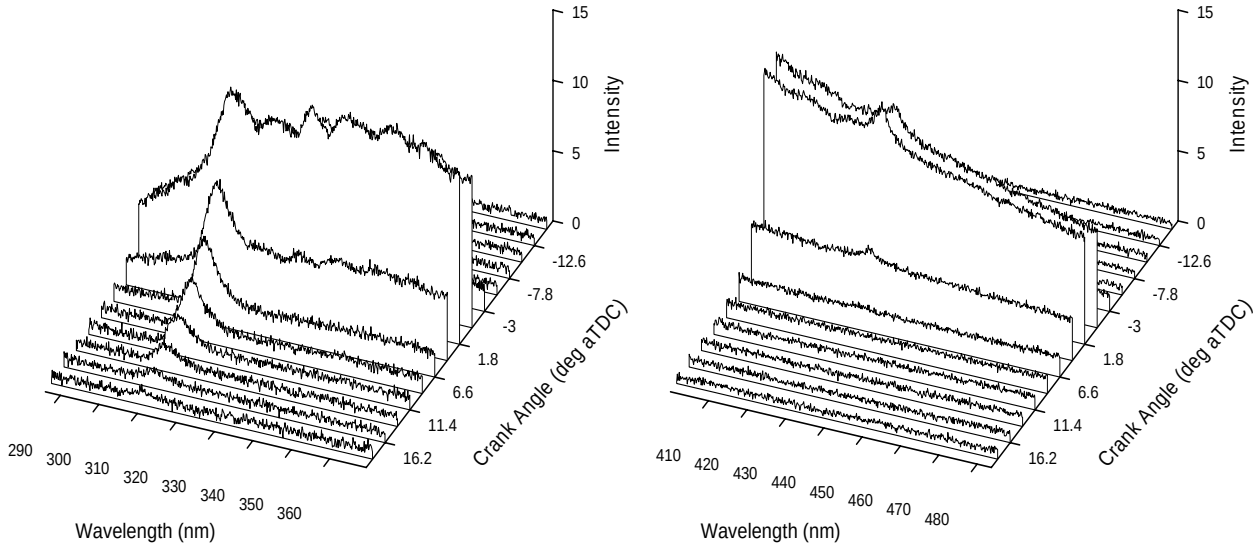

Figure 5-7 Spectra obtained at Tin = 320.3°C

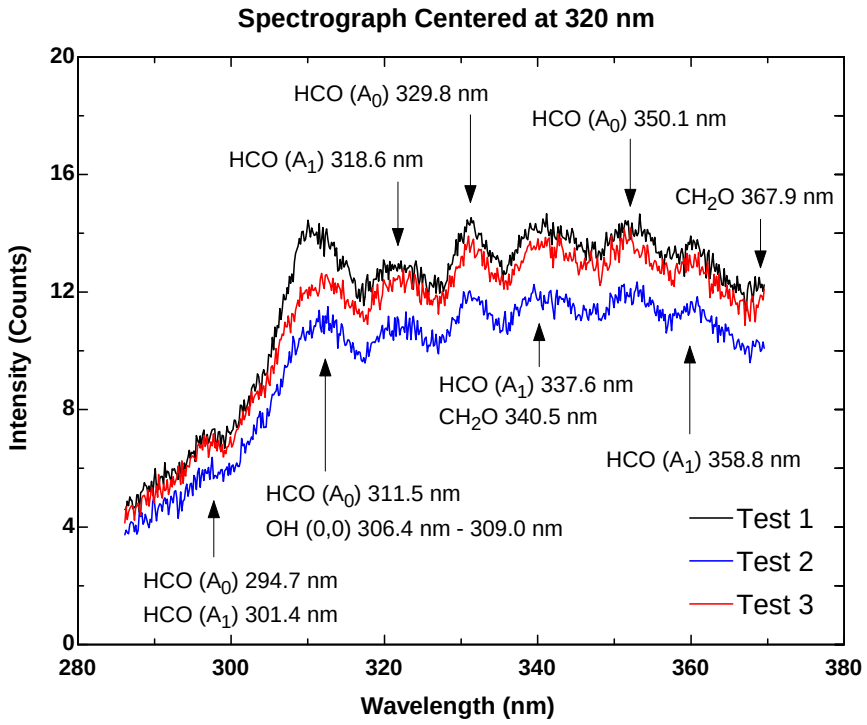

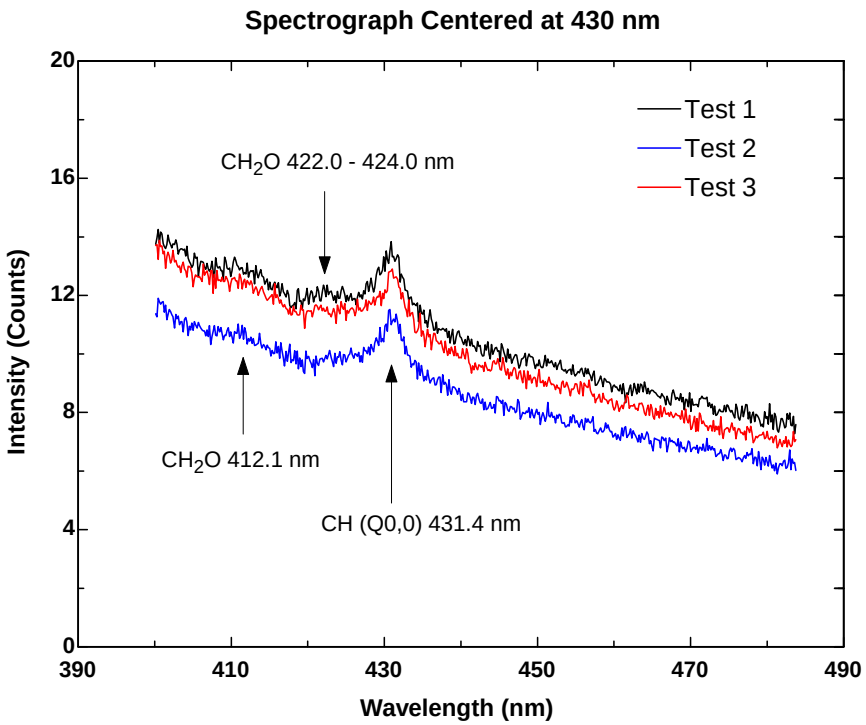

Figure 5-8 Spectrum comparison at timing closest to CA 50

Based on this comparison, it can be concluded that the intake charge temperature significantly affected the HCCI combustion phasing and heat release rate by altering the mixture reactivity and resistance to auto-ignition. However, once the reaction started, intake charge temperature does not affect the reaction sequences and intermediate species formed during the combustion process. In other words, the reaction sequences of HCCI combustion do not depend on the intake charge temperature.

The resulting spectra show several distinct features that are related to certain intermediate species. The spectra appeared as several peaks superimposed on top of a continuous spectrum. The continuous spectrum resulted from CO oxidation process that occurred throughout the combustion. As labeled in Figures 5-5 to 5-7, the peaks were identified as emissions from OH, CHO, CH_2O (Formaldehyde), and CH. With the

spectrograph centered at 550 nm, there was another peak observed at around 590 nm. This peak was attributed to emission from Sodium (Na) in the air-fuel mixture. This particular feature is not of interest since sodium is not involved in the reactions; therefore it is not included in the analysis.

Prior to the heat release period, there was no light emission; therefore the spectrum appeared as a straight line with approximately zero intensity. As soon as the ignition started, the light intensity increased rapidly with several peaks superimposed on the continuous CO-O spectrum. The peaks were corresponding to emissions from OH, CHO, CH_2O, and CH. Both OH and CHO have light emissions bands at around 310 nm; therefore the peak at that wavelength might correspond to emissions from both species. The light intensity reached a peak value close to CA 50. As the combustion progressed, the light intensity decreased and most of the peaks disappeared, except for a single peak at 309-310 nm which is very likely corresponds to OH band emissions. In all three cases, that single peak remained visible for a considerable period after CA 90. In all cases, CA 90 occurred at or before 10 deg aTDC. However, the OH band peak was still detected at 18.6 deg aTDC. At this point, the cylinder temperature was still higher than 1900 K.

The time-resolved spectra results agree with previous results cited in the literature review section, particularly about the reaction sequence in HCCI combustion. The spectra during the heat release period are dominated by the continuous CO-O oxidation spectrum. At the early stage of combustion, the continuum is superimposed over several CHO and CH_2O peaks. As the combustion progresses, the light intensity reaches a peak value close to CA 50 and CH emission at 431.5 nm is detected. Approaching CA 90, most of the peaks disappear, except for a peak corresponding to OH emission, which

remains visible for long period of time. OH is involved in many different reactions throughout the combustion process, and therefore it does not exist in large quantities until the end of the combustion, which explains why OH is the last species to be detected.

5.4 Matrix #2 Effects of Fuel Delivery Method

This data set was obtained to analyze the effects of air-fuel mixture in-homogeneity in the chemiluminescence spectra. To facilitate this experiment, the engine has been equipped with two different fuel injectors. The first fuel injector was located 1.5 meters upstream of the intake valves to allow formation of a homogeneous air-fuel mixture. This injector is referred to as the premixed fuel injector. The second injector was mounted on the cylinder head to spray fuel directly into one of the intake valves, creating some degree of in-homogeneity in the air-fuel mixture. The second injector is referred to as the stratified fuel injector. More information about the fuel injection systems setup can be found on Section 3.2.5 and 3.2.6.

The stratified fuel injection timing was controlled independently through the MotoTune software. For the data set presented in this thesis, the stratified fuel injection was set to have very late injection timing, close to the Intake Valve Closing (IVC) period. By injecting the fuel late into the compression stroke, it is expected that the fuel has shortest time to mix with the air and EGR, thus creating the most in-homogeneous mixture.

Two stratified fuel injection data points were collected at two different intake temperature settings to match the operating conditions obtained previously with the premixed fuel injector. To isolate the effects of fuel delivery method, all other engine

parameters were unchanged. Numbers related to engine performance and exhaust emissions are tabulated in Table 5-2. Figure 5-9 and 5-10 shows the heat release rate comparison with two different fuel delivery methods. In each case, the combustion phasing was very close to one another.

Parameter	**Units**	**Set 1**		**Set 2**	
Fuel Injection Type		Premixed	Stratified	Premixed	Stratified
Intake Temperature	C	320.3	319.7	312.7	313.1
IMEP	kPa	287.4	293.3	293.4	295
IMEP COV		1.5	1.7	1.2	1.9
Peak Pressure	kPa	3601	3628	3239	3133
CA 10	deg aTDC	-1.00	-1.00	2.75	3.25
CA 50	deg aTDC	1.75	1.75	6.25	7.5
CA 90	deg aTDC	4.50	4.50	10.25	11.75
EI NO	g/kg	1.27	3.71	0.35	1.02
EI CO	g/kg	13.0	16.1	15.9	21.4
EI HC	g/kg	16.2	16.1	22.8	23.3

Table 5-2 Engine performance and exhaust emissions values

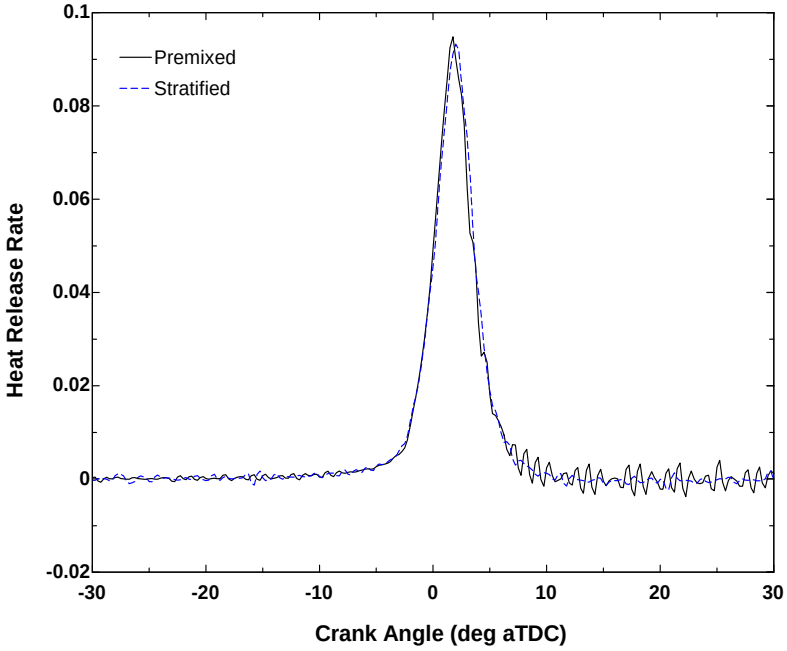

Figure 5-9 Heat release rate comparison #1 (T_{in} = 320°C)

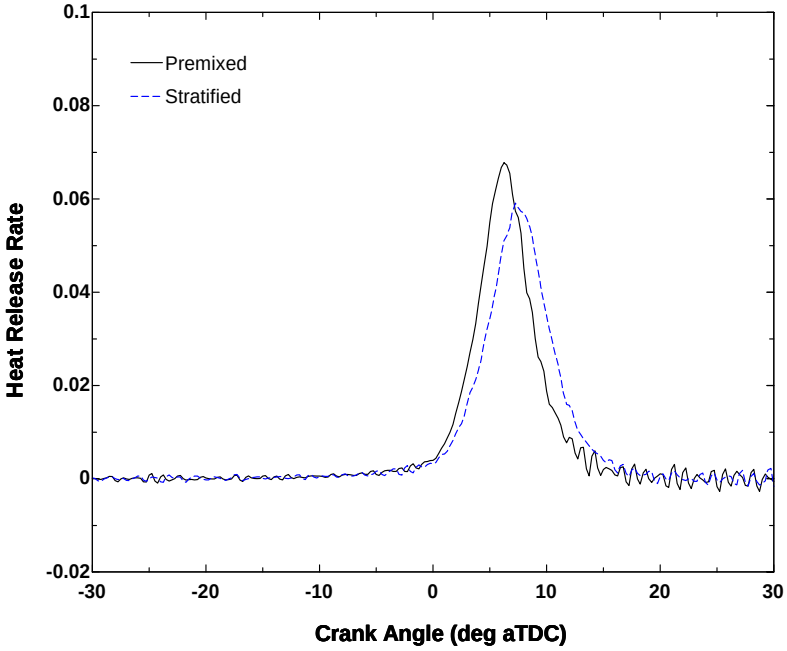

Figure 5-10 Heat release rate comparsion #2 (T_{in} = 313°C)

With different fuel delivery method, the engine performance was found to remain relatively the same. The only noticeable difference was slightly higher NO_x and CO

emissions with the stratified fuel injection. The reason behind this trend is thought to be the presence of locally rich regions in the cylinder, which burn at higher temperature. Figure 5-11 and 5-12 shows the comparison of the spectra obtained with two different fuel delivery methods with an intake temperature of 320°C. The other spectra set have very similar features; therefore they will not be presented here.

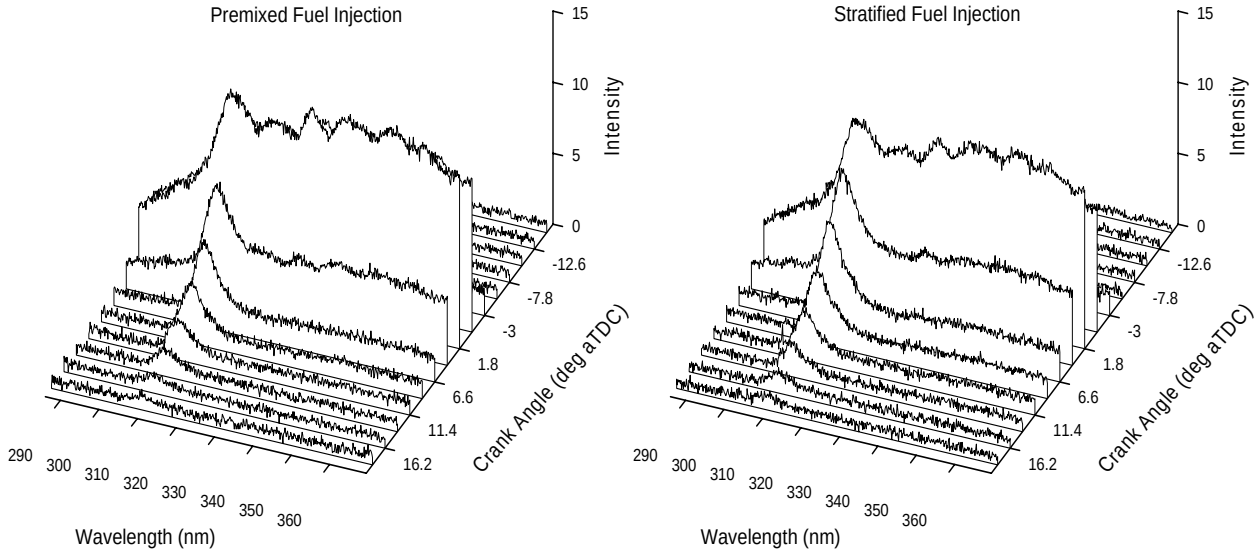

Figure 5-11 Spectra obtained with spectrograph centered at 320 nm

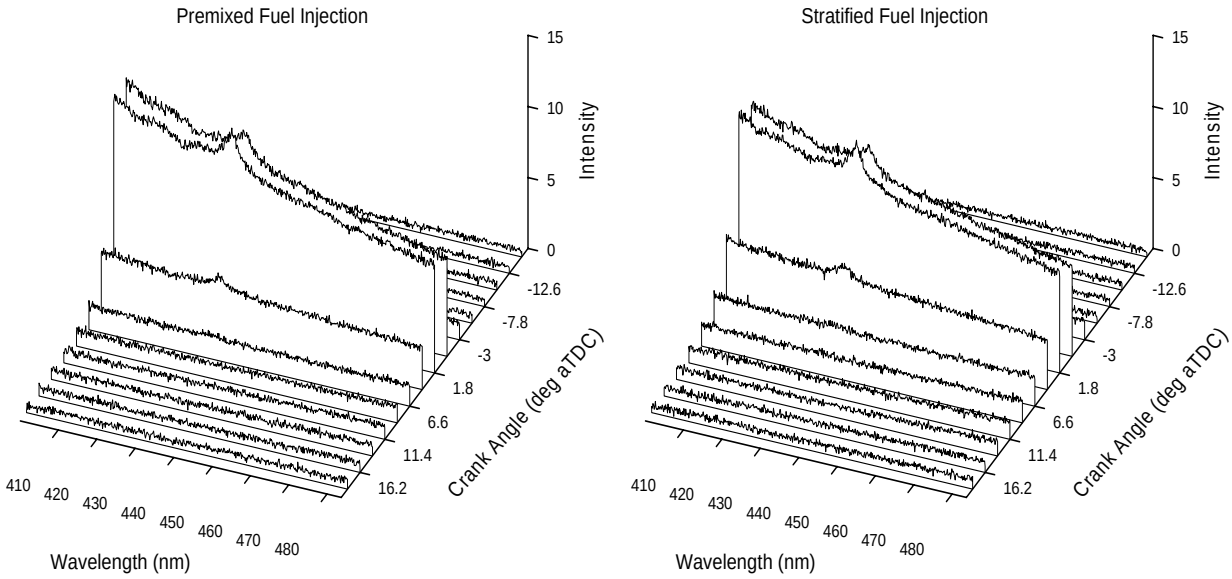

Figure 5-12 Spectra obtained with spectrograph centered at 430 nm

Looking at Figure 5-11 and 5-12, it appears that the spectral features are relatively the same no matter which fuel injector was used. For a closer look, Figure 5-13 compares the spectrum obtained at the timing most closely corresponds to CA 50. It can be seen clearly that both spectra have the same features at the same wavelengths. The only difference is slightly weaker light intensity with stratified fuel injection.

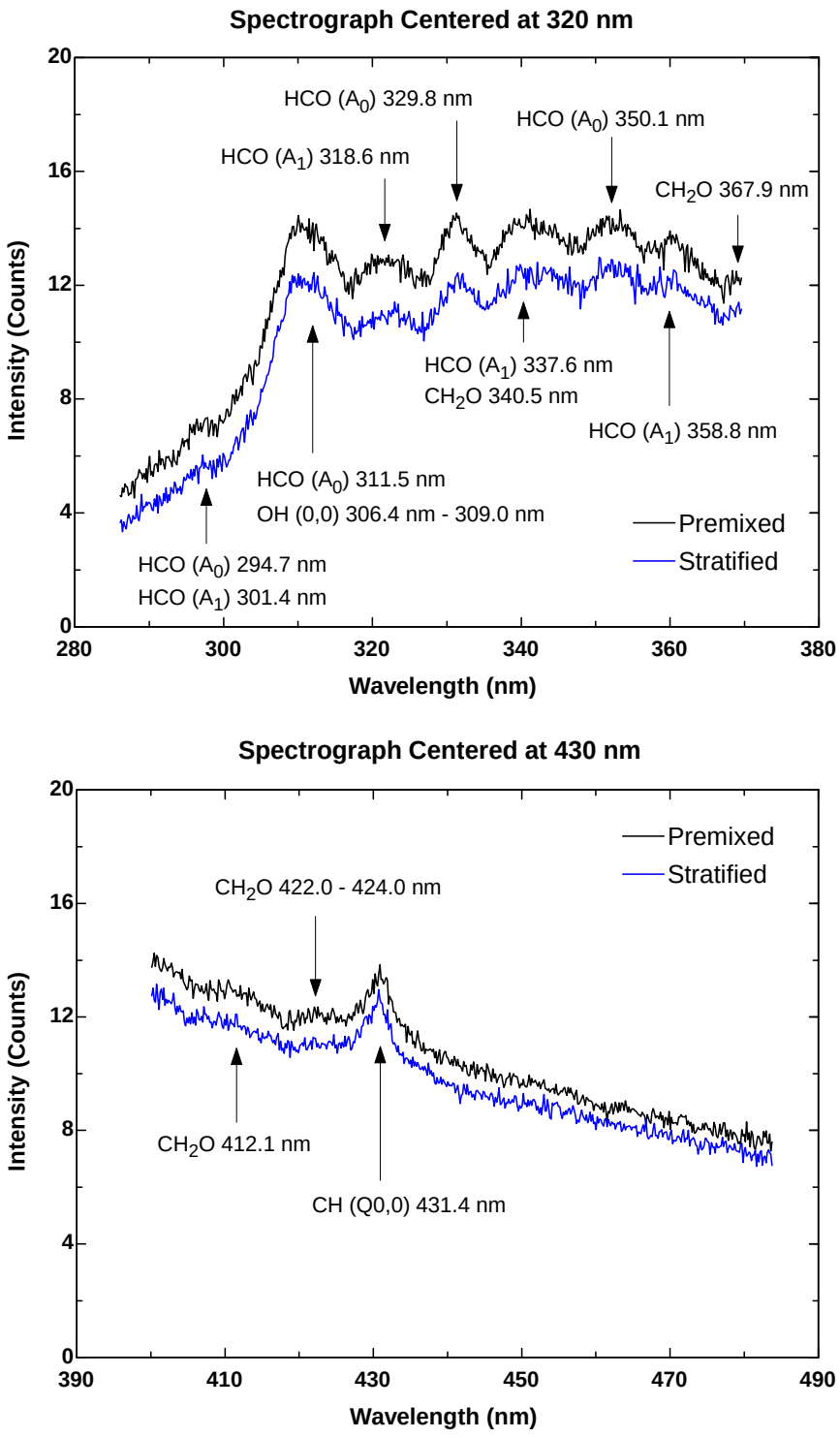

Figure 5-13 Spectrum comparison at timing closest to CA 50

The reason behind this behavior is unclear. It can be some variations in the light detection equipment sensitivity, or it may be a real effect of air-fuel mixture in-homogeneity. If it is true that there is a richer region in the cylinder, then there must be other region with leaner air-fuel ratio. Since the fiber only collects light from a small conical volume in the center of the cylinder, it is possible that the collected light is from the leaner area which burns at slightly lower temperature, emitting light of lower intensity. However, without knowing the extent of mixture in-homogeneity within the cylinder, such a conclusion can not be drawn. Another method to see if mixture in-homogeneity is indeed causing the intensity difference would be to put the fiber at a different location in the cylinder to collect light from a horizontal conical volume across the cylinder, as shown in Figure 5-14. However this method would require some modification to the cylinder head which could potentially affect the engine operating conditions. Data collected at other intake temperatures also shows similar behavior, with the stratified fuel injector resulting in slightly weaker light intensity. Figure 5-15 shows another comparison taken at different intake temperature setting (T_{in} = 316°C).

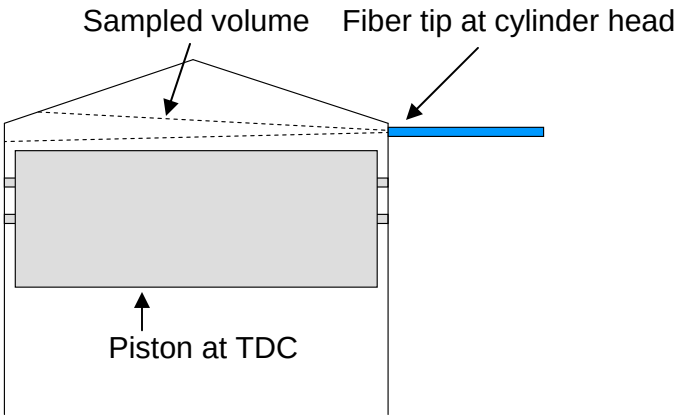

Figure 5-14 Different fiber optic setup

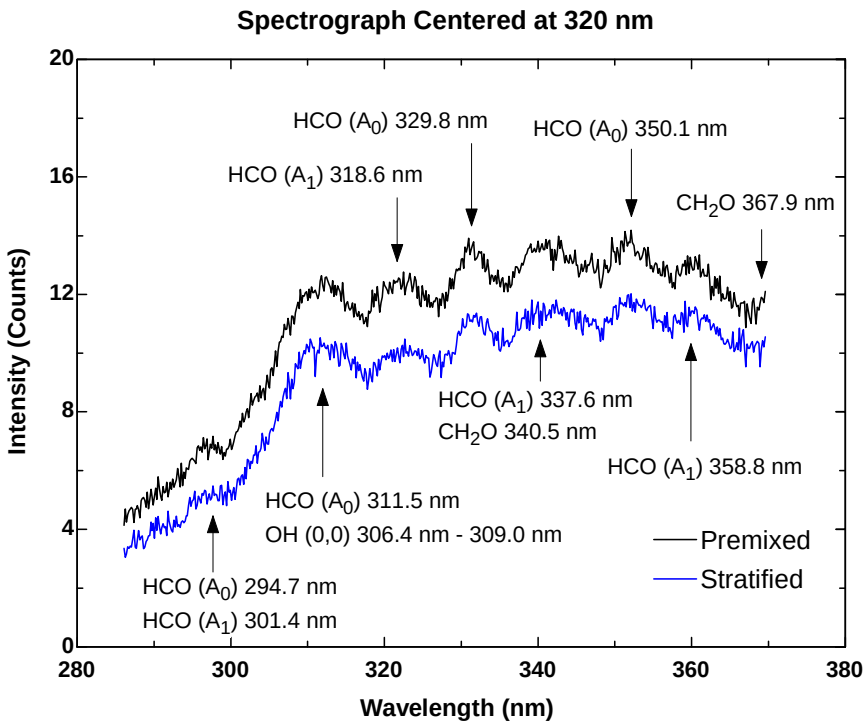

Figure 5-15 Spectrum comparison at timing closest to CA 50

Despite the difference in the intensity level, the results provided some answer to the question of how mixture in-homogeneity affects HCCI combustion. Based on the spectra, it is clear that the reaction pathways and intermediate species are the same no matter which fuel delivery method is used. The mixture in-homogeneity created by the stratified fuel injector does not seem to affect the HCCI combustion other than the changes in exhaust emissions.

5.5 Matrix #3 Effects of Fueling Rate and Air-Fuel Ratio

Previous experimental results found that increasing air-fuel ratio helps improve the combustion at lower fueling rates. This data set was designed to obtain chemiluminescence spectra under those conditions to see if there is any change in the

reaction sequences or intermediate species that might cause such behavior. The fuel used was isooctane with a fueling rate of 5 mg/cycle. Three data points were collected at three different air-fuel ratios with all other parameters being equal. The intake temperature was fixed at 365°C for all three running conditions. The resulting engine performance and exhaust emissions numbers are listed on Table 5-3. Figure 5-16 shows the heat release rate comparison of those conditions.

Parameter	**Units**	**Reference**	**Test 1**	**Test 2**	**Test 3**
Fueling Rate	mg/cycle	10	5	5	5
Air-Fuel Ratio		20:1	20:1	25:1	30:1
Intake Temperature	C	320.3	365.2	364.2	365.2
IMEP	kPa	287.4	109.8	123.1	134.9
IMEP COV		1.5	9.8	3.1	2
Peak Pressure	kPa	3601	2011	2344	2672
CA 10	deg aTDC	-1.00	1.50	-1.00	-3.75
CA 50	deg aTDC	1.75	10.50	5.25	0.75
CA 90	deg aTDC	4.50	24.00	15.00	6.50
EI NO	g/kg	1.27	0.15	0.18	0.2
EI CO	g/kg	13.0	159.2	105.5	55.6
EI HC	g/kg	16.2	79.1	47.3	33.8

Table 5-3 Engine performance and exhaust emissions values

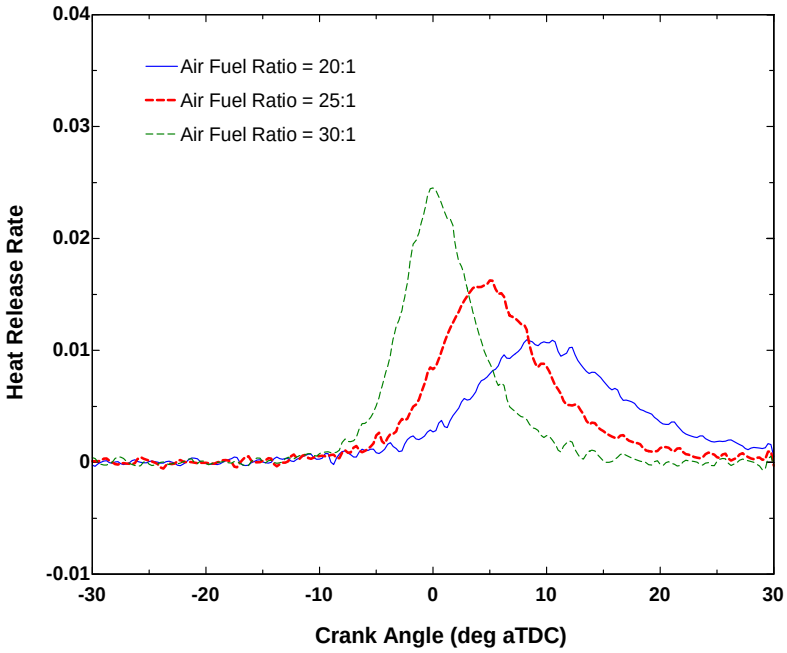

Figure 5-16 Heat release rate at different air-fuel ratios

Comparing the three lower fueling rate cases, it is clear that the data point with highest air-fuel ratio has the most advanced combustion phasing with most rapid heat release rate. In addition, that point also has the highest peak pressure and lowest COV of IMEP. Figure 5-17 shows the spectra obtained at the timing closest to CA 50 for all three air-fuel ratio conditions. For reference, a spectrum from 10 mg/cycle fueling rate case is also added to the figure. Based on the figure, the lower fueling rate cases have significantly weaker light emissions intensity compared to the higher fueling rate, as expected. Looking at Figure 5-16 and 5-17, it can be seen that chemiluminescence light intensity is closely related to heat release rate.

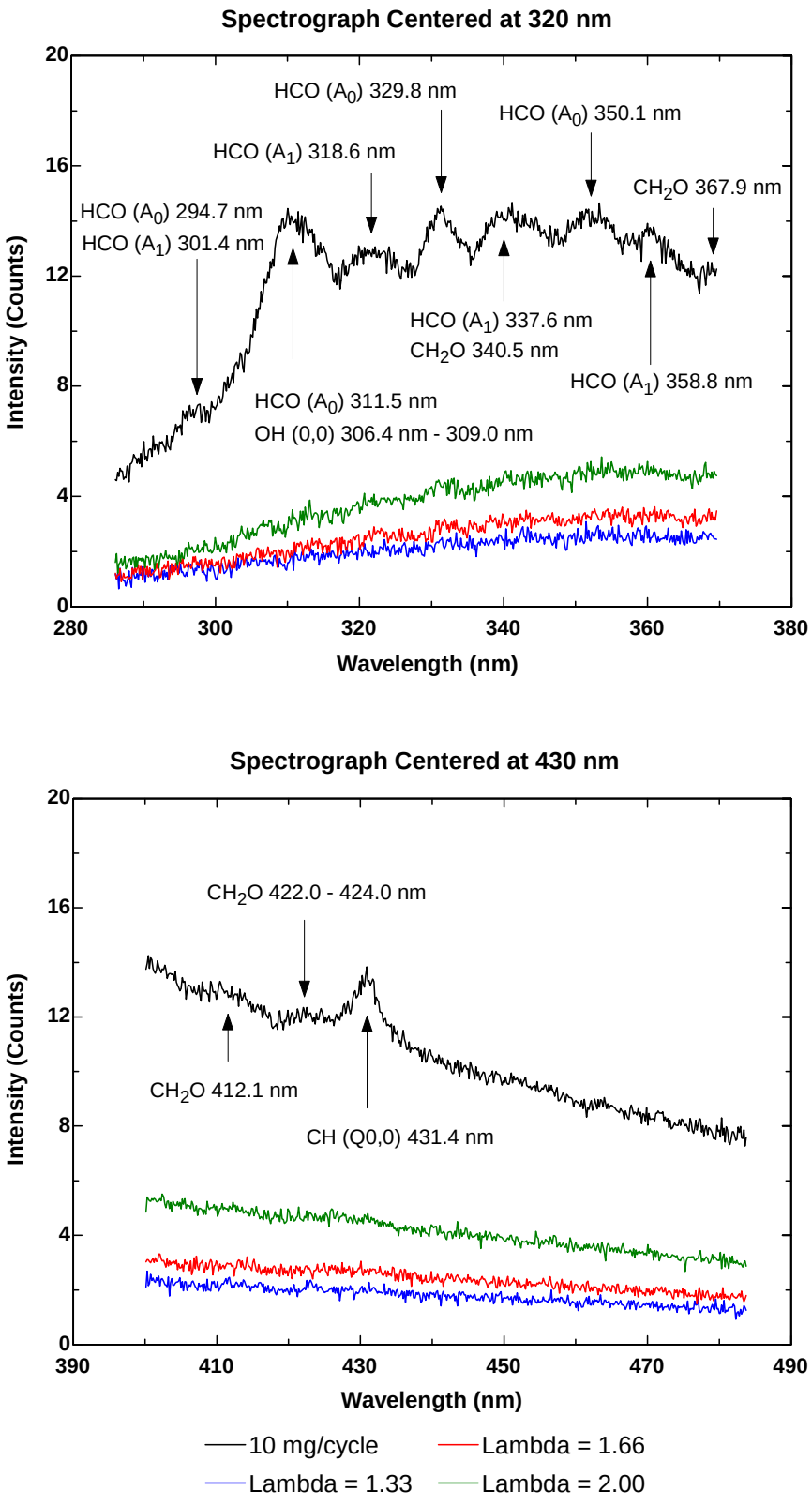

Figure 5-17 Spectrum comparison at timing closest to CA 50

From the three lower fueling rate spectra, there is not much information that could be gathered since the light intensity was too weak. Even at the peak intensity, the spectra appeared almost as a continuum without any distinct features. Therefore, a conclusion can not be drawn whether or not the reaction sequences and intermediate species changed with different air-fuel ratio. Different optical diagnostics techniques might be more suitable to investigate low fueling rate conditions.

The reason for the improvement in combustion with higher air-fuel ratio is thought to be the increasing quantity of oxygen in the cylinder. If oxygen availability is indeed causing such behavior, it is unlikely that varying the air-fuel ratio changes the reaction sequences and intermediate species. However, without further analysis, such conclusions can not be drawn.

The lower fueling rate cases produced significantly higher CO and HC emissions compared to the 10 mg/cycle cases. At the highest air-fuel ratio case, the peak cylinder temperature is approximately 1700 K. This temperature is significantly lower than the 10 mg/cycle fueling rate cases which had a peak temperature of more than 2100 K. The absence of distinct OH peak in the lower fueling rate cases spectra are consistent with previous kinetics studies results on HCCI combustion which suggested that OH generation at low cylinder temperature is not sufficient to allow for complete CO oxidation. John Dec [46] from Sandia National Laboratories suggested that 1500 K is the critical cylinder temperature, below which the CO emissions become excessive. With a peak cylinder temperature of 1700 K, the OH band emission was still not observed in the spectra, most likely because the emitted light intensity was below the detection limit of the equipment.

5.6 Matrix #4 Intake Charge Preheating (Fuel Reformation)

The fourth data set was configured to investigate the effects of intake charge preheating on the chemiluminescence spectra. It was discovered previously that certain types of fuel, such as PRF 87 and gasoline, undergo some low temperature reactions in the intake system prior to entering the cylinder. This means that the fuel entering the cylinder has been altered and has different properties. Such behavior was not observed with branched fuel structure such as isooctane. A set of data were obtained while running the engine with PRF 87 to see if the extent of pre-reactions in the intake system affects the light emission spectra.

The intake charge heating system, as described in Section 3.2.2, allows independent control of different sections in the intake system. For the first data point, the intake charge was heated to a high temperature in the intake system (T_{up} = 295°C) with a residence time of approximately 9 seconds and then allowed to cool down in the intake runner to 270°C before entering the cylinder. The idea of this data point was to allow the highest degree of pre-reaction in the intake system, and cool down the mixture as much as possible while still achieving acceptable combustion. For the second data point, the intake system temperature prior to the intake runner (T_{up}) was set at 270°C and the charge was heated as much as possible along the intake runner to reach an intake temperature of 297°C prior to entering the cylinder. The second data point was chosen to allow least amount of pre-reaction in the intake system. A third data point was selected with an intake upstream temperature (T_{up}) in between the two extremes and an intake temperature (T_{in}) that resulted in similar combustion phasing with the second data point. The engine parameters and resulting performance figures are tabulated in Table 5-4.

Parameter	Units	Test 1	Test 2	Test 3
Upstream Temperature	°C	293	272.5	278
Intake Temperature	°C	260.4	296.6	293.6
IMEP	kPa	302	300.2	293.7
IMEP COV		1.1	1.2	1.3
Peak Pressure	kPa	3065	3312	3341
CA 10	deg aTDC	3.75	2.50	2.00
CA 50	deg aTDC	8.50	6.00	5.50
CA 90	deg aTDC	14.00	9.25	9.25
EI NO	g/kg	0.12	0.37	0.29
EI CO	g/kg	23.2	18.6	15.6
EI HC	g/kg	26.1	21.6	20.0

Table 5-4 Engine performance and exhaust emissions values

The first and second data points were selected to investigate the effects of extreme upstream and intake temperature on the light emission spectra. The heat release rate plots of these data points are shown in Figure 5-18.

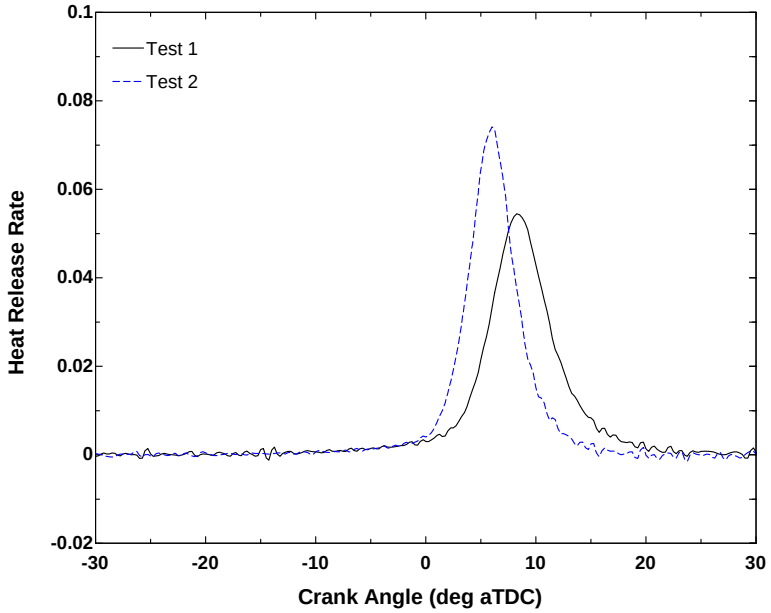

Figure 5-18 Heat release rate comparison

Despite the significant difference in the intake temperature (37°C) between point 1 and 2, the CA 50 is only offset by 2.50 CAD. This suggests that the upstream temperature is indeed affecting the auto-ignition and combustion process. The question is whether or not the pre-reaction in the intake system affects the reaction sequences and intermediate species of HCCI combustion. Figure 5-19 compares the spectra obtained under those two conditions with the spectrograph centered at 320 nm. Figure 5-20 shows the same spectra viewed from different side to give a better view of the spectra after the peak intensity. Figure 5-21 shows spectra obtained with the spectrograph centered at 430 nm.

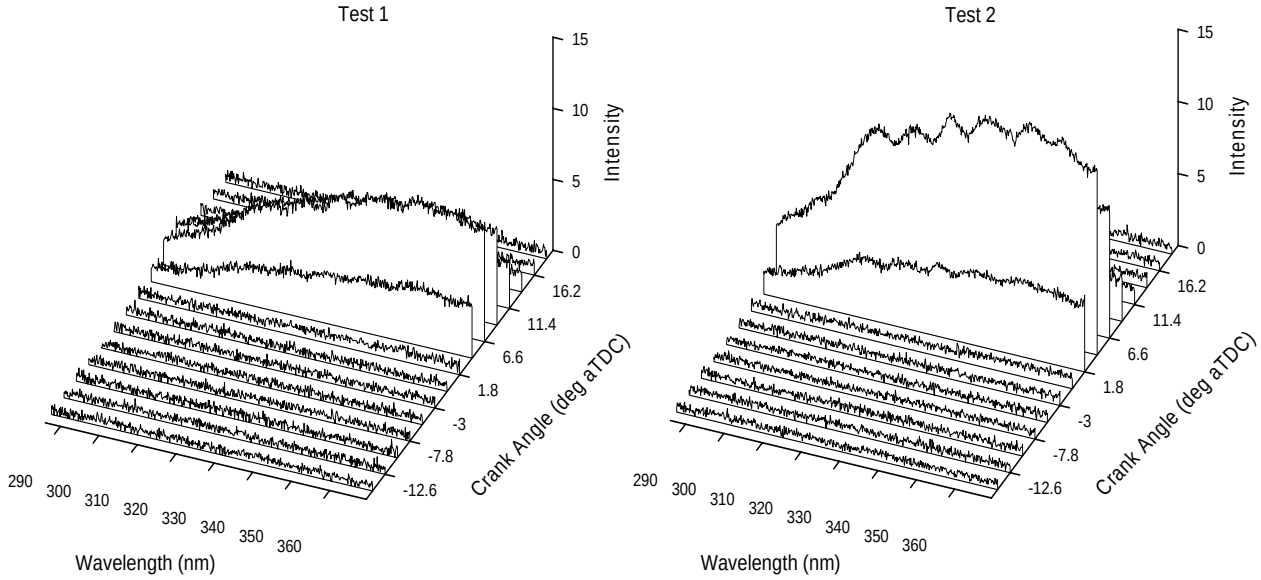

Figure 5-19 Spectra obtained with spectrograph centered at 320 nm

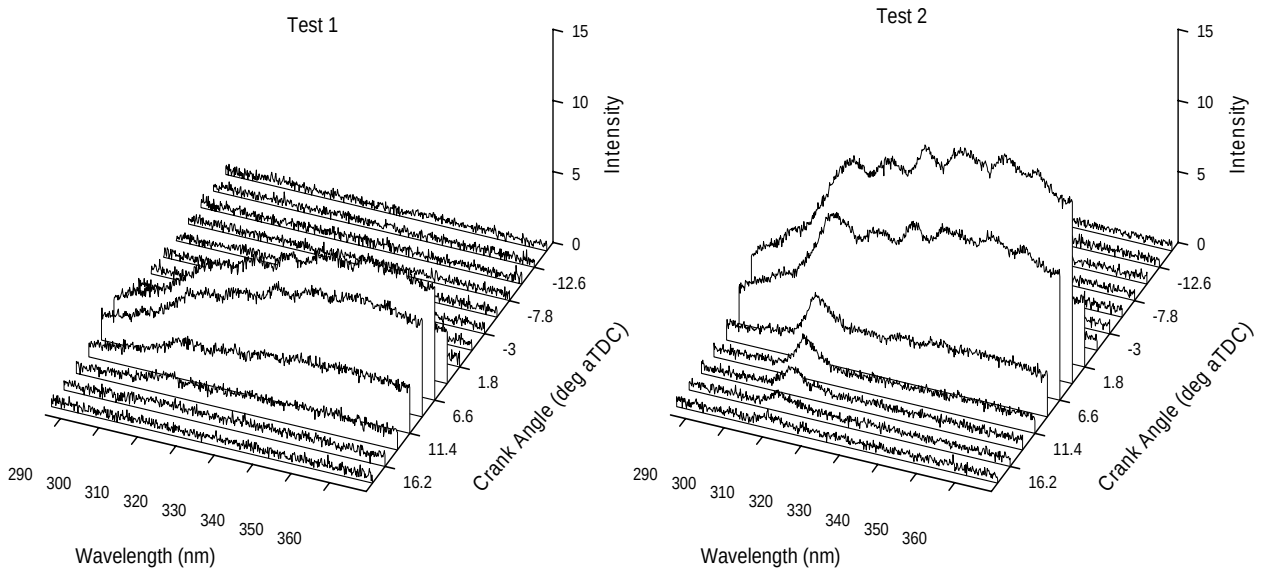

Figure 5-20 Spectra obtained with spectrograph centered at 320 nm

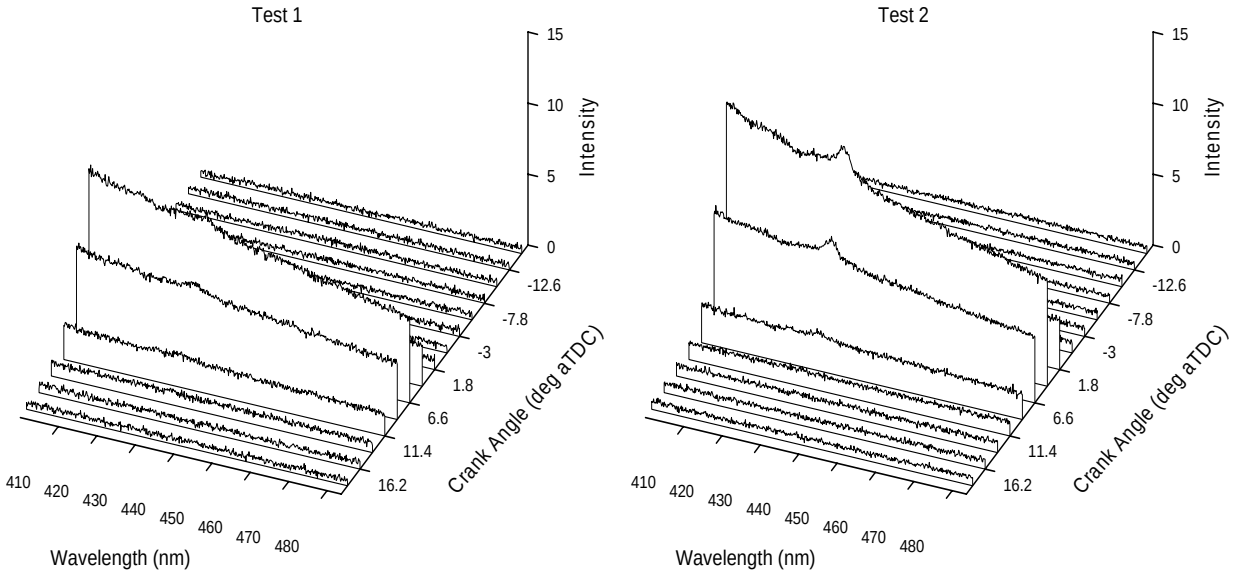

Figure 5-21 Spectra obtained with spectrograph centered at 430 nm

Looking at Figure 5-19 to 5-21, it is clear that the two data points produced similar spectral characteristics. Besides the phasing and intensity difference, the peak

locations are the same. For a closer look, Figure 5-22 compares the spectrum obtained at the timing closest to CA 50 for both test conditions.

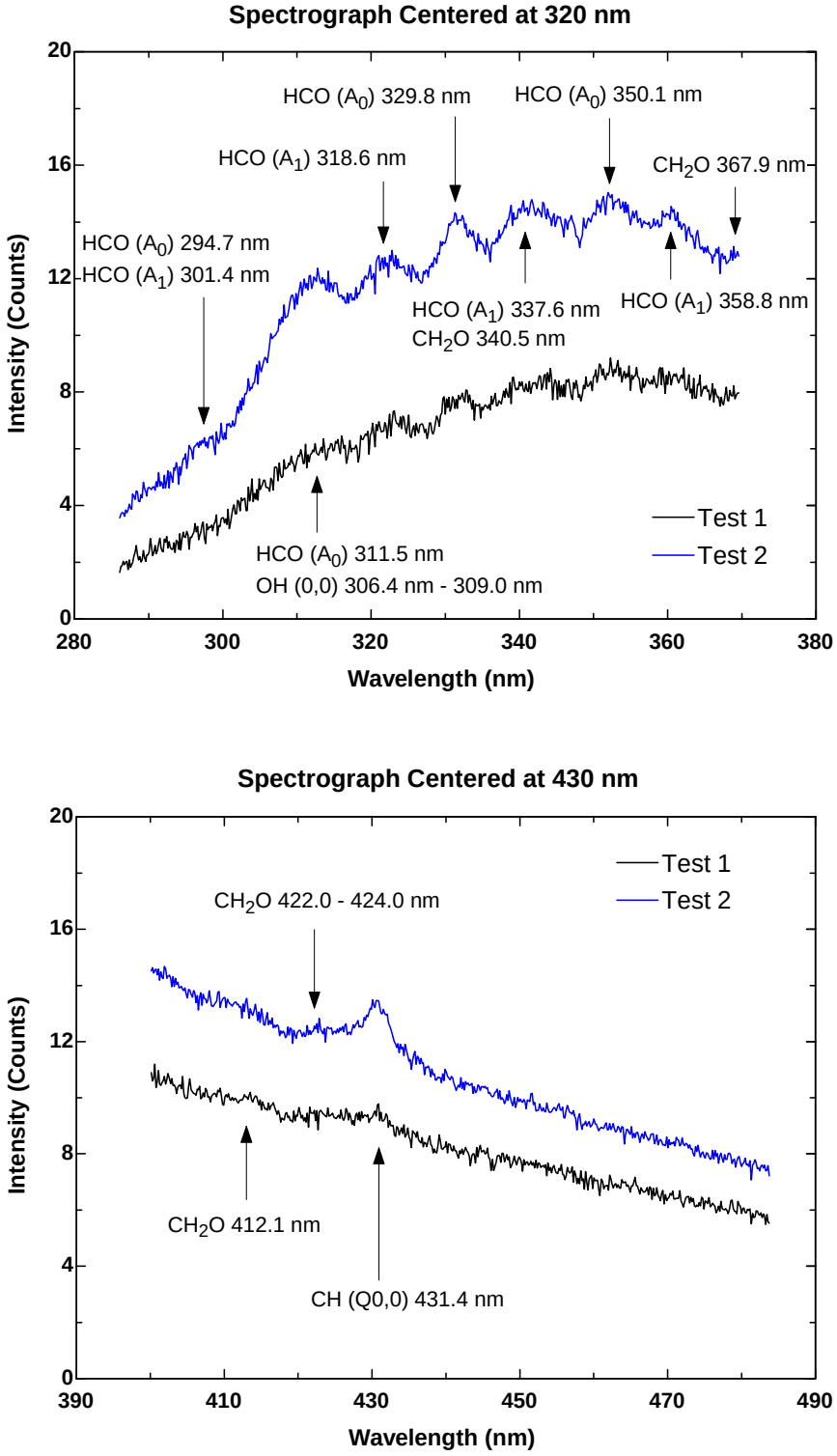

Figure 5-22 Spectrum comparison at timing closest to CA 50

Looking at the figures, it is obvious that both spectra have very similar features. The intensity difference is attributed to the difference in the heat release rate. As previously mentioned, there is a strong correlation between the intensity of light emissions and the rate of heat release. Figure 5-23 shows another spectra comparison, both obtained at 6.60 deg aTDC. At that point, the heat release rates of both conditions are almost the same. It can be seen that the overall light intensity is very close between the two spectra. In addition, the peaks occur at the same locations. However, the high intake temperature case (Data Point #2) has more pronounced features.

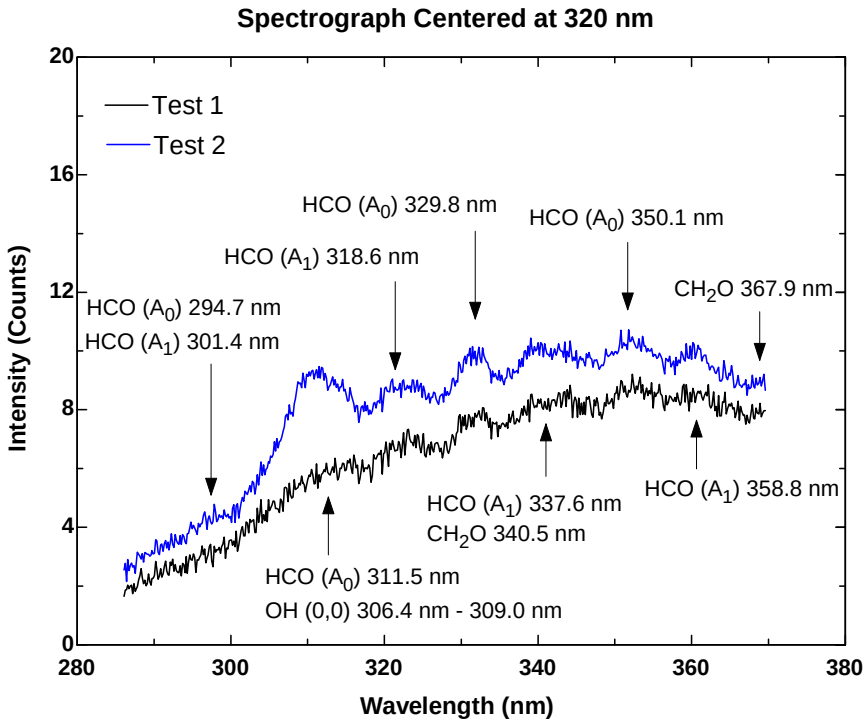

Figure 5-23 Spectrum comparison at the same heat release rate point

The second comparison was made between the second and third conditions which had similar combustion phasing and heat release rate despite the significantly different upstream and intake temperature. The heat release rate plots are shown in Figure 5-24.

Figure 5-25 and 5-26 shows the time-resolved spectra obtained with the spectrograph centered at 320 nm and 430 nm, respectively.

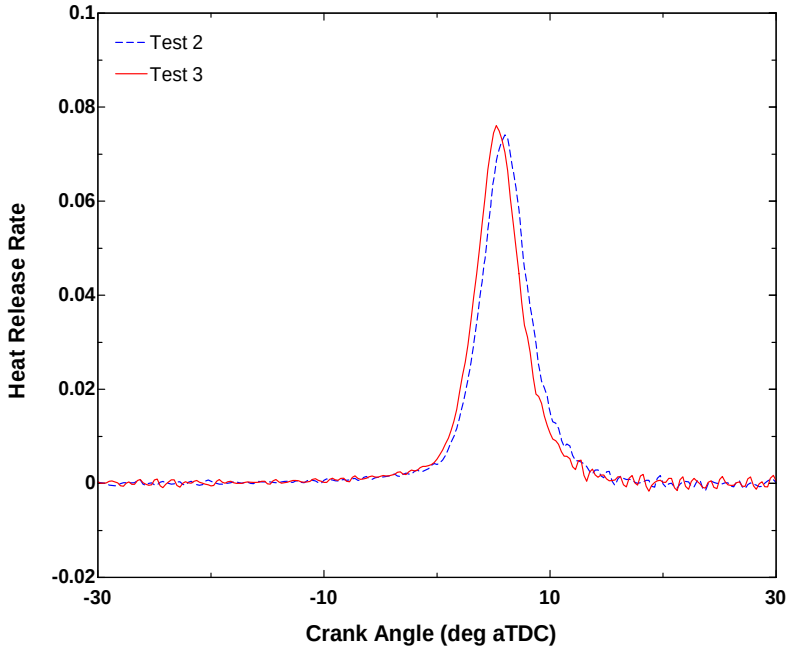

Figure 5-24 Heat Release Rate Comparison

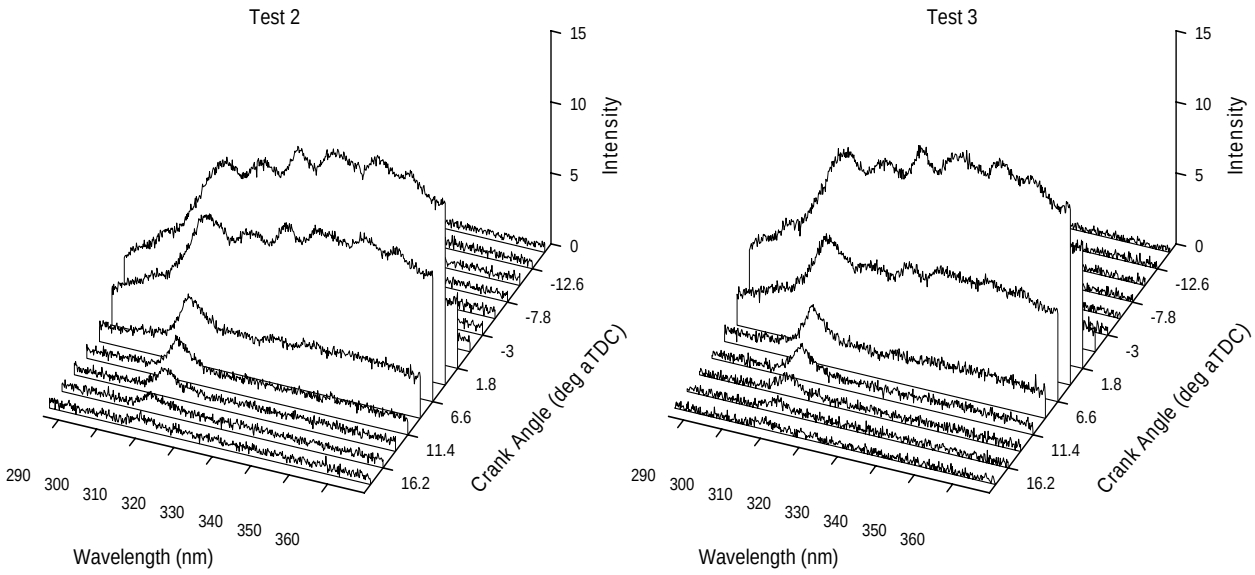

Figure 5-25 Spectra obtained with spectrograph centered at 320 nm

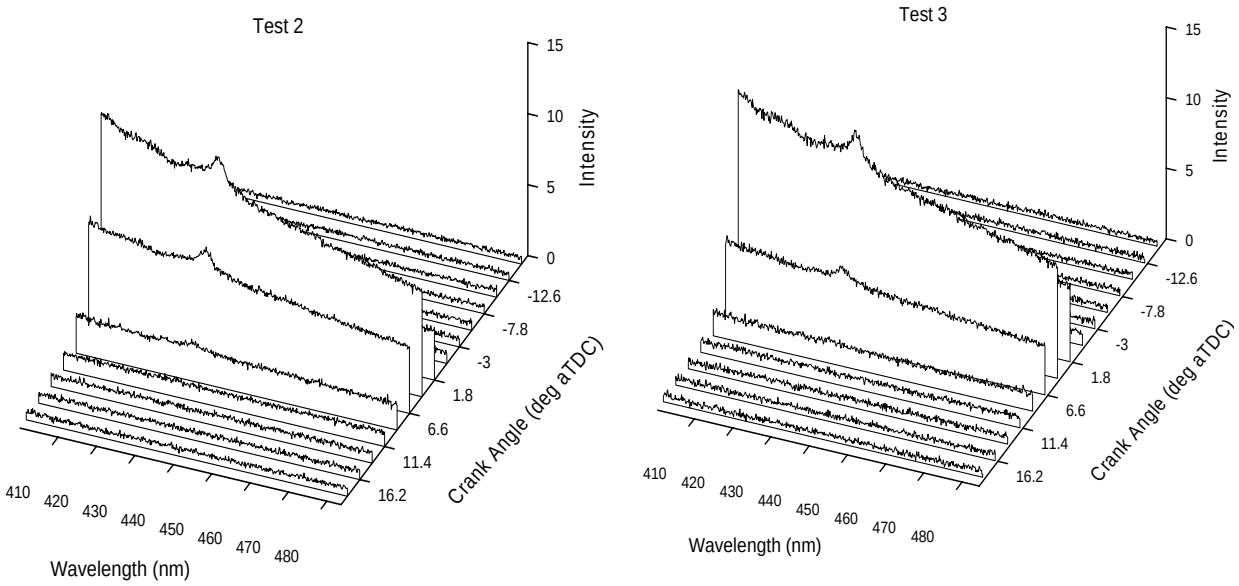

Figure 5-26 Spectra obtained with spectrograph centered at 430 nm

It can be seen that the two spectra look almost identical to each other. The phasing and intensity are very similar and the spectra have all the same features. For a closer look, Figure 5-27 shows the spectra obtained at the timing closest to CA 50.

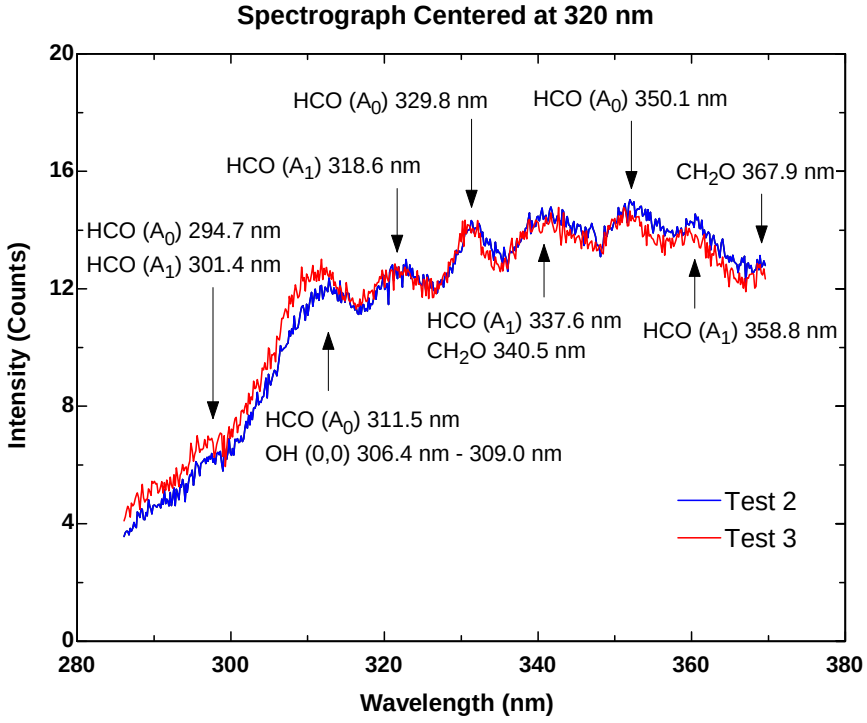

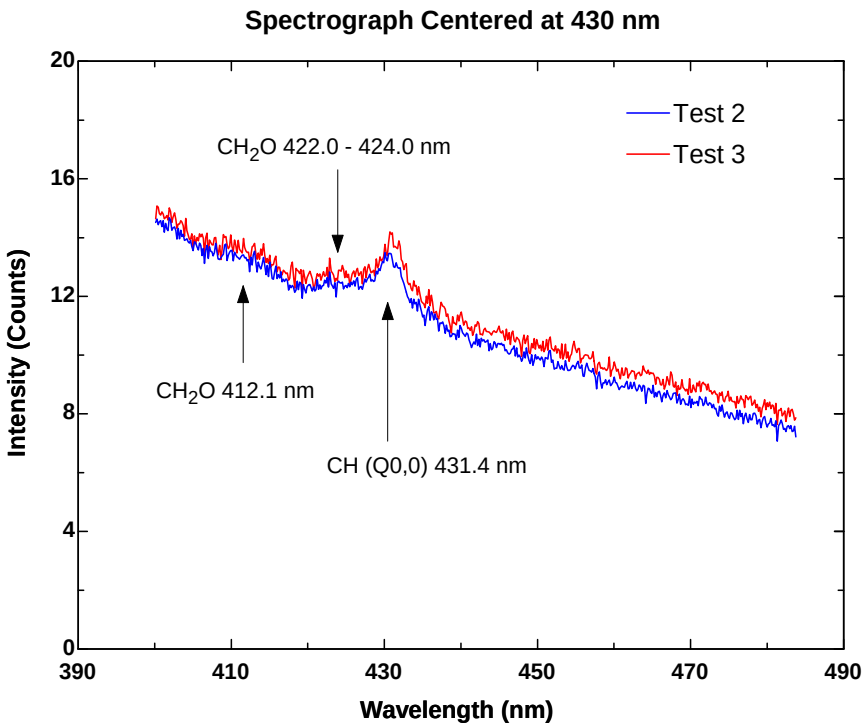

Figure 5-27 Spectrum comparison at timing closest to CA 50

From this data set results, it can be concluded that once the ignition starts, the reaction pathways and intermediate species of HCCI combustion are not affected by the thermal history of the air-fuel mixture. Looking at the first comparison, despite the significant difference in the air-fuel mixture thermal history, the spectra have very similar features, which suggest that the reaction mechanisms are the same. The same conclusion can be drawn from the second comparison, which shows almost identical spectra despite the intake temperature difference.

It is very likely that the extent of pre-reactions in the intake system alters the fuel's resistance to auto-ignition without affecting the reactions mechanism once the ignition starts. It is still possible that certain reactions or species exist prior to the start of ignition. However, with the current detection method, the presence of such species can not be detected.

Chapter 6 – Summary and Recommendations

6.1 Summary

A spectroscopic diagnostic system was designed to enable investigation of the chemiluminescence phenomena during HCCI combustion. The diagnostic system consists of an optical fiber, an imaging spectrograph, a high speed CCD camera, and a computer controller with data acquisition program. The fiber optic was installed in the existing spark plug hole to provide optical access to the cylinder without requiring any modification the engine. The CCD camera was operated in fast kinetics mode to allow data acquisition at a rate of 400 μs/spectrum, which corresponds to 2.4 CAD at an engine speed of 1000 RPM. The CCD camera is capable of acquiring data at a faster rate at the expense of weaker signal intensity.

A series of experiments were performed to investigate the effects of various engine parameters on the HCCI combustion, particularly the chemiluminescence spectra. The parameters varied were intake temperatures, fuel injector locations, fueling rate, air-fuel ratio, and intake system upstream temperatures. Two different fuels were used in this experiment, pure isooctane with an octane number of 100, and a blend of isooctane and n-heptane with an octane number of 87 (PRF 87). Throughout the experiment, the engine speed was maintained constant at 1000 RPM. The intake and exhaust pressure, coolant temperature, and oil temperature were also maintained constant to ensure data consistency.

In each experiment, only one variable was changed while all other parameters are maintained constant to isolate the effects of that particular variable. A series of time-

resolved chemiluminescence spectra were obtained at each data point. In general, light intensity signals were acquired every 2.4 CAD period, starting from 15 deg BTDC. Since the light intensity was weak, spectra from 500 sequential engine cycles were averaged to improve the signal-to-noise ratio. From analysis of the time-resolved spectra, some intermediate species created during the combustion process could be identified. The main question addressed was whether or not changing those engine parameters changes the HCCI combustion reactions sequences and the presence of intermediate species.

6.1.1 Experimental Matrix #1

The first parameter investigated was the intake temperature. As previously discovered, HCCI combustion is highly dependant on the intake temperature, with higher temperature resulting in more advanced combustion and more rapid heat release rate. The chemiluminescence spectra were found to follow this trend closely. Prior to the start of ignition, there was no light emitted in the cylinder, therefore the spectra intensity were very close to zero. As soon as the combustion started, the light intensity increased rapidly, reaching a maximum intensity close to CA 50. During this period, several peaks could be identified in the spectra, corresponding to CHO, CH_2O, OH, and CH. Those peaks were superimposed on top of a continuous emission spectrum. As the combustion progressed, the overall light intensity decreased and most of the peaks disappeared, except for one peak at 309-310 nm which is attributed to (0,0) band emissions from OH. The OH peak persisted for a considerably long duration even after CA 90.

The presence of these intermediate species agrees with results cited in the literature. The continuum is attributed to emissions from CO oxidation, which occurs

during the combustion. Early in the combustion stage, fuel is converted into different fuel radicals, which could explain why CHO and CH_2O are detected. Both OH and CHO have strong emission feature around 310 nm, therefore that particular peak could result from both OH and CHO emissions. As the combustion progresses to completion, the peaks corresponding to fuel radicals disappear as most of the fuel radicals are consumed. The presence of OH at the end of combustion is indicative of its involvement in many different reactions throughout the combustion. Large quantities of OH are not available until close to the end of combustion.

Comparing the spectra obtained at different intake temperatures, it was found that the spectral features are very similar for all cases. It can be concluded that intake temperature affects the ignition timing and heat release rate without changing the reaction pathways of the air-fuel mixture. Once the ignition starts, the reaction sequences are the same no matter what the initial temperature was.

Another conclusion that can be drawn from the results is that the light intensity is closely related to the rate of heat release. It means that the start of ignition timing can be determined by looking at the light intensity trace. This diagnostic method might be suitable to use as an external sensor to accurately determine the ignition timing of HCCI combustion.

6.1.2 Experimental Matrix #2

In this matrix, the effects of air-fuel mixture in-homogeneity on HCCI combustion were investigated. The air-fuel mixture in-homogeneity was introduced by

injecting the fuel directly into the cylinder just before intake valve closing time to allow shortest amount of air-fuel mixing time.

The resulting spectra were compared to those obtained previously using the premixed fuel injector. The resulting engine performance metrics and combustion phasing were very similar. Looking at the spectral comparison, all the features were also very similar. The peaks occurred at the same locations at the same timing. It is concluded that air-fuel mixture in-homogeneity does not affect the reaction sequences of HCCI combustion.

Looking closely at the emission spectra, it was observed that the spectra from stratified fuel injection cases had slightly weaker intensity compared to those from premixed fuel injection. The reason behind this trend is still unclear. It might be some inaccuracies in the detection equipment. It is also suspected that fuel stratifications might have caused such trend. The exhaust emission comparison shows higher NO_x and CO emissions from stratified fuel injection cases which indicate the presence of slightly richer regions within the cylinder, most likely closer to the intake valves. These richer regions burn at higher temperature, producing more NO_x. It also means that there are other areas that has slightly leaner air-fuel ratio. Since the fiber only collects light from a small conical volume in the center of the cylinder, it is possible that the fiber collects light from the leaner area, resulting in slightly weaker light intensity. However, without knowing the extent of fuel stratification within this cylinder, this hypothesis can not be confirmed.

6.1.3 Experimental Matrix #3

This data set was collected to investigate the effects of lower fueling rate, and varying the air-fuel ratio at that fueling rate, on the mission characteristic. By increasing the intake temperature, steady HCCI combustion was achieved at a 5 mg/cycle fueling rate. At this lower fueling rate, a higher air-fuel ratio resulted in a more advanced combustion with more rapid heat release rates. This trend was also captured in the light emissions spectra. At these conditions, the heat release rate and light intensity were significantly weaker, thus limiting the amount of information that could be gathered. A conclusion that can be drawn is that light intensity level follows closely the trends of heat release rate.

The reason for the combustion improvement with increasing air-fuel ratio is thought to be the increasing availability of oxygen within the cylinder. Most likely, the reaction paths of the air-fuel mixture remain unchanged. Looking at the spectra obtained under these conditions, they appear as a continuum without any distinct peaks. However, it does not mean that the intermediate species do not exist in the cylinder. The light intensity emitted by those species might be too low to be detected by the CCD camera. Different diagnostic methods might be more suitable to study HCCI combustion at the lower fueling rate conditions.

6.1.4 Experimental Matrix #4

In this data set, PRF 87 was used instead of pure isooctane. Exposed to high temperature in the intake system, PRF 87 undergoes certain low temperature reactions prior to entering the cylinder, which causes the engine’s HCCI operating window to shift.

This data set was developed to observe if the extent of reactions in the intake system affect the light emission spectra.

In the first comparison, the combustion phasing was offset by 2.5 CAD despite the significant intake temperature difference. Looking closely at the spectra, the peaks and their locations, as well as the overall trends are all the same. The only difference is in the intensity level, and this difference was attributed to the heat release rate differences between those two data points.

Another comparison was made between two cases which had very similar combustion phasing despite the considerably different intake and upstream temperatures. Once again there was no noticeable difference in the spectra. In this comparison, the spectra looked almost exactly the same.

The results of this experiment lead to a conclusion that the low temperature reactions in the intake system reduced the fuel's resistance to auto-ignition without affecting the reaction sequence of the air-fuel mixture. Once the ignition starts, the fuel seems to follow the same reaction paths independent of its thermal history. However, this does not eliminate the possibility of some difference in the early stage of combustion. It is possible that the low temperature reactions produce species that affect the fuel auto-ignition resistance. During this period, the light intensity is too weak to be detected by the CCD camera.

6.2 Conclusions

Based on the experiment results, the following conclusions can be drawn:

- There is a strong correlation between the combustion phasing, chemiluminescence light intensity and heat release rate.
- During the heat release period, the chemiluminescence spectra appear as several distinct peaks superimposed over a CO-O continuum. The peaks are identified as emissions from OH, CHO, CH_2O, and CH.
- The peaks corresponding to OH, CHO, and CH_2O are detected early in the combustion, followed by a CH peak which starts to appear closer to CA 50. After CA 50, most of the peaks disappear except for a single peak corresponding to OH (0,0) band emissions.
- HCCI combustion timing and heat release rate is highly dependent on the intake temperature. Once the ignition starts, the fuel follows the same reaction pathways and produces the same intermediate species.
- The extent of air-fuel mixture in-homogeneity generated by the stratified fuel injector does not seem to affect the engine performance, other than slight changes in NO_x and CO emissions. The slightly weaker light intensity with stratified fuel injection might be an indication of in-homogeneity within the cylinder.
- At lower fueling rates, the light intensity was too weak for the current diagnostic method.
- The extent of low temperature reactions induced by intake charge preheating reduces the fuel's resistance to auto-ignition without affecting the reaction paths

of the fuel. Once the ignition starts, the spectra appear to be the same, which means the reaction sequences and intermediate species are unchanged.

- All spectra obtained under various operating conditions have very similar features. This similarity suggests that only the intake charge thermal history determines the start of ignition timing without affecting the reaction paths of the fuel. Once the ignition starts, the fuel follows the same reaction paths regardless of the thermal history of the mixture.

6.3 Recommendations for future research

Based on the results and conclusions of this experiment, several recommendations can be made for further research. With the strong correlation between chemiluminescence light intensity, combustion phasing, and heat release rate, it might be possible to utilize a light sensor as an indicator of combustion timing in HCCI. Further investigations are needed to establish the actual correlation between light intensity level and combustion phasing.

The effects of fuel stratification can be further investigated by installing the fiber at a different location. In the current setup, the fiber is positioned in the spark plug hole, pointing down vertically. The fiber collects light from a small conical volume in the center of the cylinder. It is assumed that the light collected by the fiber is an accurate representation of light emissions from the whole cylinder volume. When the fuel is injected directly into the cylinder, it is possible that there is a region in the cylinder that is slightly richer or leaner than the global air-fuel ratio due to incomplete mixing. In such cases, the light emissions will be non-uniform. To get a more accurate representation of

the light emissions throughout the cylinder volume, the fiber must be positioned horizontally in the cylinder head. This would require some modification to the engine which could affect the engine parameters and performance characteristics. A better way to study fuel distribution within the cylinder is by utilizing the PLIF technique in the optically accessible engine. With the PLIF diagnostic method, the extent of fuel stratification in the cylinder can be determined accurately.

In the low fueling rate cases, the chemiluminescence light intensity was too weak for the current diagnostics method. The spectroscopic diagnostic equipments can also be used in light absorption measurement with the addition of an external light source. Using this technique, the presence of species in smaller concentration can be determined. It might be interesting to study the absorption spectra at the lower fueling rate cases.

The current results of the intake charge preheating experiment show that the chemiluminescence spectra are unchanged when the air-fuel mixture temperature history were altered. However, it is possible that there are some differences in the early stage of combustion. Different diagnostic methods might be more suitable to detect the presence of some species at low quantities.

BIBLIOGRAPHY

1. United States Environmental Protection Agency, Global Warming – Climate, http://yosemite.epa.gov/oar/globalwarming.nsf/content/climate.html, 2000.

2. Sher, E., Handbook of Air Pollutions from Internal Combustion Engines - Pollution Formation and Control, 1st edition, Academic Press, Chestnut Hilll, MA, 1998.

3. United States Environmental Protection Agency - Office of Mobile Sources, Regulatory Impact Analysis - Control of Air Pollution from New Motor Vehicles - Tier 2 Motor Vehicle Emissions Standards and Gasoline Sulfur Control Requirements, 1999.

4. Eng, J.A., "Characterization of Pressure Waves in HCCI Combustion", SAE Paper 2002-01-2859, 2002.

5. Iverson, R.J., "The Effects of Intake Charge Preheating and Charge Stratification on HCCI Combustion", M.S. Thesis, Mechanical Engineering Department, University of Wisconsin – Madison, 2004.

6. Onishi, S., Jo, S.H., Shoda, K., Jo, P.D., and Kato, S., "Active Thermo-Atmosphere Combustion Process for Internal Combustion Engines", SAE Paper 790501, 1979.

7. Iida, N., "Combustion Analysis of Methanol-Fueled Active Thermo-Atmosphere Combustion (ATAC) Engine Using a Spectroscopic Observation", SAE Paper 940684, 1994.

8. Najt, P.M., "Compression Ignition Homogeneous Charge Combustion", M.S. Thesis, Mechanical Engineering Department, University of Wisconsin - Madison, 1981.

9. Milovanovic, N. and Chen, R., "A Review of Experimental and Simulation Studies on Controlled Auto-Ignition Combustion", SAE Paper 2001-01-1890, 2001.

10. Callahan, C.V., Held, T.J., Dryer, F.L., Minetti, R., Ribaucour, M., Sochet, L.R., Faravelli, T., Gaffuri, P., and Ranzi, E., "Experimental Data and Kinetic Modeling of Primary Reference Fuel Mixtures", 26th Symposium (International) on Combustion, pp. 739-746, 1996.

11. Glassman, I., Combustion, 3rd Edition, Academic Press, Orlando, CA, 1996.

12. Westbrook, C.K., Pitz, W.J., and Leppard, W.R., "The Auto-Ignition Chemistry of Paraffinic Fuels and Pro-Knock and Anti-Knock Additives - A Detailed Chemical Kinetics Study", SAE Paper 912314, 1991.

13. Goodger, E.M., Hydrocarbon Fuels – Production, Properties, and Performance of Liquids and Gases, John Wiley & Sons, New York, 1975.

14. Westbrook, C.K. "Chemical Kinetics of Hydrocarbon Ignition in Practical Combustion Systems", Twenty-Eighth International Symposium on Combustion, 2000. Edinburgh, Scotland: The Combustion Institute.

15. Heywood, J.B., Internal Combustion Engine Fundamentals, McGraw-Hill, Inc., New York, NY, ISBN 0-07-028637-X, 1988.

16. Christensen, M., Johansson, B., and Einewall, P., "Homogeneous Charge Compression Ignition (HCCI) Using Isooctane, Ethanol, and Natural Gas – A Comparison with Spark Ignition Operation", SAE Paper 972872, 1997.

17. Christensen, M., Hultqvist, A., and Johansson, B., "Demonstrating the Multi Fuel Capability of a Homogeneous Charge Compression Ignition Engine with Variable Compression Ratio", SAE Paper 1999-01-3679, 1999.

18. Christensen, M., and Johansson, B., "Influence of Mixture Quality on Homogeneous Charge Compression Ignition", SAE Paper 982454, 1998.

19. Noguchi, M., Tanaka, Y., Tanaka, T., and Takeuchi, Y., "A Study on Gasoline Engine Combustion by Observation of Intermediate Reactive Products during Combustion", SAE Paper 790840, 1979.

20. Najt, P.M., and Foster, D.E., "Compression-Ignited Homogeneous Charge Combustion", SAE Paper 830264, 1983.

21. Thring, R.H., "Homogeneous Charge Compression Ignition (HCCI) Engines", SAE Paper 892068, 1999.

22. Noda, T., and Foster, D.E., "A Numerical Study to Control Combustion Duration of Hydrogen-fueled HCCI by Using Multi-zone Chemical Kinetics Simulation", SAE Paper 2001-01-0250, 2001.

23. Law, D., Kemp, D., Allen, J., Kirkpatrick, G., and Copland, T., "Controlled Combustion in an IC-Engine with a Fully Variable Valve Train", SAE Paper 2001-01-0251, 2001.

24. Christensen, M., and Johansson, B., "Supercharged Homogeneous Charge Compression Ignition (HCCI) with Exhaust Gas Recirculation and Pilot Fuel", SAE Paper 2000-01-1835, 2000.

25. Girard, J.W., Dibble, R.W., Flowers, D.L., and Aceves, S.M., "An Investigation into the Effect of Fuel-Air Mixedness on the Emissions from an HCCI Engine", SAE Paper 2002-01-1758, 2002.

26. Richter, M., Engstrom, J., Franke, A., Alden, M., Hultqvist A., and Johansson, B., "The Influence of Charge Inhomogeneity on the HCCI Combustion Process", SAE Paper 2000-01-2868, 2000.

27. Nakagome, K., Shimazaki, N., and Niimura, K., “Combustion and Emission Characteristics of Premixed Lean Diesel Combustion Engine”, SAE Paper 970898, 1997.

28. Shimazaki, N., Akagawa, H., and Tsujimura, K., “An Experimental Study of Premixed Lean Diesel Combustion”, SAE Paper 1999-01-0181, 1999.

29. Takeda, Y., Keiichi, N., and Keiichi, N., “Emission Characteristics of Premixed Lean Diesel Combustion with Extremely Early Staged Fuel Injection”, SAE Paper 961163, 1996.

30. Iwabuchi, Y., Kawai, K., Shoji, T., and Takeda, Y., “Trial of New Concept Diesel Combustion System – Premixed Compression-Ignition Combustion”, SAE Paper 1999-01-0185, 1999.

31. Aroonsrisopon, T., Werner, P., Waldman, J.O., Sohm, V., Foster, D.E., Morikawa, T., and Iida, M., "Expanding the HCCI Operation with the Charge Stratification", SAE Paper 2004-01-1756, 2004.

32. Marriott, C.D. and Reitz, R.D., "Experimental Investigation of Direct Injection-Gasoline for Premixed Charge - Compression Ignited Combustion Phasing Control", SAE Paper 2002-01-0418, 2002.

33. Suzuki, H., Koike, N., and Odaka, M., “Combustion Control Method of Homogeneous Charge Diesel Engines”, SAE Paper 980509, 1998.

34. Odaka, M., Suzuki, H., Koike, N., and Ishii, H., “Search for Optimizing Control Method of Homogeneous Charge Diesel Combustion”, SAE Paper 1999-01-0184, 1999.

35. Hultqvist, A., Christensen, M., Johansson, B., Franke, A., Richter, M., and Alden, M., “A Study of the Homogeneous Charge Compression Ignition Combustion Process by Chemiluminescence Imaging”, SAE Paper 1999-01-3680, 1999.

36. Kawahara, N., Tomita, E., and Kagajyo, H., “Homogeneous Charge Compression Ignition Combustion with Dimethyl Ether – Spectrum Analysis of Chemiluminescence”, SAE Paper 2003-01-1828, 2003.

37. Kumano, K., and Iida, N., “Analysis of the Effect of Charge Inhomogeneity on HCCI Combustion by Chemiluminescence Measurement”, SAE Paper 2004-01-1902.

38. Kim, B., Kaneko, M., Ikeda, Y., and Nakajima, T., “Detailed Spectral Analysis of the Process of HCCI Combustion”, Proceedings of the Combustion Institute, Volume 29, pp 671-677, 2002.

39. Richter, M., Franke, A., and Alden, M., “Optical Diagnostics Applied to a Naturally Aspirated Homogeneous Charge Compression Ignition Engine”, SAE Paper 1999-01-3649, 1999.

40. Graf, N., Gronki, J., Schulz, C., Baritaud, T., Cherel, J, Duret, P., and Lavy, J., “In-cylinder Combustion Visualization in an Auto-Igniting Engine using Fuel Tracer- and Formaldehyde-LIF Imaging”, SAE Paper 2001-01-1924, 2001.

41. Collin, R., Nygren, J., Richter, M., Alden, M., Hidingsson, L., and Johansson, B., “Simultaneous OH- and Formaldehyde-LIF Measurements in an HCCI Engine”, SAE Paper 2003-01-3218, 2003.

42. Chasteen, T.G., Chemiluminescence Spectroscopy, http://www.shsu.edu/%7Echemistry/chemiluminescence/CLUMIN.html.

43. Gaydon, A.G., The Spectroscopy of Flames, 2nd Edition, Chapman and Hall, London, 1974.

44. Ikeda, Y., Kaneko, M., Nakajima, T., “Local A/F Measurement by Chemiluminescence OH*, CH* and C2* in SI Engine”, SAE Paper 2001-01-0919, 2001.

45. Lancaster, D.R., Krieger,R.B., and Lienesch, J.H., "Measurement and Analysis of Engine Pressure Data", SAE Paper 750026, 1975.

46. Dec, J. Personal Communication.

Appendix A – Experimental Procedures

A.1 Spectrograph and CCD Camera Setup

The spectrograph and CCD camera do not need to be turned on until the engine is ready to run. Follow the standard procedure to warm-up the engine and emissions bench before setting up the spectrograph and CCD camera. Once the engine is ready, the following procedures can be performed

1. Connect the fiber optic SMA adapter to the fast kinetics adapter on the spectrograph input.
2. Turn on the CCD camera / spectrograph controller computer.
3. Turn on the spectrograph. The spectrograph motor will move the grating to the "home" position.
4. The CCD camera does not have an on/off switch. It is turned on automatically by the computer.
5. Adjust the spectrograph trigger parameter on the MotoTune software. This parameter determines when the CCD camera starts acquiring signal.
6. Turn on the signal generator box. Adjust the settings appropriately. The following settings are used in this experiment:
    i. Trigger Mode: External
    ii. Trigger Edge: Falling
    iii. Delay: 0.000 s
    iv. Pulse Width: 0.002 s

7. The trigger signal timing can be checked on the ACAP oscilloscope by connecting the BNC cable from the signal generator box output to the channel 2 of the DSP 4012.
8. Open the Andor MCD software
9. Open the appropriate configuration file by choosing File, Configuration Files, and Load. For this experiment, the configuration file is config1.cfg.
10. Turn on the CCD camera cooler by clicking on the temperature indicator on the bottom left corner of the screen. Set the temperature to -45°C.
11. Move the grating to the desired position:
    i. Go to Calibrate menu and select X-Calibration by Spectrograph.
    ii. Enter the desired center wavelength position.
    iii. Make sure the “Move Spectrograph” and “Apply Calibration to New Acquisitions” boxes are checked.
    iv. Click “Calibrate”. The grating will automatically move to the specified position. Do not press any button or click on anything until the spectrograph motor stop moving. Based on previous experience, the program often crashed if any button is pressed while the grating is moving.
12. Calibrate the spectrograph manually:
    i. Open the appropriate calibration file by going to File, Open.
    ii. Go to Calibrate menu and select Manual X-Calibration.
    iii. Select the peaks on the calibration file and assign specific values according to the calibration lamp specification.
    iv. Click the “Calibrate” button.

13. Open the appropriate program file by going to File, Open. On the file type option, choose Andor Program File (*.pgm). For these experiments, the program file is Fast Kinetics Auto Save.pgm. This program enables taking multiple numbers of fast kinetics spectra and save them individually for further analysis.
14. Open the setup acquisition dialog box by going to Acquisition, Setup Acquisition. Change the Trigger Mode to “External Start”. Make sure all the parameters are correct. The settings should be as follows:
    i. Acquisition Mode: Fast Kinetics
    ii. Readout Mode: Full Vertical Binning
    iii. Readout time per pixel 16 µsecs
    iv. Vertical shift speed: 4 µsecs
    v. Exposure Time: 400 µsecs
    vi. Sub Area Height: 25 rows
    vii. Number in Series: 15
15. Once the temperature reaches the set point, the data acquisition can be started.
16. Start data acquisition by pressing F5 button. Enter the number of cycles to acquire. Let the CCD camera acquire about 1000 cycles to achieve steady state dark noise level.
17. Once the dark signal reaches steady state level, the background can be collected. Turn on the Auto-Save feature, specify the directory to save the data, and acquire 500 cycles.
18. Open the shutter by choosing Hardware, Shutter Control. Check the “Permanently Open” box.

19. Change the directory setting on the Auto-save menu.
20. The system is ready for data acquisition.

A.2 Data Analysis Procedures

1. Perform the batch conversion to convert the file from *.sif to *.asc. Make sure the "Tab Delimited" box is checked.
2. Open LabVIEW program. Select "File Averager no Background.vi".
3. Open the diagram window.
4. Adjust the number of cycles appropriately.
5. Change the file directory location.
6. Click on "Run". The program will average the cycles and save into one single file.
7. Once the program has finished calculating the average, a window will pop-up and asks for a file name.
8. The averaged data can be opened with Excel or other data analysis program.
9. Subtract the background from the signal.
10. Multiply each data point with the correction factor corresponding to the spectrograph grating position.
11. The data is ready for plotting and peaks identification.

A.3 Fiber Adapter Maintenance Procedures

The fiber optics tip needs to be cleaned after every 10 hours of running to ensure data consistency. The cleaning procedures are as follows:

1. Unscrew the fiber optics SMA adapter from the spectrograph. This step is very important. The fiber will be damaged if further steps are taken without disconnecting it from the spectrograph.
2. Remove the fiber optics adapter from the spark plug hole using a slotted 14 mm socket and a ratchet wrench. Make sure the fiber is not twisted during this process.
3. Once the fiber optics is removed, the tip needs to be polished with Colloidal Alumina polishing compound. The polishing can be done at the Material Preparation Laboratory located in the Material Science & Engineering building.
4. Attach the non-abrasive nylon polishing cloth to the polishing machine. Put a drop of the polishing compound on the cloth.
5. Turn on the polisher machine and adjust the speed to medium. Hold the fiber tip on the polishing cloth while applying moderate pressure for 1-2 minutes until most of the polishing compound disappears.
6. Clean the polishing compound residue on the fiber tip with alcohol and cotton swabs.
7. Put a small amount of anti seize compound on the fiber optics adapter thread.
8. Install the fiber optics adapter back into the spark plug hole. The adapter must be properly tightened to prevent leakage from the cylinder.
9. Attach the other end of the fiber to the spectrograph.

A.4 Supplemental Laboratory Experimental Procedures

These sections provide additional information for the laboratory experimental procedures which have not been covered in the laboratory operating manual.

A.4.1 Surge Tanks and Intake Pipes Heater Strips Temperature Control

These heater strips are controlled individually. The settings can be adjusted using a LabVIEW program named “Set Zone Temps.vi”. Double click the icon on the desktop, and set the six temperatures to the desired values. Click on “Done” button, and then click the “Run” arrow. These temperatures are typically set at about 7°C to 10°C higher than the desired intake temperature.

A.4.2 Intake Runner Heater Strips Controller

The intake runner heater strips are controlled by controller #0004 labeled “Temperature Intake Air” in the controller box. The setting can be adjusted directly through the controller by following these steps:

1. Press the left button. The controller should display “SP1”
2. Press the right button. The controller should now display the current set point temperature. Adjust the set point by pressing the up/down arrow button.
3. Press the right button twice.
4. The controller will now display the second set point (the inline heater set point). Adjust this set point by pressing the up/down arrow button.
5. Press the right button again. The display should read “CNFG”
6. Press the left button.

Appendix B – Equations and Computer Codes

B.1 Air-Fuel Ratio and Emissions Calculation Equations

Orifice Air Flow Rate [mg/s]

$$\dot{m}_{air,orifice} = M \cdot \frac{P_{Upstream}}{R \cdot T_{Upstream}} + b$$

M = slope of the curve fit line from the calibration of the orifice

b = y-intercept of the curve fit line from the calibration of the orifice

R = Universal Gas Constant

Calculated Fuel Flow Rate (By Exhaust Emissions) [mg/s]

$$FuelFlow_{E.B.} = \frac{\dot{m}_{orificeAir}}{AF_{EB.Avg.}}$$

Indicated Mean Effective Pressure (IMEP) [kPa] *

$$MEP_{Indicated} = \frac{1}{V} \int_{-180}^{180} P \cdot dV$$

Coefficient of Variation of IMEP (COV_{IMEP}) *

$$COV_{IMEP} = \frac{Std.Dev._{IMEP}}{IMEP_{Average}}$$

Air/fuel Ratio using MAX Machinery Meter Fuel Flow Rate

$$AF_{MAX} = \frac{\dot{m}_{air,Orifice}}{\dot{m}_{fuel,Max}}$$

Fuel Molecular Weight

For a fuel of the format CH_yO_z

y = hydrogen / carbon ratio

z = oxygen / carbon ratio

$$MW_f = 12.011 + 1.008y + 15.99z$$

Emissions Bench Based Air/fuel Ratio via Carbon Balance

For a fuel of the format CH_yO_z

y = hydrogen / carbon ratio

z = oxygen / carbon ratio

Note: The concentrations of NO and C_3H_{3y} should be in % volume which is equal to the PPM value / 10,000.

$$AF_C = \frac{MW_a}{MW_f}\left(\frac{N}{100}\left(100 + \frac{3}{2}[H_2O] + \left(\frac{3}{2}y - 1\right)[C_3H_{3y}] - \frac{1}{2}[CO]\right) - \frac{1}{2}(y+z)\right)$$

$$N = \frac{100}{[CO] + [CO_2] + 3[C_3H_{3y}]}$$

Emissions Bench Based Air/fuel Ratio via Oxygen Balance

$$AF_O = 4.774 \frac{MW_a}{MW_f}\left(\frac{N}{100}\left([CO_2]+[O_2]+\frac{1}{2}([H_2O]+[NO]+[CO])\right)-\frac{z}{2}\right)$$

$$N = \frac{100}{[CO]+[CO_2]+3[C_3H_{3y}]}$$

Exhaust Gas Water Concentration [% Volume]

Note: The concentrations of C_3H_{3y} should be in % volume which is equal to the PPM value / 10,000.

$$[H_2O] = \frac{\frac{y}{2}\frac{100}{N}-\frac{3}{2}y[C_3H_{3y}]}{\frac{[CO]}{K_{eq}[CO_2]}+1}$$

$$K_{eq} = 3.8$$

Exhaust Gas Oxygen Concentration [% Volume]

$$[O_2] = AF_C \cdot \frac{MW_f}{MW_{air}} \cdot \frac{100}{N} \cdot \frac{1}{4.76} - \left([CO_2]+\frac{[CO]}{2}+\frac{[H_2O]}{2}+\frac{[NO]}{2}\right)$$

Exhaust Gas Hydrogen Concentration [% Volume]

$$[H_2] = \frac{1}{2}y([CO]+[CO_2])-[H_2O]$$

Carbon Dioxide Emissions Index (EI CO_2) [g/kg_{fuel}]

$$EICO_2 = [CO_2]\left(\frac{MW_{CO_2}}{MW_f\left([CO]+[CO_2]+3[C_3H_{3y}]\right)}\right)\times 1000$$

Where $MW_{CO2} = 44.010$

Carbon Monoxide Emissions Index (EI CO) [g/kg_{fuel}]

$$EICO = [CO]\left(\frac{MW_{CO}}{MW_f\left([CO]+[CO_2]+3[C_3H_{3y}]\right)}\right)\times 1000$$

Where $MW_{CO} = 28.010$

Nitrogen Oxide Emissions Index (EI NO) [g/kg_{fuel}]

$$EINO = [NO]\left(\frac{MW_{NO}}{MW_f\left([CO]+[CO_2]+3[C_3H_{3y}]\right)}\right)\times 1000$$

Where $MW_{NO} = 46.006$

Hydrocarbon Emissions Index (EI HC) [g/kg_{fuel}]

$$EICO_2 = \frac{1}{2}[C_3H_{3y}]\left(\frac{MW_{HC}}{MW_f\left([CO]+[CO_2]+3[C_3H_{3y}]\right)}\right)\times 1000$$

Where $MW_{HC} = 83.250$

B.2 Andor MCD Fast Kinetics Acquisition Code

```
rem Setup Fast Kinetics mode parameter
rem 1st parameter = exposure time
rem 2nd parameter = number of series (number of frame in 1 data set)
rem 3rd parameter = height
rem Set Full Vertical Binning mode
SetFastKinetics(400,15,25)
SetFVB()


rem #x = data set number x, each data set consists of 15 frames
rem {f} = frame number f in a particular data set


rem while loop for data acquisition
rem repeat fast kinetics for rep times
rem The last data set will be saved as run.sif
input ("Enter number of data set", rep)
z = rep+1
i = 1
while i < z
        run()
        fname$ = "run.sif"
        save(#0, fname$)
        i = i+1
if(i<rep)then
closewindow(#1)
endif
wend


rem While loops to close unnecessary windows (from windows 1 to rep will be closed)
rem Accumulated image be closed as well
rem a = 1
rem while a < z
rem     CloseWindow(#a)
rem     a = a + 1
rem wend
CloseWindow(#1)
CloseWindow(#2)
CloseWindow(#0)
```

B.3 EES Heat Release Code

Single_zone v8.3

Equations

This program is a single-zone heat release calculator
Developed by: J.B. Ghandhi
Last Modified: 3 June 2004

Notes:
1) Pressure is kPa
2) Volume in m^3 3) TDC compression is 0 degrees

Function to evaluate the specific heat ratio

function $\gamma(T)$ (1)

$\gamma = 1.392 - 7.5 \times 10^{-5} \cdot T$ (2)

end (3)

Procedure to determine the 10, 50 and 90 % burn times

procedure Crank(θ_{start}, θ_{end}, θ : CA_{10}, CA_{50}, CA_{90}, CA_5) (4)

$CA_{10} = -99$ (5)

$CA_{50} = -99$ (6)

$CA_{90} = -99$ (7)

$CA_5 = -99$ (8)

If $(theta < theta_{end})$ then $goto10$ (9)

Get out because integration is not done

$i := \theta_{start}$ (10)

$V1 = 0.1$ (11)

$V5 = 0.5$ (12)

$V9 = 0.9$ (13)

$V05 = 0.05$ (14)

repeat (15)

$i := i + .5$ (16)

$z1 = \text{Integralvalue}(i,\ cum_{hr})$ (17)

$z2 = \text{Integralvalue}(i - 0.5,\ cum_{hr})$ (18)

If $((z1 > V05 - 0.001)\ and\ (z2 < V05 + 0.001))$ then $CA_5 = i$ (19)

If $((z1 > V1 - 0.001)\ and\ (z2 < V1 + 0.001))$ then $CA_{10} = i$ (20)

If $((z1 > V5 - 0.001)\ and\ (z2 < V5 + 0.001))$ then $CA_{50} = i$ (21)

If $((z1 > V9 - 0.001)\ and\ (z2 < V9 + 0.001))$ then $CA_{90} = i$ (22)

until $(i >= \theta_{end})$ (23)

10 : (24)

end (25)

procedure TDC($\theta,\ \theta_{end},\ CA_5,\ CA_{10} : T_{TDC},\ P_{TDC},\ T_{CA5},\ T_{CA10},\ T_{m20}$) (26)

Pick out the temperature and pressure @ TDC

$T_{TDC} = 20$ (27)

$P_{TDC} = 101$ (28)

$T_{CA5} = 20$ (29)

$T_{CA10} = 20$ (30)

$T_{m20} = 20$ (31)

Initialization of the TDC Temperature and Pressure Variables

If $(\theta < \theta_{end})$ then $goto20$ (32)

Get out because integration is not done

If $(\theta >= \theta_{end})$ then (33)

$T_{TDC} = \text{Integralvalue}(0,\ T)$ (34)

$P_{TDC} = \text{Integralvalue}(0,\ P)$ (35)

$$T_{CA5} = \text{Integralvalue}(CA_5,\ T) \tag{36}$$

$$T_{CA10} = \text{Integralvalue}(CA_5,\ T) \tag{37}$$

$$T_{m20} = \text{Integralvalue}(-20,\ T) \tag{38}$$

endif (39)

20 : (40)

end (41)

$$\theta_{step} = 0.25 \tag{42}$$

Step size for integration

Use partial pressures to determine the residual fraction at IVC using measured intake and exhaust temperatures as the fresh and residual gas temperatures

Volume and Pressures

$$V_{IVC} = \text{Interpolate}(LUT\$,\ \text{'volume'},\ \text{'theta'},\ \theta = IVC) \tag{43}$$

$$P_{IVC} = \text{Interpolate}(LUT\$,\ press\$,\ \text{'theta'},\ \theta = IVC) \tag{44}$$

Pressure and Volume at Intake Valve Closure

$$V_{EVO} = \text{Interpolate}(LUT\$,\ \text{'volume'},\ \text{'theta'},\ \theta = EVO) \tag{45}$$

$$P_{EVO} = \text{Interpolate}(LUT\$,\ press\$,\ \text{'theta'},\ \theta = EVO) \tag{46}$$

Pressure and Volume at Exhaust Valve Openiing

$$V_{EVC} = \text{Interpolate}(LUT\$,\ \text{'volume'},\ \text{'theta'},\ \theta = EVC) \tag{47}$$

$$P_{EVC} = \text{Interpolate}(LUT\$,\ press\$,\ \text{'theta'},\ \theta = EVC) \tag{48}$$

Pressure and Volume at Exhaust Valve Closing

Internal EGR

$$y_{res,int} = (V_{EVC}/V_{EVO}) \cdot (P_{EVC}/P_{EVO})^{1/n_{comp}} \tag{49}$$

Yun & Mirsky correlation for internal residual fraction

$$y_{res,int} = \frac{mass_{res,int}}{mass_{res} + mass_{air} + mass_{fuel}} \tag{50}$$

Determining the amount of cylinder mass that is composed of the internal residual

$$PP_{res,int} = mass_{res,int} \cdot R \cdot T_{exhaust}/V_{IVC} \tag{51}$$

Determining the Partial Pressure of the internal residual

External EGR

$$PP_{freshair} = (mass_{air} + mass_{fuel}) \cdot R \cdot T_{intake}/V_{IVC} \quad (52)$$

Partial Pressure of the air and fuel masses entering the cylinder through the intake valve

$$mass_{res,ext} = (P_{IVC} - PP_{freshair} - PP_{res,int}) \cdot V_{IVC}/R/T_{intake} \quad (53)$$

Determing the amount of the inlet gasses that is composed of exhaust residual

IVC Conditions

$$mass_{res} = mass_{res,int} + mass_{res,ext} \quad (54)$$

Total mass of exhaust Residuals

$$T_{IVC} = P_{IVC} \cdot \frac{V_{IVC}/R}{(mass_{air} + mass_{fuel} + mass_{res})} \quad (55)$$

Calculation of the cylinder gas temperature at intake valve closure

$$y_{res} = \frac{mass_{res}}{(mass_{res} + mass_{air} + mass_{fuel})} \quad (56)$$

Determining the mass fraction of the residual gasses

Determine the compression polytropic coefficient

$$P1 = \text{Interpolate}(LUT\$,\ press\$,\ \text{'theta'},\ \theta = IVC + 5) \quad (57)$$

$$V1 = \text{Interpolate}(LUT\$,\ \text{'volume'},\ \text{'theta'},\ \theta = IVC + 5) \quad (58)$$

Pressure and volume 5 degrees after intake valve closure

$$P2 = \text{Interpolate}(LUT\$,\ press\$,\ \text{'theta'},\ \theta = -30) \quad (59)$$

$$V2 = \text{Interpolate}(LUT\$,\ \text{'volume'},\ \text{'theta'},\ \theta = -30) \quad (60)$$

Pressure and volume 30 degrees before top dead center

$$n_{comp} = abs\left(\frac{\log(P2/P1)}{\log(V2/V1)}\right) \quad (61)$$

calculates the polytropic coefficient of compression for the cut off points defined above

$$V_{disp} = \text{Lookup}(LUT\$,\ 1,\ \text{'volume'}) - \text{Lookup}(LUT\$,\ 180/ca,\ \text{'volume'}) \quad (62)$$

Total volume displaced by one stroke of the piston

$$Q = mass_{fuel} \cdot LHV \cdot \eta_c \quad (63)$$

Amount of fuel energy available in the cylinder

$$Ru = 8.314 \ [\mathrm{kJ/kmol \cdot K}] \tag{64}$$

Universal gas constant

$$R = \frac{Ru}{\mathrm{MW\,(air\,)}} \tag{65}$$

Gas constant for air

$$speed = \frac{60/RPM}{360} \tag{66}$$

Inverse of the Engine Speed

$$V_p = \frac{2 \cdot Stroke}{time} \tag{67}$$

Mean speed of the piston

$$time = \frac{60}{RPM} \tag{68}$$

Time per revolution

$$EVC = 375 \tag{69}$$

Crank angle where the exhaust valve closes

$$p = \mathrm{Interpolate}(LUT\$,\ press\$,\ \text{'theta'}\ ,\ \theta = \theta) \tag{70}$$

Pressure at the integral step

$$dp = \mathrm{Differentiate}(LUT\$,\ press\$,\ \text{'theta'}\ ,\ \theta = \theta) \tag{71}$$

Calculated change in pressure for the integral step

$$T = p \cdot \frac{V/R}{(mass_{air} + mass_{fuel} + mass_{res})} \tag{72}$$

Calculated temperature at each integral step

$$V = \mathrm{Interpolate}(LUT\$,\ \text{'volume'}\ ,\ \text{'theta'}\ ,\ \theta = \theta) \tag{73}$$

Actual volume at each integral step

$$dV = \mathrm{Differentiate}(LUT\$,\ \text{'volume'}\ ,\ \text{'theta'}\ ,\ \theta = \theta) \tag{74}$$

Change in volume for each integral step

$$gam = \gamma\,(T) \tag{75}$$

Specific heat ratio for each integral step using a temperature correction

$$\frac{V}{gam-1}\cdot dp + gam\cdot p\cdot dV/(gam-1) + dQ_{ht} = dQ_{hr} \tag{76}$$

Calculated amount of heat released at each integral step

$$dQ_{ht} = HT\cdot h\cdot Area\cdot(T - T_{wall})\cdot speed \tag{77}$$

Calculated amount of heat transfer at each integral step

$$h = 0.131\cdot\left(D^{0.2}\right)\cdot\frac{(p/101.3)^{0.8}}{T^{0.53}}\cdot\left(W^{0.8}\right) \tag{78}$$

Calculated convective heat transfer coefficient from Woschni's correlation

$$W = 2.28\cdot(V_p + C2\cdot 0.0136\cdot(V_{disp}/V_{IVC})\cdot((p/P_{IVC}) - (V_{IVC}/V)^{n_{comp}})\cdot T_{IVC}) \tag{79}$$

Woschni correlation for the mean gas velocity

$$Area = 2\cdot\left(\pi\cdot\frac{D^2}{4}\right) + \pi\cdot D\cdot\left(V/\left(\pi\cdot D^2/4\right)\right) \tag{80}$$

Disk-shaped chamber surface area

$$Q_{tot} = \int_{\theta_{start}}^{\theta_{end}} dQ_{hr}\, d\theta \tag{81}$$

Total amount of calculated heat released

$$cum_{hr} = Q_{tot}/Q \tag{82}$$

Fraction of heat released to heat available for release

$$Diff = (Q - Q_{tot})^2 \tag{83}$$

Difference between the integrated heat released and the actual heat released

$$Q_{ht} = \int_{\theta_{start}}^{\theta_{end}} dQ_{ht}\, d\theta \tag{84}$$

Heat transfered to the cylinder walls

```
$integraltable theta:0.25, dQ_hr,dQ_ht,cum_hr, T, p
```

Generates a table of these parameters from 45 degrees before TDC to 45 degrees after TDC

$$\text{call Crank}(\theta_{start}, \theta_{end}, \theta : CA_{10}, CA_{50}, CA_{90}, CA_5) \tag{85}$$

Determines several points of the combustion phasing

$$\text{call TDC}(\theta, \theta_{end}, CA_5, CA_{10} : T_{TDC}, P_{TDC}, T_{CA5}, T_{CA10}, T_{m20}) \tag{86}$$

Determines cylinder properties at various points in the cycle

$$Duration = CA_{90} - CA_{10} \tag{87}$$

Duration of the combustion

B.4 EES Minimization Code

minimization

Equations

This program is used to calculate a multiplication factor to minimize the difference between the light intensity and the lamp specification

Developed by: Rinaldo Augusta

1) Column 1 in Lookup Table = Light intensity measured by the CCD camera

2) Column 2 in Lookup Table = Actual lamp specification from the manufacturer

duplicate $i = 1, 512$ (1)

$sig_i = \text{Lookup}(\text{'lookup 1'}, i, 1)$ (2)

$act_i = \text{Lookup}(\text{'lookup 1'}, i, 2)$ (3)

end (4)

duplicate $i = 1, 512$ (5)

$$c_i = \left(A \cdot \frac{sig_i}{act_i} - 1 \right)^2 \quad (6)$$

end (7)

$$sum = \sum_{i=1}^{512} c_i \quad (8)$$

A = multiplication factor that results in minimum difference between the light intensity and the lamp specification